Biomineralised Hydroxyapatite as a Cement Coating

Ronald Joseph Turner

Thesis

Submitted for the fulfilment of the requirements for the degree of

Doctor of Philosophy

Department of Civil and Environmental Engineering

University of Strathclyde, Glasgow, UK

2018

Declaration / Copyright

Signed:

Date: 23rd October 2018

Acknowledgements

Thanks to my supervisors – Dr Andrea Hamilton and Dr Joanna C Renshaw – for their support, practical advice, and guidance in producing this thesis. Thanks to Amy Romaniuk and Chris Wong for their support throughout the PhD process. Thank you to Dr Charles Knapp, Dr Pieter Bots, and Dr Susan Cumberland for a great deal of advice. A special thanks to my mother Christine Turner, for her continual advice and support.

Ronnie Turner

Dated: 23rd October 2018

Abstract

Ordinary Portland Cement (OPC) is the World's most widely used building material. Cement is thus vulnerable to degradation through many processes. Bacteria are capable of generating minerals, in a process called biomineralisation. This may lead to the formation of many different minerals. There is precedent for applying biomineralisation processes to the repair and preservation of cements and concretes.

In this thesis, we observe and describe for the first time the bacterially-mediated deposition of a hydroxyapatite coating onto OPC, and describe the biochemical mechanisms underlying this process. The biogenic hydroxyapatite deposition takes place in a synergistic process with the cement substrate material; utilising a *Pseudomonas fluorescens* biofilm, phosphates from the growth medium, and calcium from the cement substrate and pore solution.

We additionally investigate the capacity of *P. fluorescens* to form biofilms under varied environmental conditions of temperature and carbon source availability, which is relevant to the application of the identified biogenic deposition system in the built environment. The investigation of *P. fluorescens* biofilms under these conditions is yet to be reported in the literature. We also establish that varied *P. fluorescens* morphologies may emerge under different environmental conditions, and carry out a novel structural characterisation and assay the fitness of these varied colony morphologies.

Developing upon these initial investigations, we characterise this biogenic hydroxyapatite in detail using TEM, SEM-EDS, XRD, synchrotron-SAXS, and Mossbauer spectroscopy. We identify that this biogenic hydroxyapatite presents a less crystalline; plate like morphology, and reduced primary particle size in comparison to abiotic hydroxyapatite.

The functional capacities of this biogenic hydroxyapatite as an OPC coating material are also investigated. We use focus-variation microscopy to characterise the surface topography of the

coating, nanoindentation to measure the hardness and elastic modulus of the biogenic and abiotic hydroxyapatites, in combination with X-CT analysis to establish the completeness of the deposition process, and contact-angle measurements to investigate the hydrophobicity of the coating.

Table of Contents

Chapter 1: Introduction

1.1 Introduction – Microorganisms and Cement

Microorganisms are an important factor in the deterioration of ceramic materials such as concrete, natural stone, and glass.[1] Microbially induced concrete corrosion (MICC) has been well researched due to the widespread use of concrete in the built environment, and the subsequent economic impact promoting research interest.[2] MICC associated with sewerage and water transport systems has been particularly well characterised.[3–6]

In comparison with the level of research involving concretes, the interactions of bacteria with cement paste alone is not as well studied. However there have been recent investigations into the association of selected bacterial species with medical cements,[7] and surfaces relevant to food safety.[8] The degradation mechanisms of Portland cement pastes by organic acids produced by Fungi such as *Aspergillus* and the physical damage caused by fungal mycelia have been a topic of recent research interest .[9,10]

There has been very little study to date regarding the capacity of bacteria to preserve or repair – rather than degrade – cement materials. Some recent studies have established that biofilm material will generate a cement which is more resistant to water ingress,[11] or that biofilms may provide some shielding from environmental attack.[12] While microbially-induced calcite precipitation is an established method for cement repair, [13] the use of bacterially generated hydroxyapatite to preserve cements and protect new buildings remains unstudied and the underlying biochemical processes have not been characterised.

1.2 Biofilms

The dominant mode of bacterial growth in the environment is in the form of a biofilm[14–17]. Biofilms are multicellular communities which consist of a matrix of extracellular polymeric substances (EPS) within which the microbial cells and some inorganic materials are suspended. The resultant gel is primarily anionic.[18] These dense, multicellular communities are irreversibly adhered to a solid substrate, an interface, or indeed to other microorganisms.[19] Bacteria living within biofilms are considered 'sessile', and generally express an altered phenotype in terms of growth rate and gene transcription than found in equivalent planktonic (free-swimming) cells.[19]

Figure 1: A 3D Image of a Biofilm

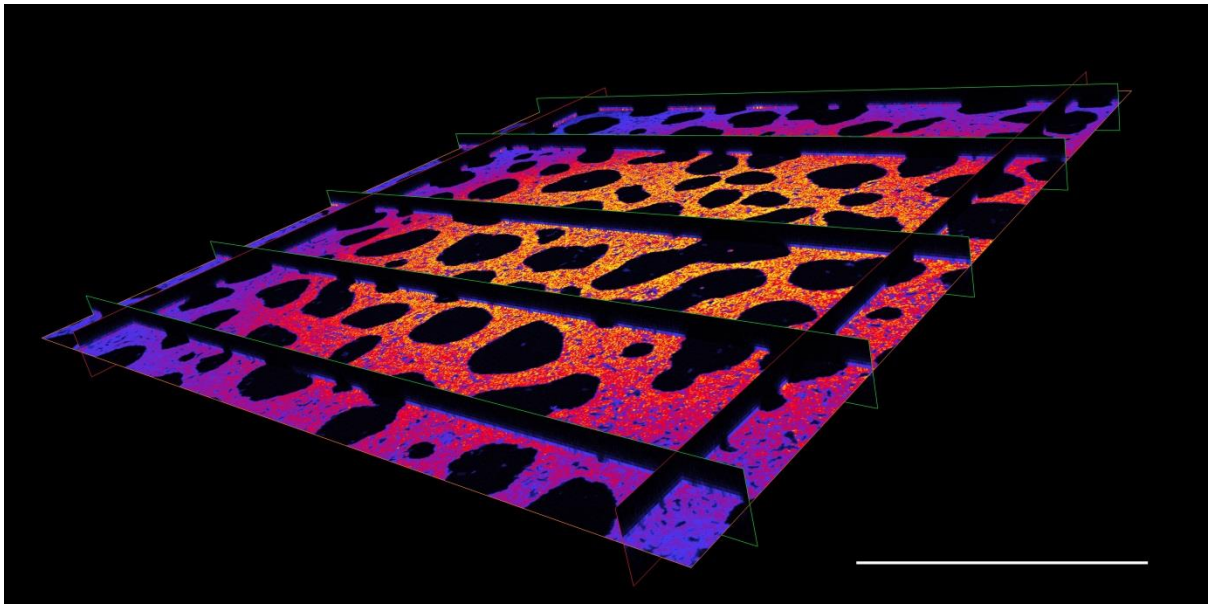

Figure 1: A 3D image of a biofilm attached to a glass substrate, visualised using confocal microscopy. The image illustrates the extracellular matrix which makes up a biofilm (purple-orange), which encases individual cells. Voids and pores are also visible (black areas), which allow for nutrient flow and waste product removal from the biofilm. Scale bar is 100µm. Image is own work.

Biofilms are widely associated with the built environment, such as through colonisation of metal surfaces [18] and drinking water systems.[20] Biofilms are capable of forming in a broad range of

environments, and so have relevance to a diverse range of industrial activities, including aviation,[21] the oil industry,[18] and nuclear waste disposal. [22] Bacteria are known to grow on the surface of cement materials in the form of a biofilm.[7,16,23] It is therefore highly likely that most bacterial communities will interact with cementitious materials as biofilms.[14–16] Thus, when investigating interactions between bacteria and cement pastes it is natural to focus studies on the activity of biofilms rather than planktonic cells.

a. Biofilms and Cement

The association of bacterial biofilms with cement pastes has been studied to a limited extent in the context of medical ceramics,[7,24] and food safety.[16] These investigations generally have very different aims and outcomes from those concerning biofilms in a civil engineering context. The influence of the microorganisms on the ceramic substrate tends to be of less interest in food safety and medical investigations, with measurements of bacterial growth and activity as influenced by the substrate taking precedence.

The presence of fungi in biofilms is also relevant to the corrosion of cement pastes, and their role in this process has been investigated.[9] It has been noted that fungi are relevant to the degradation of cement at near-surface nuclear repositories.[10] Fungal metabolism in biofilms may generate organic acids, leading to chemical attack of the underlying cement paste. Investigations have generated a model of Portland cement degradation by acetic, butyric, lactic and oxalic acids secreted by *Aspergillus niger* [9]

Further work has characterised the mechanisms of cement structure degradation caused by citric, tartaric, and oxalic acids using techniques such as electron-probe micro analysis (EPMA), XRD, and SEM [25]. While chemical attack is the predominant form of fungi-associated cement degradation, physical attack by intrusion of hyphal growth into cement pores has also been reported [9].

The growth of a mixed-culture biofilm of isosaccharinic acid degrading microorganisms taken from an alkaline analogue site on the cement-based NRVB (Nirex Reference Vault Backfill) was investigated by Nirex [26]. Electron microscopy was used to characterise the biofilm. The biofilm was found to trap inorganic debris and carbonation was observed close to the biofilm/grout interface, although the biofilm could not penetrate more than a millimetre into the porous NRVB structure.

b. Microbially Induced Concrete Corrosion

Microbially induced concrete corrosion (MICC) has been reported in a variety of environments, such as sewage pipelines and waste water treatment systems.[27,28] Corrosion of the concrete materials found in wastewater collection systems has a significant economic impact.[4,29] The cost of maintaining the wastewater collection infrastructure in the USA is an estimated $4.5 billion per year.[30]

This economic impact has promoted significant interest in elucidating the mechanisms behind MICC. Various microorganisms have been shown to participate in the corrosion of concrete. Commonly associated with this process are the aerobic Sulphur Oxidising Bacteria (SOB), the anaerobic Sulphate Reducing Bacteria (SRB), and the nitrifying bacteria *Nitrosomonas* and *Nitrobacter* [1,3]. However, nitrifying bacteria are generally only relevant to MICC above the ground; as they are generally deposited onto the concrete substrate from atmospheric dust.[1]

MICC is typically associated with bacterial growth on the concrete in the form of a biofilm.[3,29] Many of the microorganisms and general mechanisms involved in MICC have been known for decades, with recent advancements in molecular-based approaches allowing more detailed descriptions of the microbial activity behind these processes. MICC in underground systems has been associated with biogenic sulphuric acid. Underground MICC is typically associated with environments which contain sulphate, which leads to biogenic sulphuric acid attack of the concrete through the combined actions of sulphate reducing bacteria (SRB) and sulphur oxidising bacteria (SOB).

SRB obtain energy/electrons from molecular hydrogen or organic compounds, using sulphate as a terminal electron acceptor. SRB couple the oxidisation of organic compounds or molecular hydrogen to the reduction of sulphate to hydrogen sulphide, and so will produce hydrogen sulphide (H_2S) from sulphate (SO_4^{2-}). SRB are generally anaerobic.[1] The generated H_2S may react with atmospheric oxygen to generate elemental sulphur, sulphide, and thiosulphate.[28]

SOB such as *Thiobacillus* are able to grow with reduced sulphur compounds as their only energy/electron source, and CO_2 as the only carbon source. Energy can be obtained from the oxidisation of hydrogen sulphide, producing (biogenic) sulphuric acid. These sulphur oxidising prokaryotes can oxidise a variety of reduced inorganic sulphur compounds, including hydrogen sulphide, sulphur, sulphite, thiosulphate, and a variety of polythionates.[31] Many SOB species are either obligate aerobes or facultative anaerobes. [30–32]

The reduction in pH caused by SOB production of sulphuric acid can cause dissolution of calcium hydroxide ($Ca(OH)_2$) leading on to the precipitation of gypsum from solution. Following dissolution of $Ca(OH)_2$ at lower pH, cement hydrates such as calcium silicate hydrate (CSH), calcium aluminate hydrate (CAH) and tetra-calcium aluminoferrite (C4AF) decompose as a result of the loss of calcium, and convert to amorphous silica, alumina and ferric hydrogel.[28] The calcium aluminate sulphate mineral ettringite may form in deeper sections of the concrete, where the pH remains relatively high.[28] Ettringite is expansive, and so occupies a greater volume than the monosulfoaluminate it replaces. This creates expansive stresses that can cause cracking and deterioration.[33]

c. Microbially-Induced Biomineralisation as a Cement Treatment Method

Where 'biomineralisation' is discussed in this thesis, it refers to 'biologically induced mineralisation' rather than 'biologically controlled mineralisation', which is not relevant to this work.[34,35] Specifically, in biologically controlled mineralisation the organism controls the process of mineralisation to a high degree; typically independently of environmental conditions which generate

a mineral form specific to that particular species, such as through the production of an organic matrix.[35,36] Examples include magnetite formation by bacteria and silica deposition by diatoms.[36] In comparison, in biologically induced mineralisation the synthesis of the mineral is generally dependent upon environmental conditions which may be generated by the organism – such as the reduction of CO_2 by algae [35] - and does not use any specialised structures or molecular mechanisms unique to the organism.[35,36]

The use of biomineralisation to repair the built environment is presently best studied in the form of 'microbially induced calcite precipitation' (MICP). There has been significant research interest in the use of bacteria such as *S. pasteurii* to seal cracks in concretes through the precipitation of calcite to generate a consolidating surface finish.[13] This process relies upon the generation of an alkaline microenvironment around the bacterial cell via metabolic processes such as the breakdown of urea by the enzyme urease, with the resulting increase in pH associated with calcium carbonate precipitation.[37–39]

Calcite treatments of building materials are associated with increased strength of the substrate material,[40] but have shown limited capacity to bind stone particles together[36] and may be more susceptible to environmental degradation than other biominerals such as the relatively less soluble hydroxyapatite.[41] Hydroxyapatite is a calcium phosphate mineral which closely resembles bone material and there is an emerging interest in the use of hydroxyapatite coatings for the consolidation and preservation of marble and limestone buildings and sculptures. [42–46] Hydroxyapatite coatings have been observed to display excellent consolidation abilities, and are more resistant to environmental degradation than calcites.[47,48]

While the use of hydroxyapatite as a building material treatment is a developing area of research, the use of biomineralised hydroxyapatite in this context remains unstudied. All work to date has utilised chemical methods to deposit this hydroxyapatite, with methods including immersion of

calcite-bearing samples in phosphate solutions[45], as well as more aggressive plasma-spraying and electrochemical deposition processes.[49,50]

There have been limited studies investigating biogenic hydroxyapatite formation on solid surfaces. Macaskie et al. (2005) used the Gram-negative bacterium *Serratia* NCIMB 40259 to deposit an extracellular polymeric matrix of biomass onto polyurethane and titanium substrate materials. This EPS was then used as a 'scaffold' for enzymatic nucleation of bio-hydroxyapatite when a source of calcium is added, producing a hydroxyapatite layer bound to the scaffold.[51] *Pseudomonas* and *Serratia* species have also been used to produce nanoscale bio-hydroxyapatite while encapsulated in a sol-gel. [52]

Therefore there is significant scope to investigate the capacity of bacteria to generate hydroxyapatite coatings on OPC-based substrate materials. Bacterial deposition of bio-hydroxyapatite onto concrete may produce a thinner, more flexible, or stronger film than has been achieved with plasma spraying, electrochemical deposition, or biomimetic deposition.[50,53] There are several practical applications for this biogenic hydroxyapatite. This may include the consolidation of cement-based construction materials, as has been investigated with inorganically synthesised hydroxyapatites by other researchers,[42,48] or the generation of cement coatings with the capacity to uptake environmental contaminants such as heavy metals and radionuclides.[51]

In this work, we aim to establish a method for the deposition of hydroxyapatite onto a cement-based substrate material using the model environmental bacterium *Pseudomonas fluorescens* SBW25. We intend to examine the growth of this strain under different conditions relevant to this deposition processes, including the use of different carbon sources and growth temperatures. We will also characterise this deposited 'biogenic' hydroxyapatite as compared against an 'abiotic' hydroxyapatite, in terms of its chemical and structural composition, and the properties of this hydroxyapatite as a cement coating material for practical applications in the built environment.

We have utilised the model environmental bacterium *Pseudomonas fluorescens* to generate a hydroxyapatite coating on the surface of an OPC substrate. We describe the biochemical mechanisms underlying this deposition process. (Chapter 3) Additional work examined the crystallographic nature and chemical composition of this biogenic hydroxyapatite. (Chapter 5)

There has been little investigation of the effects of temperature and carbon source variation on the formation of *P. fluorescens* biofilms. In this thesis (Chapter 4), we identify that alterations in carbon source concentration and composition have variable effects on adhered biofilm cell density, and that reduced temperatures promote emergence of a fuzzy spreader phenotype. The crystal violet binding assay, coupled with confocal microscopy allowed characterisation of changes in biofilm cell morphology and bulk structure which were associated with different environmental conditions.

In this work, we describe and quantify the effects of temperature, carbon source concentration, and carbon source composition on the capacity of *Pseudomonas fluorescens* to form an adhered biofilm at the liquid-solid interface. We establish that two distinct morphologies emerge under varied conditions, and quantify the differences between these morphologies in detail using confocal microscopy. The data presented in Chapter 4 is relevant to the potential applications of the biofilm-mediated deposition of biogenic hydroxyapatite by *P. fluorescens*, providing an outline of the environmental conditions where this deposition process may be successfully applied.

We demonstrate in Chapter 6 that this deposition process uniformly coats the substrate material, as visualised using X-CT. The biogenic hydroxyapatite has an increased surface roughness, with a subsequent increase in coating surface area which is useful for bioremediation applications as well as potential applications in medical devices. We additionally demonstrate that this biogenic hydroxyapatite layer is hydrophobic, which is a significant benefit for preserving new cement structures due to the limitation of water and chloride ingress; both of which are associated with cement deterioration. (Chapter 6)

References

[1] M. Diercks, W. Sand, E. Bock, *Experientia* **1991**, *47*, 514.

[2] H. Yuan, P. Dangla, P. Chatellier, T. Chaussadent, *Cem. Concr. Res.* **2013**, *53*, 267.

[3] H. Satoh, M. Odagiri, T. Ito, S. Okabe, *Water Res.* **2009**, *43*, 4729.

[4] S. Okabe, M. Odagiri, T. Ito, H. Satoh, *Appl. Environ. Microbiol.* **2007**, *73*, 971.

[5] A. L. Ling, C. E. Robertson, J. K. Harris, D. N. Frank, C. V. Kotter, M. J. Stevens, N. R. Pace, M. T. Hernandez, *PLoS One* **2015**, *10*, 1.

[6] L. Cheng, M. W. House, W. J. Weiss, M. K. Banks, *Water Res.* **2016**, *89*, 321.

[7] V. Adetunji, A. Kehinde, O. Bolatito, J. Chen, *J. Food Prot.* **2014**, *77*, 599.

[8] S. Stepanović, I. Ćirković, V. Mijač, M. Švabić-Vlahović, *Food Microbiol.* **2003**, *20*, 339.

[9] L. De Windt, P. Devillers, *Cem. Concr. Res.* **2010**, *40*, 1165.

[10] H. Lajili, P. Devillers, C. Grambin-Lapeyre, J. P. Bournazel, *Mater. Struct.* **2008**, *41*, 1633.

[11] S. Grumbein, D. Minev, M. Tallawi, K. Boettcher, F. Prade, F. Pfeiffer, C. U. Grosse, O. Lieleg, *Adv. Mater.* **2016**, 8138.

[12] S. Soleimani, B. Ormeci, O. B. Isgor, *Appl. Microbiol. Biotechnol.* **2013**, *97*, 1093.

[13] A. Richardson, K. A. Coventry, A. M. Forster, C. Jamison, *Struct. Surv.* **2014**, *32*, 265.

[14] W. G. Characklis, *Water Res.* **1973**, *7*, 1113.

[15] G. A. O'Toole, R. Kolter, *Mol. Microbiol.* **1998**, *28*, 449.

[16] B. Joseph, S. K. Otta, I. Karunasagar, I. Karunasagar, *Int. J. Food Microbiol.* **2001**, *64*, 367.

[17] J. W. Costerton, *The Biofilm Primer*, Springer-Verlag Berlin Heidelberg, Berlin, **2007**.

[18] H. a Videla, L. K. Herrera, *Int. Microbiol.* **2005**, *8*, 169.

[19] R. M. Donlan, J. W. Costerton, *Clin. Microbiol. Rev.* **2002**, *15*, 167.

[20] M. M. Keinänen-Toivola, R. P. Revetta, J. W. Santo Domingo, *FEMS Microbiol. Lett.* **2006**, *257*, 182.

[21] L. M. Brown, J. P. McComb, M. D. Vangsness, L. L. Bowen, S. S. Mueller, L. M. Balster, C. a. Bleckmann, *Int. Biodeterior. Biodegrad.* **2010**, *64*, 253.

[22] N. R. Smart, A. P. Rance, B. Reddy, L. Hallbeck, K. Pedersen, A. J. Johansson, **2014**, *49*, DOI 10.1179/1743278214Y.0000000213.

[23] N. B. Hallam, J. R. West, C. F. Forster, J. Simms, *Water Res.* **2001**, *35*, 4063.

[24] D. Neut, E. P. De Groot, R. S. Z. Kowalski, J. R. Van Horn, H. C. Van Der Mei, H. J. Busscher, *J. Biomed. Mater. Res. - Part A* **2005**, *73*, 165.

[25] S. Larreur-Cayol, a. Bertron, G. Escadeillas, *Cem. Concr. Res.* **2011**, *41*, 882.

[26] United Kingdom Nirex Ltd, *Report S/95/011 - Nirex Near Field Research: Report on Current Status in 1994*, **1995**.

[27] R. L. Islander, J. S. Devinny, F. Mansfeld, A. Postyn, H. Shih, *J. Environ. Eng.* **1991**, *117*, 751.

[28] S. Soleimani, O. B. Isgor, B. Ormeci, *Cem. Concr. Res.* **2013**, *53*, 229.

[29] E. Vincke, N. Boon, W. Verstraete, *Appl. Microbiol. Biotechnol.* **2001**, *57*, 776.

[30] V. Gomez-Alvarez, R. P. Revetta, J. W. Domingo, *BMC Microbiol.* **2012**, *12*, 122.

[31] C. G. Friedrich, D. Rother, F. Bardischewsky, A. Quentmeier, J. Fischer, *Appl. Environ. Microbiol.* **2001**, *67*, 2873.

[32] E. Drobner, H. Huber, R. Rachel, K. O. Stetter, *Arch. Microbiol.* **1992**, *157*, 213.

[33] J. J. Thomas, H. Jennings, “Materials of Cement Science Primer: The Science of Concrete,” can be found under http://iti.northwestern.edu/cement/, **2008**.

[34] N. K. Dhami, S. M. Reddy, A. Mukherjee, in *Adv. Top. Biominer.*, **2012**, pp. 137–164.

[35] H. Lowenstam, *Science (80-.).* **1981**, *211*, 1126.

[36] W. De Muynck, N. De Belie, W. Verstraete, *Ecol. Eng.* **2010**, *36*, 118.

[37] C. Rodriguez-Navarro, F. Jroundi, M. Schiro, E. Ruiz-Agudo, M. T. González-Muñoz, *Appl. Environ. Microbiol.* **2012**, *78*, 4017.

[38] S. Dupraz, M. Parmentier, B. Ménez, F. Guyot, *Chem. Geol.* **2009**, *265*, 44.

[39] B. Krajewska, *J. Adv. Res.* **2017**, *13*, 59.

[40] N. K. Dhami, M. S. Reddy, A. Mukherjee, *Ecol. Eng.* **2012**, *39*, 31.

[41] E. Sassoni, E. Franzoni, *Built Herit. 2013 Monit. Conserv. Manag.* **2013**, 1287.

[42] G. Graziani, E. Sassoni, E. Franzoni, G. W. Scherer, *Appl. Surf. Sci.* **2016**, *368*, 241.

[43] E. Sassoni, G. Graziani, E. Franzoni, *Constr. Build. Mater.* **2016**, *102*, 931.

[44] E. Sassoni, G. Graziani, E. Franzoni, *Constr. Build. Mater.* **2016**, *102*, 918.

[45] E. Franzoni, E. Sassoni, G. Graziani, *J. Cult. Herit.* **2015**, *16*, 173.

[46] F. Yang, Y. Liu, *Mater. Lett.* **2014**, *124*, 201.

[47] S. Naidu, C. Liu, G. W. Scherer, *J. Cult. Herit.* **2014**, *16*, 94.

[48] E. Sassoni, S. Naidu, G. W. Scherer, *J. Cult. Herit.* **2011**, *12*, 346.

[49] N. Eliaz, O. Ritman-Hertz, D. Aronov, E. Weinberg, Y. Shenhar, G. Rosenman, M. Weinreb, E. Ron, *J. Mater. Sci. Mater. Med.* **2011**, *22*, 1741.

[50] J. L. Ong, D. C. N. Chan, *Crit. Rev. Biomed. Eng.* **2000**, *28*, 667.

[51] L. E. Macaskie, P. Yong, M. Paterson-Beedle, A. C. Thackray, P. M. Marquis, R. L. Sammons, K. P. Nott, L. D. Hall, *J. Biotechnol.* **2005**, *118*, 187.

[52] A. Khanafari, T. Akbari, M. R. Sohrabi, *Nanomed J* **2014**, *1*, 276.

[53] Q. Zhang, Y. Leng, R. Xin, *Biomaterials* **2005**, *26*, 2857.

Chapter 2: Analytical Techniques

A broad range of analytical techniques can be applied to characterisation of biofilms and biominerals. Aspects of biofilms that are typically characterised include structure, chemical composition, and activity.[1] A review of the chemical and physical methods for biofilm characterisation was prepared by Wingender et al. in 2007.[2] A review of the methods for characterising biominerals (with a focus on pathological biominerals such as kidney stones) was prepared by Gianossi (2012).[3]

The techniques described in this chapter were used in these studies to examine biofilm formation and other microbial activities. We also characterise the hydroxyapatite biomineral layer in terms of morphology, crystal structure, chemical composition, as well as substrate coverage and layer thickness.

a. Biofilm Characterisation

The growth of biofilms may be quantified using culture-based techniques. These techniques rely upon the examined organism being culturable under laboratory conditions. The use of microtitre plates as a culture vessel for biofilm formation - coupled to crystal violet staining to quantify the adhered cells – has been applied successfully to quantify biofilm adherence.[4–7] However, crystal violet staining techniques have the inherent limitation of measuring total biomass but not viability; as live cells, dead cells, and extracellular material will all uptake the crystal violet stain.[8]

Direct quantification of adhered biofilm cells overcomes these limitations, but requires more time and materials. This quantification may be done by 'scraping' the biofilm from the colonised substrate material into a suspension buffer, homogenising the resultant suspension, and quantifying the number of biofilm cells in CFU/ml via serial dilutions and plate counting.[9] Similar approaches have been successfully applied to the evaluation of biofilm formation on antibiotic-loaded ceramics[10] and biofilms formed by *Streptococcus*.[8] This methodology also permits the bacterial colony morphology

to be examined, which allows for a positive identification of the bacterial strain, and is also of relevance to studies of 'adaptive radiation'.[11]

We utilise a culture-based 'fitness assay' based on maximal growth rate to establish differences in environmental fitness of different *P. fluorescens* SBW25 morphologies, which is a commonly utilised method to quickly and easily establish a proxy of bacterial fitness.[12] In our study, we measure OD_{600} over a time course for two differing *P. fluorescens* SBW25 morphologies to compare their fitness for growth at different temperatures.

Confocal laser scanning microscopy (CLSM) allows the three-dimensional structure of biofilms to be directly visualised, and parameters such as biofilm thickness, biomass, and roughness to be quantified via image analysis.[13–16] CLSM is presently the 'gold standard' method for biofilm structural studies,[17] due to the relatively mild sample preparation conditions in comparison to higher-resolution imaging techniques such as conventional SEM.[18]

b. Biomineral Characterization

i. X-Ray Powder Diffraction (XRD)

XRD is an X-ray based analytical technique which allows the phase composition and crystal structure of materials (mineralogical composition) to be determined, based on the diffraction of X-rays from the structure of these crystalline or semi-crystalline materials.[19,20] In the context of this thesis, we utilise XRD to identify the presence of hydroxyapatite minerals. Additionally, Rietveld refinement techniques allow for the quantification in variations of the crystalline structure of different materials, such as cements.[21]

XRD require a homogenous material, which in the case of our work was typically generated by grinding the sample into a powder where possible. XRD is also relatively poor at quantifying low amounts (<2%) of components in a mixed sample, and does not provide any information on the

chemistry of the material examined, only its crystallography. These issues were overcome by complementing XRD studies with FT-IR, ICP-OES, and SEM/TEM.

ii. Fourier-Transform Infra-Red Spectroscopy (FT-IR)

FT-IR is a 'vibrational spectroscopy' technique, working by way of the detection of internal vibrations in the molecules constituting the analysed material.[22] FT-IR may be applied to detect and quantify microbial biomass,[22] as well as to characterise inorganic materials such as cements.[23] By measuring the IR absorption (or transmittance, or emission) spectra of a sample which interacts with infrared radiation, it is possible to make inferences about the molecular structure of that sample.

In order for any vibrational spectroscopy technique to work effectively, the sample must be 'IR active' – the molecule must have to capacity to vibrate in some mode such as stretching/rocking/twisting etc. In most organic materials, this will be evident the movement of hydrogen atoms bonded to carbon. In the case of hydroxyapatite – an inorganic mineral – it is possible to observe signals from carbonates (CO_3^{2-}), phosphates (PO_4^{3-}), and hydroxides/water molecules.

iii. Electron Microscopy (SEM and TEM)

SEM is an electron microscopy technique allowing a high level of magnification, with a maximum resolution of approximately 10nm. TEM allows an even higher level of magnification, with a maximum resolution of approximately 0.2nm, allowing almost atomic-level imaging of materials. Both of these techniques rely upon a beam of electrons to create images of the sample. Both techniques can be paired with electron dispersion spectroscopy, which allows for a concurrent elemental analysis of the sample. However, the elemental analysis is less sensitive than that which can be attained with alternative spectroscopic or emissions-based techniques such as ICP-OES. Consequently, in the context of this study SEM and TEM are most useful as a method of visualising particle morphology, complementing X-ray diffraction and ICP-OES measurements. SEM and other

electron or optical techniques such as focus-variation microscopy also provide textural data such as surface roughness.

SEM and TEM both require sample preparation techniques. Ceramics require gold-coating prior to SEM imaging, and TEM imaging requires the generation of either thin sections or dispersions of small particle numbers onto a sample grid. If SEM is used to visualise biofilms, it is possible to generate high resolution images compared to techniques such as CLSM, but this comes at the expense of sample dehydration or disruption during sample preparation.

iv. Synchrotron Techniques – Small-Angle X-Ray Scattering (SAXS)

Synchrotron radiation allows for the generation of high-energy, high brilliance X-rays when compared to laboratory X-ray sources.[24] SAXS pattern analysis allows for information on particle sizing and nanoscale structure to be determined, and is often employed to examine biomolecules such as proteins.[25] In the context of this thesis, we use SAXS to complement TEM analyses of particle size. Being very closely related to XRD, SAXS shares the same advantages and limitations common to most X-ray diffraction techniques; requiring a homogenous sample and providing only crystallographic information.

v. X-ray Computed Tomography (X-CT)

X-CT relies upon the differential absorption of X-rays by materials with different attenuation coefficients, which are converted into greyscale values to generate a 3D image of the sample. We utilise X-CT to image the distribution of a biogenic hydroxyapatite over the surface of a cement substrate material.

X-CT provides a non-destructive method to visualise the 3D structure of materials, which may include biomineral layers or biofilms. This visualisation can be carried with minimal sample preparation. Image analysis techniques can allow the differentiation of differing mineral phases based upon their varied X-ray attenuation properties, however it is necessary to validate these

observations using XRD to confirm phase composition, and no specific elemental or chemical information is generated.

vi. Inductively coupled plasma optical emission spectroscopy (ICP-OES)

ICP-OES (sometimes referred to as ICP-AES) is an emission spectroscopy technique. A plasma is generated and utilised to ionise a sample material. This process will generate radiation at wavelengths which are characteristic of the elements being ionised. It is necessary to use chemical standards of known concentrations against which the sample emission spectrum may be compared. This method provides highly quantitative information regarding the chemical composition of the analyte material, but offers no information regarding sample crystal structure or particle morphology. This makes ICP-OES highly complementary to X-ray diffraction and electron imaging techniques.

References

[1] V. Lazarova, J. Manem, *Water Res.* **1995**, *29*, 2227.

[2] E. Denkhaus, S. Meisen, U. Telgheder, J. Wingender, *Microchim. Acta* **2007**, *158*, 1.

[3] V. S. Maria Luigia Giannossi, in *An Introd. to Study Mineral.* (Ed.: C. Aydinalp), **2012**, p. 154.

[4] S. M. Kwasny, T. J. Opperman, *Curr. Protoc. Pharmacol.* **2010**, 1.

[5] G. A. O'Toole, R. Kolter, *Mol. Microbiol.* **1998**, *28*, 449.

[6] C. A. White-Ziegler, S. Um, N. M. Pérez, A. L. Berns, A. J. Malhowski, S. Young, *Microbiology* **2008**, *154*, 148.

[7] C. E. Zago, S. Silva, P. V. Sanitá, P. A. Barbugli, C. M. I. Dias, V. B. Lordello, C. E.

Vergani, *PLoS One* **2015**, *10*, 1.

[8] K. Welch, Y. Cai, M. Strømme, *J. Funct. Biomater.* **2012**, *3*, 418.

[9] J. W. Costerton, J. C. Nickel, T. I. Ladd, in *Bact. Nat.* (Eds.: J.S. Poindexter, E.R. Leadbetter), Plenum Publishing Group, New York City, **1986**, pp. 49–84.

[10] D. Neut, E. P. De Groot, R. S. Z. Kowalski, J. R. Van Horn, H. C. Van Der Mei, H. J. Busscher, *J. Biomed. Mater. Res. - Part A* **2005**, *73*, 165.

[11] P. B. Rainey, M. Travisano, *Nature* **1998**, *394*, 69.

[12] M. J. Wiser, R. E. Lenski, *PLoS One* **2015**, *10*, DOI 10.5061/dryad.4875k.Funding.

[13] P. S. Stewart, R. Murga, R. Srinivasan, D. de Beer, *Water Res.* **1994**, *29*, 2006.

[14] J. J. Harrison, H. Ceri, J. Yerly, C. a Stremick, Y. Hu, R. Martinuzzi, R. J. Turner, *Biol. Proced. Online* **2006**, *8*, 194.

[15] T. Inaba, T. Hori, H. Aizawa, A. Ogata, H. Habe, *npj Biofilms Microbiomes* **2017**, *3*, 5.

[16] A. Heydorn, A. T. Nielsen, M. Hentzer, C. Sternberg, M. Givskov, B. K. Ersboll, S. Molin, *Microbiology* **2000**, *146*, 2395.

[17] J. a. J. J. Haagensen, D. Verotta, L. Huang, A. Spormann, K. Yang, *Antimicrob. Agents Chemother.* **2015**, *59*, AAC.05037.

[18] M. Alhede, K. Qvortrup, R. Liebrechts, N. Høiby, M. Givskov, T. Bjarnsholt, *FEMS Immunol. Med. Microbiol.* **2012**, *65*, 335.

[19] P. E. Stutzman, P. Feng, J. W. Bullard, *J. Res. Natl. Inst. Stand. Technol.* **2016**, *121*, 47.

[20] J. Skibsted, C. Hall, *Cem. Concr. Res.* **2008**, *38*, 205.

[21] G. Le Saoût, V. Kocaba, K. Scrivener, *Cem. Concr. Res.* **2011**, *41*, 133.

[22] J. Schmitt, H.-C. Flemming, *Int. Biodeterior. Biodegradation* **1998**, *41*, 1.

[23] M. a. Trezza, M. F. Ferraiuelo, *Cem. Concr. Res.* **2003**, *33*, 1039.

[24] F. Guirado, S. Galí, *Cem. Concr. Res.* **2006**, *36*, 2021.

[25] N. Kirby, S. Mudie, A. Hawley, H. D. T. Mertens, N. Cowieson, V. Samardzic-Boban, U. Felzmann, N. Mudie, J. Dwyer, *ACA Trans. 2013* **2013**, 27.

Chapter 3 – Biogenic Hydroxyapatite: A New Material for the Preservation and Restoration of the Built Environment

All literature reviews, practical work, data analysis, and manuscript preparation was carried out by Ronald Turner, with guidance provided by Andrea Hamilton and Joanna Renshaw, with the following exceptions:

- OPC/Hydroxyapatite thin-sections were prepared under contract by Petrolab Ltd (Cornwall, UK)
- FT-IR data collection and analysis were provided under contract by The James Hutton Institute (Craigiebuckler, Aberdeen, UK)

The following section (Chapter 3) is formatted for and was published in ACS Applied Materials and Interfaces, Volume 9, Issue 37, Pages 31401-31410 (2017).

Chapter 3 - Biogenic Hydroxyapatite: A New Material for the Preservation and Restoration of the Built Environment

Ronald J Turner, Joanna C Renshaw, and Andrea Hamilton*

Department of Civil and Environmental Engineering, University of Strathclyde, Glasgow

E-mail: Andrea.Hamilton@strath.ac.uk

Keywords: Cement, Hydroxyapatite, Biomineralisation, Bioceramics, Medical Implant Materials, Architectural Preservation, Nuclear Waste Disposal, Environmental Remediation

Abstract

Ordinary Portland Cement (OPC) is by weight the world's most produced man-made material, and consequently is used in a variety of applications in environments ranging from buildings, to nuclear wasteforms, and within the human body. In this paper, we present for the first time the direct deposition of biogenic hydroxyapatite onto the surface of OPC, in a synergistic process which relies upon the unique properties of the cement substrate. The synthesised hydroxyapatite is very similar to that found in nature; having a crystallite size, iron and carbonate substitution, and a semi-crystalline structure which identify that this biogenic hydroxyapatite is akin to that found in natural bone and tooth enamel. Hydroxyapatites with such a structure are known to be mechanically stronger and more biocompatible than synthetic or biomimetic hydroxyapatites. The formation of this biogenic hydroxyapatite coating therefore has significance in a range of contexts. In medicine, hydroxyapatite coatings are linked to improved biocompatibility of ceramic implant materials. In the built environment, hydroxyapatite

coatings have been proposed for the consolidation and protection of sculptural materials such as marble and limestone, with biogenic hydroxyapatites having reduced solubility in comparison with synthetic apatites. Hydroxyapatites have also been established as effective for the adsorption and remediation of environmental contaminants such as radionuclides and metals. We further identify that in addition to providing a biofilm scaffold for nucleation, the metabolic activity of *Pseudomonas fluorescens* increases the pH of the growth medium to a suitable level for hydroxyapatite formation. The generated ammonia reacts with phosphate in the growth medium, producing ammonium phosphates, which are a precursor to the formation of hydroxyapatite under conditions of ambient temperature and pressure. Subsequently, this biogenic deposition process takes place in a simple reaction system under mild chemical conditions, which are cheap and easy to apply to fragile biological or architectural surfaces.

1 Introduction

Hydroxyapatite (HAP) is a calcium phosphate mineral with the general chemical formula $Ca_{10}(PO_4)_6(OH)_2$.[1] HAP is an example of a 'bioceramic',[2] a novel class of materials with potential applications ranging from bone implants,[3] to drug delivery.[4] Hydroxyapatite coatings have been used to reinforce bone cements, enhancing load-bearing capacity,[5] and promoting proliferation and differentiation of human osteoblast-like cells.[6,7] In addition, there is an emerging interest in the use of hydroxyapatite coatings for the consolidation and preservation of marble and limestone buildings and sculptures.[8–12]

OPC is among the most utilised materials in society. Cement and concrete have been commonly used building materials throughout the 20th Century and there is significant interest in repairing concrete structures to reduce the amount of cement consumed worldwide. Cement is also used as a encapsulant for radioactive waste storage and the use of hydroxyapatites for the remediation of radionuclide[13,14] and heavy metal[15] contaminants from the environment has been a subject of recent research interest.

The crystal structure of HAP is too complex to be accurately mimicked by synthetic crystalline apatites, and the use of these synthetic apatites has been observed to result in poor adhesion and low mechanical strength of dental treatments,[16] as well as reduced radionuclide sorption capacity.[13] Hydroxyapatite produced through the direct actions of a living organism - termed 'biogenic' hydroxyapatites - may offer a solution to these limitations, through properties such as reduced solublity, and particle sizes comparable to those found in natural hydroxyapatites.[16–18]

Here we identify and elucidate a new method for deposition of a biogenic hydroxyapatite onto the surface of OPC; using the Gram negative bacterium *Pseudomonas fluorescens*. Unlike existing techniques, this method does not require the addition of an external calcium source and uses a simple bioreactor design with a common environmental microorganism. Importantly it is achieved using few reagents, requiring only *Pseudomonas fluorescens*, LB broth, and a phosphate pH buffer. Unlike synthetically grown HAP[16,19] and biomimetic HAPs,[20] this phase is easily formed at room temperature and pressure, making it applicable to the building industry and relatively economical.

The location, crystal structure, chemistry and morphology of the hydroxyapatite produced on OPC are investigated using XRD, FT-IR, and SEM-EDX. We identify that this biogenic hydroxyapatite has similarity to natural hydroxyapatites; which is of relevance to a range of applications, particularly nuclear waste disposal, medical implant materials, and architectural preservation. We additionally identify and describe for the first time the bacterially mediated biochemical mechanism behind this deposition process, which relies upon the metabolic generation of ammonium phosphate minerals.

2 Methods

2.1 OPC Sample Preparation

OPC Powder 'Multicem 32,5R (CEM-II/A-LL)' (Hanson Heidelberg) was hydrated with 200g water per 500g OPC powder (water:cement ratio = 0.4). The paste was mixed for 15 minutes using a Rotary Mixer on a low speed setting. The paste was then poured into silicone moulds and stored at 100 %relative humidity and 20°C for 24 hours. Samples were removed and cured in a saturated solution of $Ca(OH)_2$ ($1.5gL^{-1}$) for 28 days at 20°C. The cement coupons were stored in this solution at 20°C until required.

2.2 Biofilm Growth on Cured OPC Coupons

Growth medium was prepared from $20gL^{-1}$ LB Broth (Sigma-Aldrich), $9.4gL^{-1}$ KH_2PO_4 (Sigma-Aldrich), $2.2gL^{-1}$ K_2HPO_4 (Fluka), dissolved in deionised water in a 2L Duran flask, The flask was heated on a magnetic stirrer plate at 70°C to dissolve all components. Then100 ml volumes were decanted into Erlenmeyer flasks which were sealed with non-absorbent cotton wool bungs (Cowens Ltd) and autoclaved. OPC samples were rinsed thoroughly in DI water, and aseptically transferred into thel Erlenmeyer flasks (1 coupon per flask). The inoculum of *P. fluorescens* strain SBW25 was grown overnight at ambient temperature with continual shaking, in 100ml LB broth to an OD600 = 0.1. Test flasks were inoculated with 100uL of this overnight culture. Control flasks were not inoculated. All flasks were incubated at ambient temperature on a shaking tray, inside a fume hood for 20 days. Control and test samples were aseptically retrieved from the flasks after 20 days and rinsed thoroughly in DI water to remove any biofilm material, then vacuum packed to minimise cement carbonation prior to analysis. To determine if contaminating bacteria were present on the control samples, and verify that *Pseudomonas* was growing successfully on test samples, scrapings from the surface were taken, homogenised via sonication, inoculated onto Tryptone Soya Agar plates (Oxoid), and incubated for 4 days at 20°C. No contamination was observed on the control

samples, and *Pseudomonas* growth was apparent on all test samples.

2.3 Examination of Ammonium Phosphate Mineral Formation

Growth medium was prepared as described above, but with the addition of $15gL^{-1}$ agar (Sigma-Aldrich) prior to autoclaving. The medium was then aseptically dispensed into Petri dishes, cooled, and stored overnight at room temperature. The following day, 3x plates were streak-inoculated with *P. fluorescens* culture overnight. 3x plates were kept as non-inoculated controls. All plates were then incubated at 20°C for 12 days and pH was measured. After a 6 day incubation period, the plates were imaged and a fine opaque crystalline precipitate was observed within the bacterial colonies when viewed with an optical microscope (Nikon Eclipse LV100IVD) using a 10x objective lens and reflected light. There was no bacterial growth or precipitate observed on the control plates. After a 12 day incubation period large crystal precipitates were observed, associated with the bacterial colonies on the test plates. The crystals were imaged under a 10x objective lens, using cross-polarised light microscopy in incident mode. No bacterial growth or crystal precipitates were observed on the control plates.

2.4 SEM-EDS Analysis

Polished thin cross-sections of the cement samples were made by resin impregnation followed by grinding and polishing the sample to a final thickness of 30 μm . For analysis sections were gold coated and imaged using an S-3700 SEM (Hitachi) fitted with an 80mm X-Max detector (Oxford Instruments) for EDS analysis. All SEM Images and EDS Maps were gathered at a 10mm working distance and 15.0kV accelerating voltage.. SEM images without EDS analysis were collected using an SU6600 SEM (Hitachi) and all images were processed using ImageJ.[21]

2.5 X-ray Diffraction (XRD) analysis

XRD patterns were collected through the body of intact samples and smears from bacterial colonies grown on agar plates using an X-ray Diffractometer (Bruker D8 Advance). Patterns were collected in the 2theta scan range 6-60° using a step size of 0.02°, and a scan speed of 0.5 seconds/step. A Cu shutter tube generating X-rays with a wavelength of 1.5418 Angstrom (0.15418nm) was used with a 0.6mm X-ray slit. Samples were continually rotated during pattern collection. XRD data was processed using DiFFRAC EVA software (Bruker) and compared with mineral phases from the ICSD (Inorganic Crystal Structure Database) An estimate of hydroxyapatite crystallite size was calculated using Scherrer's equation,[22] based on the full width at half maximum (FWHM) of the (002) reflection at 26° 2theta.

2.6 X-ray Fluorescence (XRF) Analysis

All samples were ground into a fine powder prior to analysis. XRF analysis of OPC powder and fully cured hydrated OPC paste powders was carried out using a Bruker S4 Explorer instrument.

2.7 FT-IR Analysis

IR spectra were recorded using a Bruker Vertex 70 Fourier Transform Infrared Spectrometer. Representative portions of the sample surface were transferred on to the sample area of a single reflection diamond attenuated total reflectance (DATR) accessory, fitted with a KRS-5 substrate.

2.8 Confocal Microscopy of Biofilms

Biofilm-coated OPC samples were removed from the incubation flasks and rinsed in a 1x concentration phosphate buffered saline (PBS) solution. The samples were then transferred into a 50ml staining bottle containing 0.1 % w/v acridine orange (Alfa-Aesar) in 1x PBS

solution. The biofilms were stained for 5 minutes, removed from the solution, and then examined using a confocal microscope (Leica SP5 II). A laser excitation wavelength of 458nm was used to excite the fluorescent stain, and a photon multiplier tube with an emission collection wavelength of 475-550nm was used to collect the image data from the sample. Images were obtained using a 40x dry objective lenses and confocal maps were collected using 100 frames per optical section.

3 Results and discussion

3.1 Characterisation of Calcium Phosphates on OPC Samples

OPC samples were incubated in phosphate-buffered LB broth (initial pH 6.2) with (test) and without (control) *P. fluorescens* inoculum for 20 days and then analysed using SEM-EDS, XRD and FT-IR.

Calcium phosphate mineralisation occurred on the surface of all OPC samples incubated in the medium, regardless of the presence of *P. fluorescens*. SEM-EDS analyses clearly demonstrate the presence of a calcium phosphate layer on the surface of the test sample, which was not observed on the un-treated OPC control (Fig 1).

However, XRD (Fig 2) and FT-IR (Fig 3) analysis showed that the phosphate layer deposited on the control sample was brushite (Fig 2A), a highly crystalline calcium phosphate mineral with the formula $CaHPO_4.2H_2O$. This could be expected, as the pH of the control solution was 7.4, which is too low to precipitate hydroxyapatite.[23] However, on samples incubated with *Pseudomonas*, biofilm growth was evident and associated with the formation of a hydroxyapatite layer on the OPC surface (Figs 1A, 2B, 3), forming below the biofilm. The location of the phosphate layer presents opportunities for generating hydroxyapatite coated cements, which could overcome the limited mechanical performance, such as low fracture toughness of synthetic calcium-phosphate based ceramics.[24,25]

The broad X-ray diffraction reflections in the XRD spectrum (Fig 2B) indicate that

the bacterially deposited hydroxyapatite is a poorly crystalline material, particularly when compared to the sharp reflections from brushite (Fig 4) observed on the control samples. Biogenic hydroxyapatite typically consists of poorly crystalline carbonated hydroxyapatite.[26,27] In contrast, non-biologically generated calcium phosphate minerals typically present higher crystallinity.[20] Further comparisons of our hydroxyapatite with a carbonate substituted hydroxyapatite (ICSD-289992) and a synthetic hydroxyapatite (ICSD-203027) identifies that the hydroxyapatite generated by *Pseudomonas fluorescens* appears most similar to the carbonated hydroxyapatite (Supplementary Fig 1, 2).

Biological hydroxyapatites have been observed to incorporate different ions into their crystal structures.[27] The FT-IR spectrum of the bacterially deposited hydroxyapatite (Fig 3B) displays peaks at 1456, 1415, and 874 cm^{-1}. These peaks indicate the presence of carbonate ions $(CO_3)^{-2}$, partially replacing $(PO_4)^{-3}$ sites in the hydroxyapatite crystal structure.[27] This creates an inherent disorder when compared with synthetic hydroxyapatites, which have higher crystallinity.[20] Carbonate substitution of phosphate groups is a common characteristic of other biogenic hydroxyapatite crystals described in the literature.[20] Additionally, the XRD pattern of the hydroxyapatite produced matches to that of 289992-ICSD - a calculated structure for a carbonate-substituted hydroxyapatite (Supplementary Fig 1).[28] These observations indicate that this bacterial hydroxyapatite is comparable to natural hydroxyapatites found in bone and dental enamels, in terms of both ionic substitution and crystal structure.

The hydroxyapatite layer was observed to consist of a granular assembly of individual nanoscale particles, with size ranging from 30-100nm (Fig 3A). The observed morphology is consistent with nano-hydroxyapatite morphologies reported in the literature.[16,29]

Application of Scherrer's equation to the (002) reflection of the biogenic hydroxyapatite XRD patterns determined the crystallite size to be approximately 30nm (Fig 2B). This is similar to the particle size of natural hydroxyapatite found in teeth[24] and corresponds well to literature values for biologically generated hydroxyapatites made using this same methodology; sizes typically ranging from 20-40nm.[22,30]

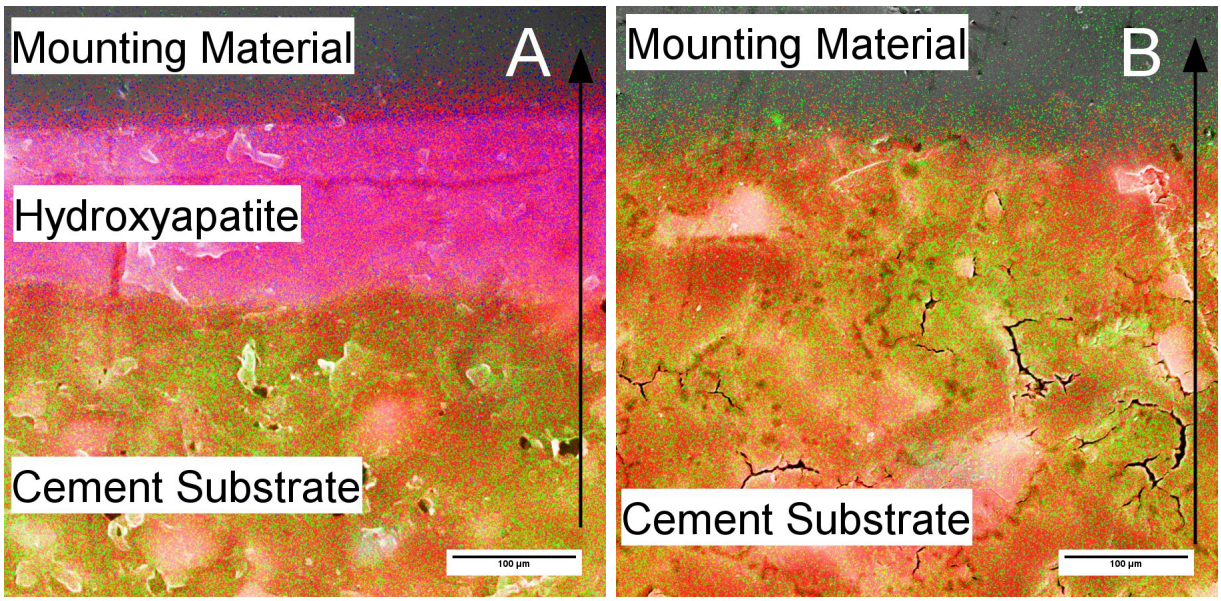

Figure 1: A) SEM-EDS map of the test OPC sample cross section. Image illustrates the interface at the top surface of the sample against the mounting material. The SEM-EDS map shows distribution of calcium (Red), silicon (Green) and phosphorus (Blue) through the sample cross-section. A calcium phosphate layer (Magenta) is clearly visible at the interface between the cement and the sample mounting material, representing the 'top' surface where the biofilm has been active. B) SEM-EDS Map of unmodified OPC sample cross-section cured for 28 days with no further modification. Image illustrates the interface at the top surface of the sample against the mounting material. The SEM-EDS map of calcium (Red) and silicon (Green) distribution in the sample is shown. No phosphorus was detected during EDS mapping of the control sample. The direction of the black arrows indicate the 'top' of the sample cross-section.

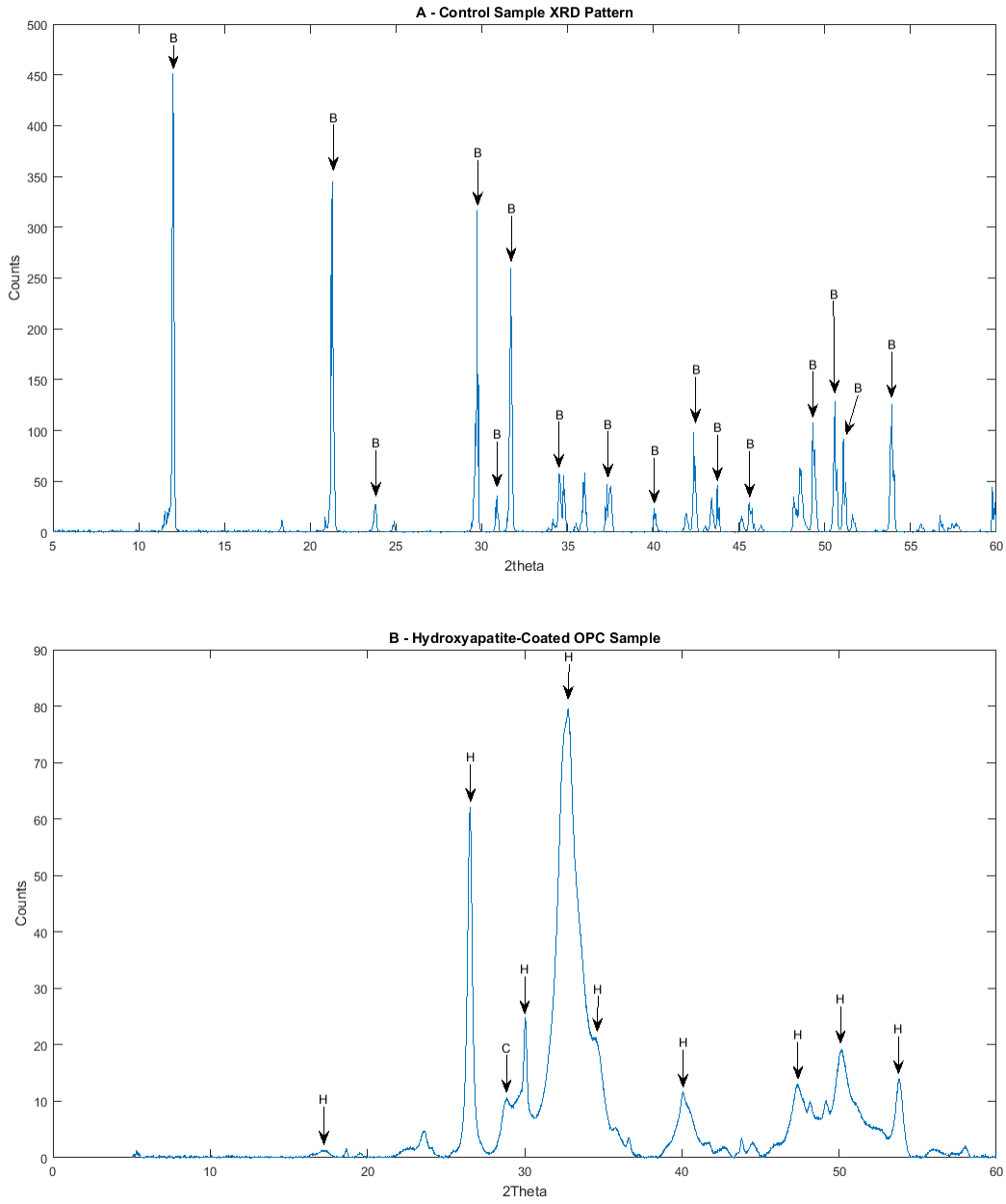

Figure 2: A) XRD pattern of control OPC sample. The pattern was matched to PDF 00-009-0077 (Brushite) as annotated (B). B) XRD pattern of *Pseudomonas*-treated OPC sample. Reflections were matched to 289992-ICSD (hydroxyapatite) as annotated (H). A calcite peak (C) is also annotated on the test coupon, which was matched to 250-ICSD (PDF 01-070-0095). The (002) reflection can be observed at c. 26° 2theta. The size of the hydroxyapatite crystallites based on the (002) reflection FWHM was calculated as c. 30nm using Scherrer's equation.

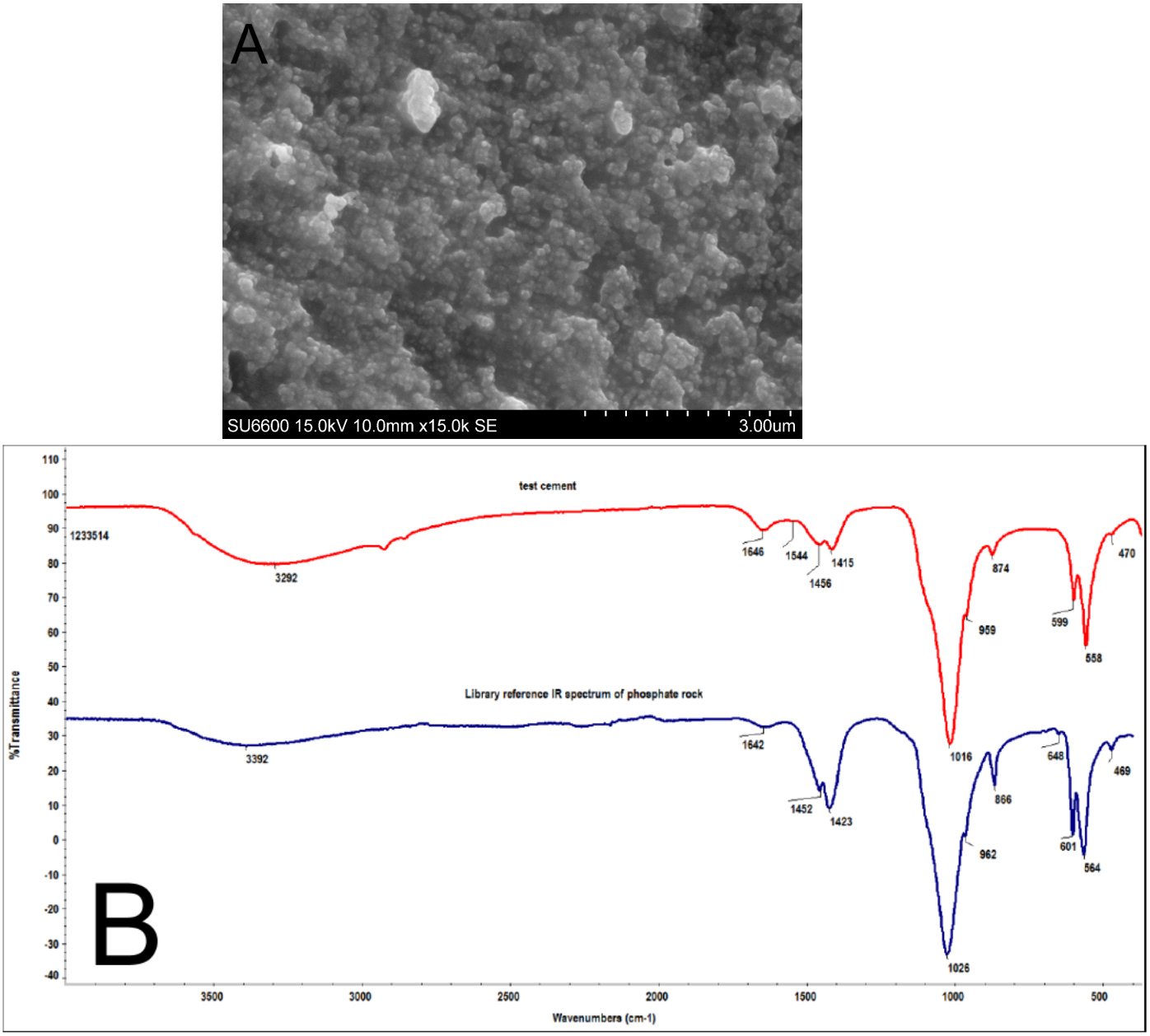

Figure 3: A) SEM micrograph of hydroxyapatite layer deposited onto the OPC substrate. Image is of a polished cross-section of the hydroxyapatite layer. The hydroxyapatite presents a relatively coarse morphology, consisting of an assembly of nanoscale particles. Individual particle sizes are 30-100nm. B) The IR spectrum of surface material from the same sample, which indicated that it consisted primarily of a phosphate, with a structure similar to hydroxyapatite (formula, $Ca_{10}(PO_4)_6OH_2$) and some $CaCO_3$. It showed strong similarities to a reference IR spectrum of a phosphate rock which contains hydroxyapatite

3.2 Interactions between *Pseudomonas fluorescens*, OPC, and Hydroxyapatite

*Pseudomonas*and other bacteria are capable of producing nano-hydroxyapatite with physical properties very similar to natural bone material.[31] Research on the bacterial generation of hydroxyapatite has generally required immobilisation of the bacteria on a matrix, such as sol-gels or alginate beads, prior to mineral formation;[31] and the addition of a specific calcium source to stimulate hydroxyapatite production.[32]

It is significant that these steps are not necessary when bio-hydroxyapatite is generated on an OPC substrate material, as shown in this study. OPC has several properties which may have contributed to this. The OPC block provides a fixed substrate for hydroxyapatite deposition; negating the requirement for a sol-gel or similar matrix. In previous studies, calcium phosphate loading was found to be necessary when generating bio-hydroxyapatite on polyurethane or titanium,[31] and the addition of calcium and phosphorus donors was also necessary when using sol-gel or alginate substrates.[32] In the case of OPC, calcium is present in sufficient quantities (Table 1) both on the OPC surface and in the surrounding solution.

A pH of 7.4 or higher is necessary for the chemical synthesis of hydroxyapatite.[23] For chemical deposition of biomimetic hydroxyapatite, pH values ranging from 7.3-11.5 are typical,[19,22,33–35] and the presence of calcium and phosphate precursors is necessary. Previous studies of biogenic hydroxyapatite production involve multi-step processes and use a controlled rise in pH.[31,32] In this work, a rise in pH was observed in both the control and test systems, compared to the initial pH of the LB broth (Table 2), despite the presence of the phosphate pH buffer. This rise in pH is due to $Ca(OH)_2$ leaching from the cement. In the control system, the pH rise was limited to pH 7.4 (from an initial pH of pH 6.2); in the absence of higher pH, brushite was formed rather than hydroxyapatite. However, in the systems containing *P. fluorescens*, the increase was much greater, rising to pH 9.1. In the course of this work, we identified that attempting to grow *P. fluorescens* in this batch reaction system with no pH buffering capacity was not possible, due to an almost immediate

rise in growth medium pH to 12.5 which inhibits *P. fluorescens* growth.

P. fluorescens is a non-lactose fermenting microorganism. Consequently, in a growth medium such as LB broth which contains amino acids as the carbon and nitrogen sources, *P. fluorescens* will secrete ammonia, amines, and amides as by-products from the metabolic breakdown of amino acids.[36]The secretion of these metabolic products accounts for the pH increase observed in the medium, which was greater than that caused by OPC alone (Table 2). The generation of an alkaline micro-environment around the bacterial cell is a well characterised process which occurs during the initial stages of calcite biomineralisation, with oxidative deamination of amino acids and the resulting increase in pH associated with calcium carbonate precipitation.[37,38]

The metabolic generation of ammonia by *Pseudomonas* can be expected to instigate a similar reaction to that which occurs during the generation of urolithiasis-associated struvite, calcite, and hydroxyapatite crystals by non-lactose fermenting microorganisms such as *Pseudomonas*, *Staphylococcus*, *Klebsiella*, and *Proteus*.[39–42] The reaction mechanism behind the bacterial production of struvite has also been linked to the generation of hydroxyapatite under conditions of increased calcium concentration such as the use of calcium acetate by Sanchez-Roman *et al*, (2007)[39] but a cement substrate has never been used before in this context.

The reaction produces ammonium phosphates, via the bacterial generation of ammonia in a reaction system containing phosphates.[43] Ammonium phosphates are used as chemical precursors to hydroxyapatite, and have been used as such for the consolidation of limestones.[44–46]Hydroxyapatite does not form when OPC is placed in buffered LB broth without *Pseudomonas* (Fig 1B). We propose that in our system, *P. fluorescens* breaks down amino acids, and in doing so raises the pH and generates ammonia, leading to the formation of ammonium phosphate precursors for hydroxyapatite formation. We have identified that *Pseudomonas fluorescens* will generate ammonium phosphate minerals when grown in buffered LB medium (Fig 4), using a combination of optical microscopy and XRD analysis. It has

been noted that hydroxyapatite production using carbonate and ammonium phosphate precursors occurs at room temperature and pressure,[45] which is in agreement with the findings of this work; and supports this proposed chemical mechanism underlying hydroxyapatite production by *Pseudomonas*. The synergistic interactions between bacterial metabolism, the growth medium, and the OPC substrate which lead to hydroxyapatite biomineralisation are summarised in Figure 5.

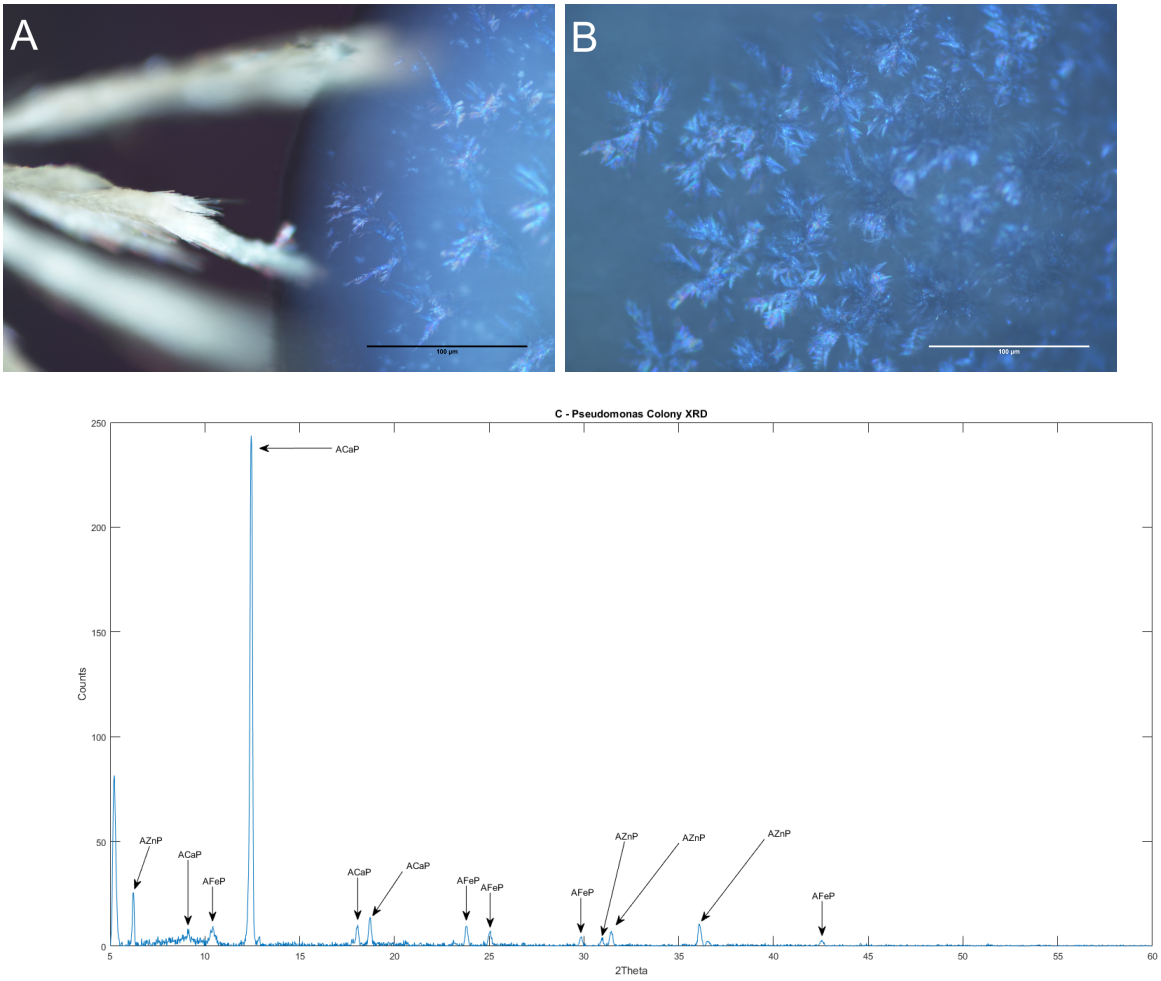

Figure 4: A) Cross-polarised transmitted light microscopy image of ammonium phosphate crystals precipitated into buffered LB agar by *P. fluorescens*. The image shows the edge of a single *P. fluorescens* colony (right hand side) on an agar plate. Precipitation can be observed both within the colony itself, and projecting from the surface of the colony as dendrites. B) Cross-polarised transmitted light microscopy image of ammonium phosphate crystals precipitated into buffered LB agar. The image shows the central portion of single *P. fluorescens* colony on an agar plate. Crystalline precipitates are observed to be dispersed as dendritic crystals throughout the bacterial colony. C) XRD patterns collected from extracted crystalline material after 12 days of incubation. Peaks annotated 'ACaP' were matched to PDF 00-035-0226 (ammonium calcium phosphate hydrate). Peaks annotated 'AFeP' were matched to PDF 00-031-0053 (ammonium iron phosphate hydrate). Peaks annotated 'AZnP' were matched to PDF 00-020-1429 (ammonium zinc phosphate hydrate).

It has been observed that bacteria control the process of bio-mineralisation, facilitating nucleation and growth of the mineral particles.[47] This is perhaps best characterised in the bio-mineralisation of calcium carbonate,[38,47,48] as well as magnetite deposition by the

magnetotactic bacteria, and silica deposition by diatoms.[49] The EPS skeleton generated by bacteria has been used as a nucleation point for the crystallisation of hydroxyapatite on titanium and foam substrates.[32] In this context, the mechanism for this deposition process has been observed to use the cohesive, tightly adherent biofilm generated by the bacterium Serratia, which acts as a scaffold for the enzymatically mediated nucleation of calcium phosphate minerals.[32] The biofilm matrix produces a confined 'reaction space' which prevents agglomeration of the nanocrystals, aiding the generation of nanoscale hydroxyapatite particles.[32] We observed that *P. fluorescens* generates a biofilm scaffold (Fig 6) which may support the nucleation process.

In the built environment, hydroxyapatite coatings can be expected to reduce the dissolution of calcites in limestone and marble;[45] however this protection has been observed to be less than anticipated.[8] This has been partially attributed to the high thickness of the HAP films being prone to cracking, as well as layer porosity.[8] Limestone is also a significant component of the OPC material (CEM-II/A-LL) used in this study, consisting of 6-20 % of the OPC mass.[50]XRF analysis of our cement finds a CaO weight % of 66% (Table 1), literature values of CaO content marbles and limestones are relatively close to this value, with measurements of approximately 55% appearing typical.[51,52] As such, we would suggest that limestone and marble are likely to be suitable alternative substrate materials for the deposition process described in this work.

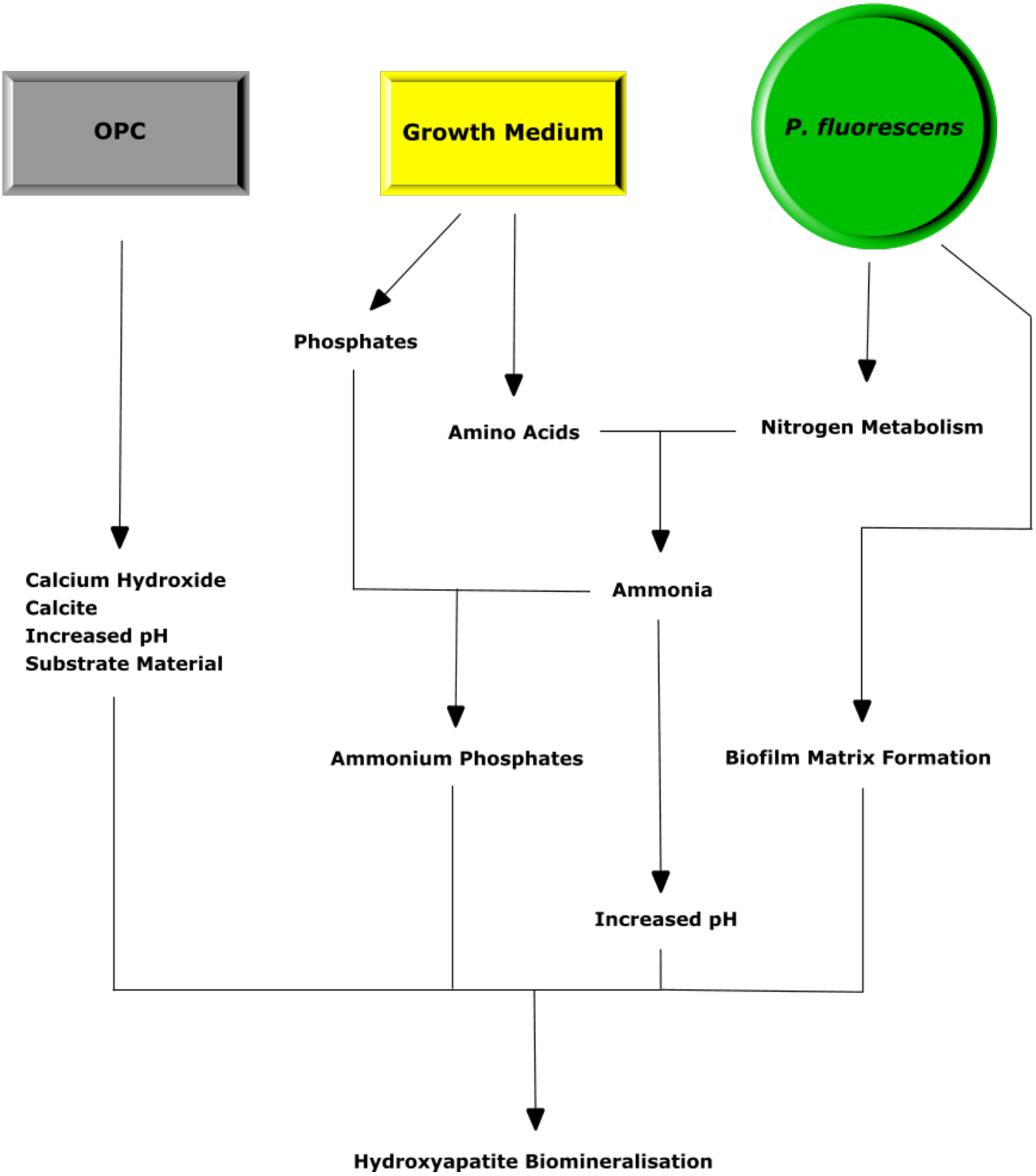

Figure 5: A flow chart illustrating the synergistic interactions between components in the reaction system, which produces hydroxyapatite biomineralisation on the surface of the OPC substrate.

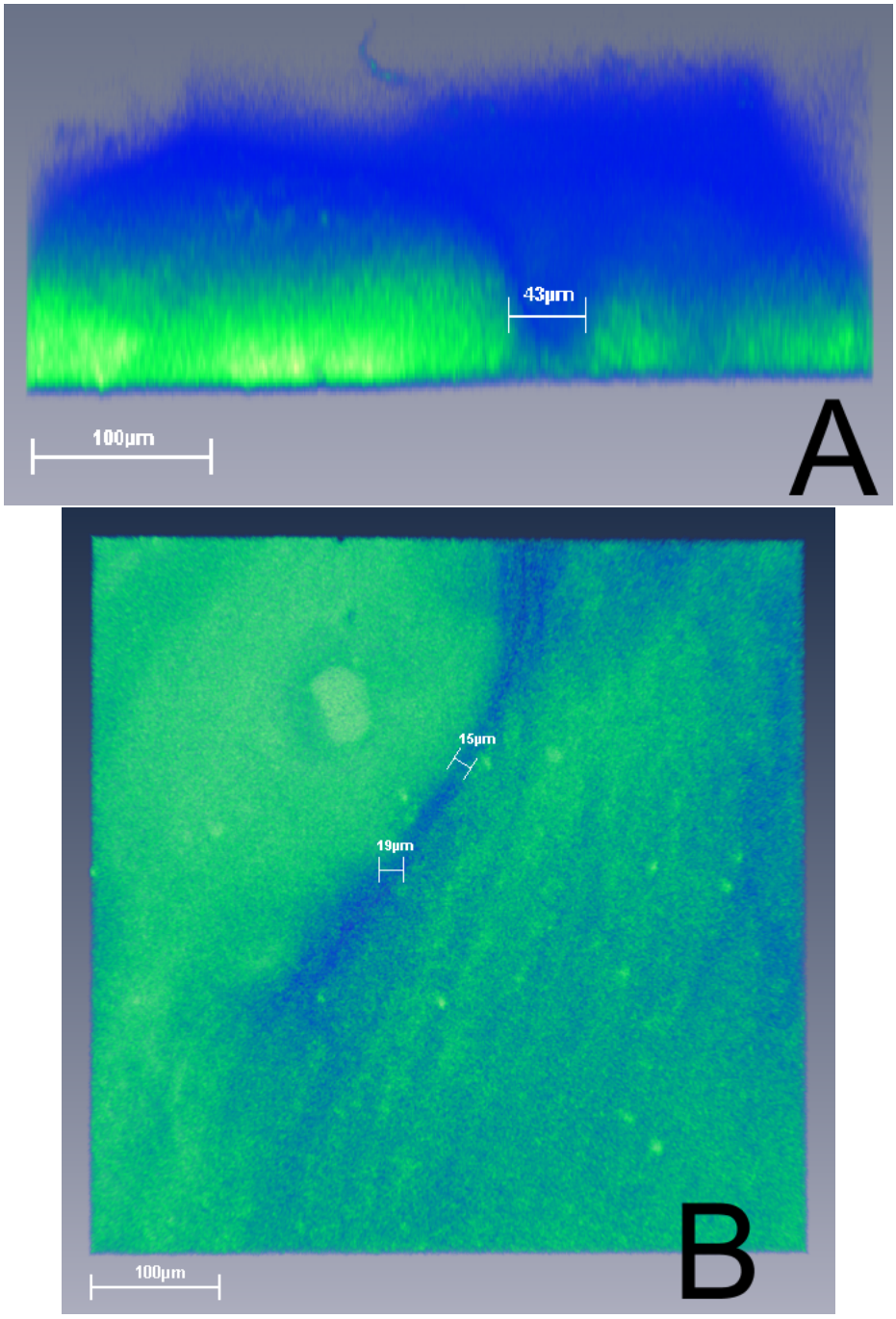

Figure 6: Confocal microscopy images of a *P. fluorescens* biofilm on the surface of an OPC coupon. The image shows A) XZ and B) XY projections of the biofilm. A 'channel' of lower biofilm density can be observed, measuring approximately 43μm (annotated) across at the 'entry' point as observed on the XZ projection and narrowing to breadths of approximately 15-19μm (annotated) further into the 'channel' as observed in the XY projection. Blue represents areas of lower biofilm signal intensity, green represents areas of higher biofilm signal intensity; the highest signal intensity areas are shown in Yellow.

4 Tables

4.1 XRF Table

Table 1: XRF Analysis

Analyte	Chemical Form	Dry OPC Powder[1]	Hydrated OPC Paste[1]
Calcium	CaO	72.05	66.15
Silica	SiO_2	21.76	21.08
Alumina	Al_2O_3	5.1	4.67
Iron	Fe_2O_3	3.34	3.17
Magnesium	MgO	2.17	1.72
Titanium	TiO_2	0.21	0.2
Sodium	Na_2O	0.33	0.09
Potassium	K_2O	0.87	0.13
Phosphorus	P_2O_5	0.11	0.09
Zinc	ZnO	0.12	0.12
Sulfur Trioxide	SO_3	3.38	2.29
Sulfur	S	1.35	0.92

[1] All values are weight%

4.2 pH Table

Table 2: pH Measurements

Sample	pH[2]
Test	9.065±0.027
Control	7.445±0.201
Buffered LB (No OPC)	6.204±0.007

[2] All values are mean of n=3 ± standard error of the mean

5 Conclusions

We have demonstrated for the first time that a biogenic hydroxyapatite can be directly biomineralised onto the surface of Ordinary Portland Cement, and described the biochemical mechanisms behind this deposition process. Both XRD and FT-IR analysis illustrate that the disorder, carbonation, crystal structure, and crystallite size of this deposited hydroxyapatite are similar to natural apatite materials; with associated advantages over synthetic apatites

which have been described elsewhere.[13,16–18] The direct biomineralisation of hydroxyapatite on OPC has never been reported before; and as such the biochemical mechanisms underlying this unique synergistic process have not been investigated or described in the literature to date.

The described method presents a rapid, simple, and cheap method of promoting in-situ biomineralisation of hydroxyapatite onto the OPC substrate, with associated advantages arising from the formation of this biogenic hydroxyapatite in comparison with more widely studied biomimetic hydroxyapatites. Significantly, we have observed that the bacterium *Pseudomonas fluorescens* will produce this biogenic hydroxyapatite under mild reaction conditions within a relatively simple reaction system, in a synergistic process which uses the chemical and physical properties of a Portland cement substrate material. We suggest that OPC has properties which make it a favourable substrate for bacterial hydroxyapatite deposition, namely the presence of accessible calcium,[39] which in combination with the pH rise and ammonia production arising from microbial metabolic processes, favours hydroxyapatite formation.[23] There is significant potential to investigate this deposition process on other calcium-rich substrate materials, such as marbles and limestones.

Acknowledgement

The authors gratefully acknowledge the Engineering and Physical Sciences Research Council (EPSRC) for funding the research as a Doctoral Training Partnership. Thanks to Gerry Johnston, Fiona Sillars, and Tiziana Marrocco of the University of Strathclyde AMRL for assistance with SEM-EDX and XRD data collection; and thanks to Gillian Robb and Graeme MacKenzie of the University of Strathclyde Centre for Biophotonics for assistance with confocal microscopy.

References

(1) Elliott, J. C. *Structure and Chemistry of the Apatites and Other Calcium Orthophosphates*; Elsevier Science, 1994; pp 1–389.

(2) Lin, K.; Xia, L.; Gan, J.; Zhang, Z.; Chen, H.; Jiang, X.; Chang, J. Tailoring the nanostructured surfaces of hydroxyapatite bioceramics to promote protein adsorption, osteoblast growth, and osteogenic differentiation. *ACS Appl. Mater. Interfaces* **2013**, *5*, 8008–8017.

(3) Mistry, S.; Kundu, D.; Datta, S.; Basu, D. Comparison of bioactive glass coated and hydroxyapatite coated titanium dental implants in the human jaw bone. *Aust. Dent. J.* **2011**, *56*, 68–75.

(4) Sarath Chandra, V.; Baskar, G.; Suganthi, R. V.; Elayaraja, K.; Ahymah Joshy, M. I.; Sofi Beaula, W.; Mythili, R.; Venkatraman, G.; Narayana Kalkura, S. Blood compatibility of iron-doped nanosize hydroxyapatite and its drug release. *ACS Appl. Mater. Interfaces* **2012**, *4*, 1200–1210.

(5) Moursi, A. M.; Winnard, A. V.; Winnard, P. L.; Lannutti, J. J.; Seghi, R. R. Enhanced osteoblast response to a polymethylmethacrylate-hydroxyapatite composite. *Biomaterials* **2002**, *23*, 133–144.

(6) Dalby, M. J.; Di Silvio, L.; Harper, E. J.; Bonfield, W. Increasing hydroxyapatite incorporation into poly(methylmethacrylate) cement increases osteoblast adhesion and response. *Biomaterials* **2002**, *23*, 569–576.

(7) Dalby, M. J.; Di Silvio, L.; Harper, E. J.; Bonfield, W. Initial interaction of osteoblasts with the surface of a hydroxyapatite-poly(methylmethacrylate) cement. *Biomaterials* **2001**, *22*, 1739–1747.

(8) Graziani, G.; Sassoni, E.; Franzoni, E.; Scherer, G. W. Hydroxyapatite coatings for marble protection: Optimization of calcite covering and acid resistance. *Appl. Surf. Sci.* **2016**, *368*, 241–257.

(9) Sassoni, E.; Graziani, G.; Franzoni, E. An innovative phosphate-based consolidant for limestone. Part 2: Durability in comparison with ethyl silicate. *Constr. Build. Mater.* **2016**, *102*, 931–942.

(10) Franzoni, E.; Sassoni, E.; Graziani, G. Brushing, poultice or immersion? The role of the application technique on the performance of a novel hydroxyapatite-based consolidating treatment for limestone. *Journal of Cultural Heritage* **2015**, *16*, 173–184.

(11) Yang, F.; Liu, Y. Artificial hydroxyapatite film for the conservation of outdoor marble artworks. *Mater. Lett.* **2014**, *124*, 201–203.

(12) Sassoni, E.; Graziani, G.; Franzoni, E. An innovative phosphate-based consolidant for limestone. Part 1: Effectiveness and compatibility in comparison with ethyl silicate. *Constr. Build. Mater.* **2016**, *102*, 918–930.

(13) Handley-Sidhu, S.; Renshaw, J. C.; Moriyama, S.; Stolpe, B.; Mennan, C.; Bagheri-asl, S.; Yong, P.; Stamboulis, A.; Paterson-Beedle, M.; Sasaki, K.; Pattrick, R. A. D.; Lead, J. R.; MacAskie, L. E. Uptake of Sr 2+ and Co 2+ into biogenic hydroxyapatite: Implications for biomineral ion exchange synthesis. *Environ. Sci. Technol.* **2011**, *45*, 6985–6990.

(14) Sasaki, K.; Goto, T. Immobilization of Sr2+ on naturally derived hydroxyapatite by calcination of different species of fish bones and influence of calcination on ion-exchange efficiency. *Ceram. Int.* **2014**, *40*, 11649–11656.

(15) Chen, X.; Wright, J. V.; Conca, J. L.; Peurrung, L. M. Evaluation of Heavy Metal Remediation Using Mineral Apatite. *Water, Air, Soil Pollut.* **2000**, *98*, 57–78.

(16) Li, L.; Pan, H.; Tao, J.; Xu, X.; Mao, C.; Gu, X.; Tang, R. Repair of enamel by using hydroxyapatite nanoparticles as the building blocks. *J. Mater. Chem.* **2008**, *18*, 4079.

(17) Sadat-Shojai, M.; Khorasani, M. T.; Dinpanah-Khoshdargi, E.; Jamshidi, A. Synthesis methods for nanosized hydroxyapatite with diverse structures. *Acta Biomater.* **2013**, *9*, 7591–7621.

(18) Pinchuk, N.; Parkhomey, O.; Sych, O. In Vitro Investigation of Bioactive Glass-Ceramic Composites Based on Biogenic Hydroxyapatite or Synthetic Calcium Phosphates. *Nanoscale Res. Lett.* **2017**, *12*, 111.

(19) Rusu, V. M.; Ng, C. H.; Wilke, M.; Tiersch, B.; Fratzl, P.; Peter, M. G. Size-controlled hydroxyapatite nanoparticles as self-organized organic-inorganic composite materials. *Biomaterials* **2005**, *26*, 5414–5426.

(20) Liu, Q.; Huang, S.; Matinlinna, J. P.; Chen, Z.; Pan, H. Insight into biological apatite: physiochemical properties and preparation approaches. *BioMed Res. Int.* **2013**, *2013*.

(21) Abràmoff, M. D.; Magalhães, P. J.; Ram, S. J. Image processing with imageJ. *Biophotonics International* **2004**, *11*, 36–41.

(22) Müller, L.; Conforto, E.; Caillard, D.; Müller, F. A. Biomimetic apatite coatings-Carbonate substitution and preferred growth orientation. *Biomol. Eng.* **2007**, *24*, 462–466.

(23) Eiden-Aßmann, S.; Viertelhaus, M.; Heiß, A.; Hoetzer, K. A.; Felsche, J. The influence of amino acids on the biomineralization of hydroxyapatite in gelatin. *J. Inorg. Biochem.* **2002**, *91*, 481–486.

(24) Kalita, S. J.; Bhardwaj, A.; Bhatt, H. A. Nanocrystalline calcium phosphate ceramics in biomedical engineering. *Mater. Sci. Eng., C* **2007**, *27*, 441–449.

(25) Tanner, K. Small but extremely tough. *Science* **2012**, *336*, 1237–1238.

(26) Beniash, E. Biominerals- hierarchical nanocomposites : the example of bone. *Wiley Interdiscip. Rev.: Nanomed. Nanobiotechnol.* **2011**, *3*, 47–69.

(27) Fleet, M. E. *Carbonated Hydroxyapatite: Materials, Synthesis, and Applications*; Pan Stanford Publishing, 2014.

(28) Ulian, G.; Valdrè, G.; Corno, M.; Ugliengo, P. Periodic ab initio bulk investigation of hydroxylapatite and type a carbonated apatite with both pseudopotential and all-electron basis sets for calcium atoms. *Am. Mineral.* **2013**, *98*, 410–416.

(29) Huang, S. B.; Gao, S. S.; Yu, H. Y. Effect of nano-hydroxyapatite concentration on remineralization of initial enamel lesion in vitro. *Biomed. Mater.* **2009**, *4*, 1–6.

(30) da Cunha, M. R.; Menezes, F. A.; dos Santos, G. R.; Pinto, C. A. L.; Barraviera, B.; Martins, V. d. C. A.; Plepis, A. M. d. G.; Ferreira Junior, R. S. Hydroxyapatite and a New Fibrin Sealant Derived from Snake Venom as Scaffold to Treatment of Cranial Defects in Rats. *Mater. Res. (Sao Carlos, Braz.)* **2015**, *18*, 196–203.

(31) Khanafari, A.; Akbari, T.; Sohrabi, M. R. Comparison of nano-hydroxyapatite productivity by Pseudomonas aeruginosa and Serratia marcescense through encapsulation method Nano-hydroxyapatite productivity by encapsulation method. *Nanomed. J.* **2014**, *1*, 276–284.

(32) Macaskie, L. E.; Yong, P.; Paterson-Beedle, M.; Thackray, A. C.; Marquis, P. M.; Sammons, R. L.; Nott, K. P.; Hall, L. D. A novel non line-of-sight method for coating hydroxyapatite onto the surfaces of support materials by biomineralization. *J. Biotechnol.* **2005**, *118*, 187–200.

(33) Roveri, N.; Battistella, E.; Bianchi, C. L.; Foltran, I.; Foresti, E.; Iafisco, M.; Lelli, M.; Naldoni, A.; Palazzo, B.; Rimondini, L. Surface enamel remineralization: biomimetic apatite nanocrystals and fluoride ions different effects. *J. Nanomater.* **2009**, *2009*, 8.

(34) Li, S.; Wu, H. H.; Xu, G. J.; Xiao, X. F. Facile Biomimetic Fabrication of Hollow Hydroxyapatite with Hierarchically Porous Microstructure Using Hyperbranched Gemini Surfactant as Template. *Adv. Mater. Res. (Durnten-Zurich, Switz.)* **2014**, *1015*, 355–358.

(35) Zhang, Q.; Leng, Y. Electrochemical activation of titanium for biomimetic coating of calcium phosphate. *Biomaterials* **2005**, *26*, 3853–3859.

(36) Rhodes, M. E. The Characterization of Pseudomonas fluorescens. *J. Gen. Microbiol.* **1959**, *21*, 221–263.

(37) Dupraz, S.; Parmentier, M.; Ménez, B.; Guyot, F. Experimental and numerical modeling of bacterially induced pH increase and calcite precipitation in saline aquifers. *Chem. Geol.* **2009**, *265*, 44–53.

(38) Rodriguez-Navarro, C.; Jroundi, F.; Schiro, M.; Ruiz-Agudo, E.; González-Muñoz, M. T. Influence of substrate mineralogy on bacterial mineralization of calcium carbonate: Implications for stone conservation. *Appl. Environ. Microbiol.* **2012**, *78*, 4017–4029.

(39) Sánchez-Román, M.; Rivadeneyra, M. A.; Vasconcelos, C.; McKenzie, J. A. Biomineralization of carbonate and phosphate by moderately halophilic bacteria. *FEMS Microbiol. Ecol.* **2007**, *61*, 273–284.

(40) Grases, F.; Söhnel, O.; Vilacampa, A. I.; March, J. G. Phosphates precipitating from artificial urine and fine structure of phosphate renal calculi. *Clin. Chim. Acta* **1996**, *244*, 45–67.

(41) Kim, J. W.; Yoon, C. Y.; Park, H. S.; Lee, J. G.; Moon, D. G.; Oh, M. M. Precipitation of amorphous magnesium ammonium phosphate: Is it a precursor for staghorn stones? *Urolithiasis* **2014**, *42*, 283–284.

(42) Palma, D.; Langston, C.; Gisselman, K.; McCue, J. Canine struvite urolithiasis. *Compendium Contin. Educ. Vet.* **2013**, *35*, 457–458.

(43) Beavon, J.; Heatley, N. G. The occurrence of struvite (magnesium ammonium phosphate hexahydrate) in microbial cultures. *J. Gen. Microbiol.* **1963**, *31*, 167–9.

(44) Sassoni, E.; Graziani, G.; Franzoni, E. Repair of sugaring marble by ammonium phosphate: Comparison with ethyl silicate and ammonium oxalate and pilot application to historic artifact. *Mater. Des.* **2015**, *88*, 1145–1157.

(45) Naidu, S. Novel Hydroxyapatite Coatings for the Conservation of Marble and Limestone. Ph.D. thesis, Princeton, 2014.

(46) Sassoni, E.; Naidu, S.; Scherer, G. W. The use of hydroxyapatite as a new inorganic consolidant for damaged carbonate stones. *Journal of Cultural Heritage* **2011**, *12*, 346–355.

(47) Barabesi, C.; Galizzi, A.; Mastromei, G.; Rossi, M.; Tamburini, E.; Perito, B. Bacillus subtilis gene cluster involved in calcium carbonate biomineralization. *J. Bacteriol.* **2007**, *189*, 228–235.

(48) Zamarreño, D. V.; Inkpen, R.; May, E. Carbonate crystals precipitated by freshwater bacteria and their use as a limestone consolidant. *Appl. Environ. Microbiol.* **2009**, *75*, 5981–5990.

(49) Bauerlein, E. Biomineralization of unicellular organisms: An unusual membrane biochemistry for the production of inorganic nano- and microstructures. *Angew. Chem., Int. Ed.* **2003**, *42*, 614–641.

(50) British Standards Institute, *BS EN 197-1:2011 - Cement Part 1: Composition, Specifications and Conformity Criteria for Common Cements*; 2011.

(51) Vaggelli, G.; Serra, M.; Cossio, R.; Borghi, A. A New Approach for Provenance Studies of Archaeological Finds: Inferences from Trace Elements in Carbonate Minerals of Alpine White Marbles by a Bench-to-Top μ-XRF Spectrometer. *Int. J. Mineral.* **2014**, *2014*.

(52) Hemeda, S. Geotechnical Characterization of Sakakini's Palace Stones and Other Construction Materials, Cairo-Egypt. *Geomaterials* **2013**, *3*, 38–46.

Chapter 4: Effect of Carbon Source Concentration and Growth Temperature on Pseudomonas fluorescens SBW25 Biofilm Formation, Morphology, and Structure

Statement

All literature reviews, practical work, data analysis, and manuscript preparation was carried out by Ronald Turner, with guidance provided by Andrea Hamilton and Joanna Renshaw. The presented manuscript was amended based on anonymous peer review comments provided during submission to the American Society for Microbiology journal 'Applied and Environmental Microbiology' in June 2017 and December 2017.

Chapter 4: Effect of Carbon Source Concentration and Growth Temperature on *Pseudomonas fluorescens* SBW25 Biofilm Formation, Morphology, and Structure

Abstract

The growth of biofilms has considerable relevance to many emergent practical applications such as microbial fuel cells and biomineralisation. These applications present a diverse set of environmental conditions, and so the characterisation of biofilm formation and structure under different environmental conditions is of relevance to a range of disciplines. The ubiquitous bacterium *Pseudomonas fluorescens* SBW25 is capable of forming biofilms in a range of environments, and as such is an excellent model microorganism for the investigation of biofilm formation. *P. fluorescens* SBW25 has also been the model organism for many studies of 'adaptive radiation' – the emergence of niche-adapted, diversified morphologies from an ancestral species. While *P. fluorescens* SBW25 biofilm and cell morphologies have been well-studied in terms of their genetic basis, the effects of temperature on adaptive radiation of *P. fluorescens* and the characterisation of links between biofilm cell colony morphology and bulk biofilm structure remains unstudied.

In this study, we demonstrate that the Fuzzy Spreader (FS) and Smooth (SM) morphologies of *P. fluorescens* SBW25 have several adaptations which may favour their emergence under different temperature conditions. We identify that the FS morphology has a competitive advantage at reduced incubation temperatures versus the SM morphology. We link this observation to measured structural variations in the bulk biofilm formed when these colony morphologies are present in different proportions. These structural variations may be

directly linked to altered fitness to different environmental niches. These effects were observed across a range of carbon sources, and the changes in biofilm structure observed are relevant to a number of practical applications including wastewater treatment, microbial fuel cells, and biomineralisation.

Keywords: Biofilms, Pseudomonas fluorescens, Temperature, Carbon Source, Confocal Microscopy, Biofilm Assays

Introduction

Bacterial biofilms are ubiquitous in the environment, forming on virtually any surface submerged in or exposed to an aqueous solution. They form under a wide range of conditions and can be found in natural, industrial and medical systems. Biofilm formation is useful in a number of practical applications, such as wastewater treatment [1], and the operation of microbial fuel cells [2,3]. These processes rely upon the development of mature biofilms, often onto a specifically engineered substrate designed to maximise process efficiencies [1,2]. Both wastewater treatment processes and microbial fuel cells may use a range of temperatures [3,4], carbon sources, and carbon source concentrations [5,6]. Potentially, MFCs could perform well at relatively low temperatures, ranging from 4^{o}C – 15^{o}C [3]. Consequently, the investigation and description of biofilm growth at lower temperatures is of particular significance to researchers in a number of fields.

Pseudomonas species are used in waste water treatment and microbial fuel cells [7–9], and there has been recent interest in the use of *Pseudomonas* bacteria to promote biomineralisation [10,11]. The generation of calcium phosphate minerals by these bacteria has been linked with the formation of biofilms [12], and in a previous study we demonstrated the

formation of a hydroxyapatite layer on a cement surface by a biofilm of *P. fluorescens* SBW25 [13]. The minerals deposited by these biofilms may be useful in a number of diverse settings, from use in medical implants [14,15], the preservation of architectural materials [16], to nuclear waste remediation [17].

In this study, we investigated *P. fluorescens,* a motile, obligate aerobic, Gram-negative, rod-shaped bacterium, ubiquitous in the environment. The organism is commonly associated with natural materials such as soil, water, and plants[18] and can form biofilms in a range of environments.[19] Varied *P. fluorescens* SBW25 colony morphologies have been observed to emerge under different environmental conditions, notably the 'Smooth' (SM), 'Fuzzy Spreader' (FS), and 'Wrinkly Spreader' (WS) morphologies.[20] The emergence of varied phenotypes from a common ancestor morphology is called 'adaptive radiation', and *P. fluorescens* SBW25 has acted as the preeminent model microorganism to study this effect in the *Bacteria*.[21–25]

Both the FS and SM morphologies have been observed to exist in biofilms at the base of test tube microcosms, with competition between these strains being the topic of several studies.[20,26,27] However, there has been relatively little investigation of the effects of temperature and carbon source on biofilm formation and adaptive radiation by *P. fluorescens* SBW25. There is scope for variations in colony morphology to be linked with variations in bulk biofilm morphology or even individual cell morphology, as observed in *V. cholerae*.[28] Individual colony morphology is associated with cell positioning within a microcosm in recent computational models.[29] Consequently, observations of variation in colony morphology may link to bulk biofilm structural changes, and hence impact on biofilm

activity relevant to many industrial processes such as wastewater treatment,[1] the operation of microbial fuel cells,[2,3] and biomineralisation.[13,30]

In this work, we investigated the effect four different carbon sources (sodium pyruvate, sodium benzoate, glucose and glycerol; $1gL^{-1}$ and $5gL^{-1)}$, and incubation temperatures of 25°C and 9°C, on biofilm formation by *P. fluorescens* SBW25 at the solid-liquid interface. The effect on biofilm structure, adhered biofilm cell CFU/ml, and colony morphology was investigated after incubation periods of 2, 6 and 10 days. King's B medium was then utilised for a more detailed comparison of differences in colony morphology abundance at an incubation temperatures of 9°C versus 25°C.

Results and Discussion

Effect of carbon source, concentration and temperature on biofilm growth and morphology

In general (and as expected) the adhered cell concentration at 9°C was lower, compared to 25°C for all four carbon sources (sodium pyruvate, sodium benzoate, glucose and glycerol) at both concentrations, and all time points. At the reduced incubation temperature (9°C), the carbon source concentrations appeared to have no effect on the amount of adhered biofilm cells at each time point, and a decrease in adhered biofilm CFU/ml was observed between days 6 and 10, for all carbon sources. Generally, at 9°C there was little difference in cell concentration between carbon sources and concentrations.

Across all time points sodium pyruvate at a concentration of $5gL^{-1}$ was the only carbon source where an increase in concentration was linked to a significantly increased amount of adhered biofilm cells (**Figure 1**). In the case of sodium benzoate and D-glucose, a decrease in adhered cells was observed with increasing carbon concentration (Fig 1) after the 10 day

incubation period. It should be noted that the initial quantification point (2 days) may be too late in the incubation period to detect initial differences in growth rate with variations in carbon source and temperature.

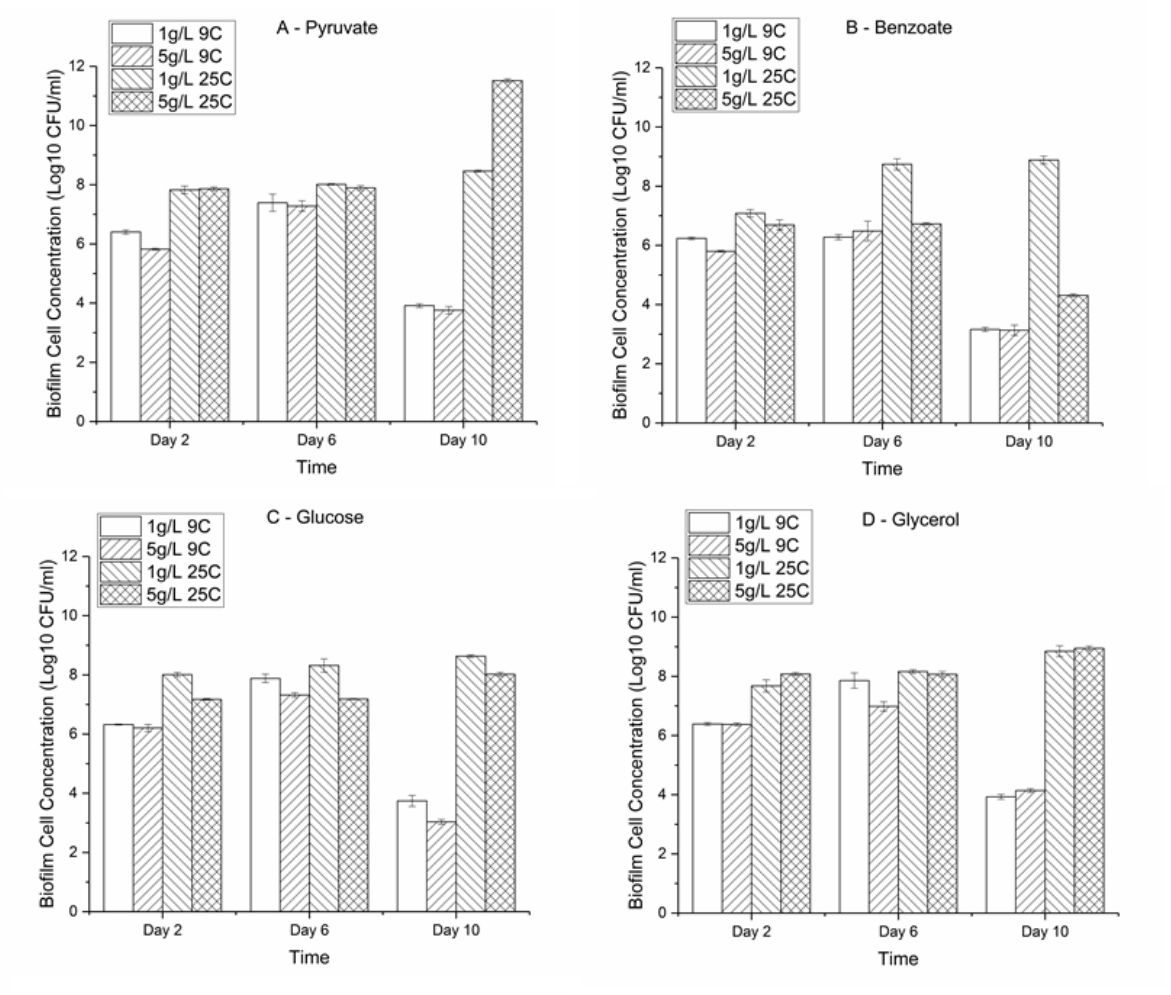

Figure 1: The effects of carbon source and temperature on Biofilm cell CFU/ml measured at 2, 6, and 10 day incubation periods. Variations on biofilm cell CFU/ml are associated with changes in carbon source and incubation temperature. All measurements are mean of N=3 +/- SEM.

In general when viewed across all examined time points and incubation temperatures, the lowest quantity of adhered cells was observed with sodium benzoate as the carbon source, with a mean adhered cell concentration of $3.35x10^5$ CFU/m. The highest quantity of adhered cells was observed with sodium pyruvate, which generated a mean adhered cell concentration of $2.28x10^7$ CFU/ml.

Two distinct phenotypes were observed for the adhered biofilm cells – a Smooth phenotype and a Fuzzy Spreader phenotype (Appendix 2, Supplementary Figure 4).[27] The smooth morphology has been generally observed to colonise the liquid phase of static broth microcosms, forming small, smooth colonies. In comparison, the fuzzy spreader has been observed to colonise the microcosm floor where O_2 levels are lower; forming large, spreading colonies [20,27,31].

All cultures were inoculated with an ancestral SM phenotype. At 25^oC the SM phenotype still dominated in the early stages of the incubation period; FS was only observed with $1gL^{-1}$ pyruvate (**Table 1**). By day 6, the FS morphology appeared to become more dominant, with a more even mix between FS and SM morphologies observed across all carbon sources and temperatures by day 10.

Carbon Source	Day 2, 25°C	Day 6, 25°C	Day 10, 25°C	Day 2, 9°C	Day 6, 9°C	Day 10, 9°C
Glycerol 5gL^{-1}	SM	FS	FS	FS	FS	FS
Glycerol 1gL^{-1}	SM	FS	FS	FS	FS	FS
Benzoate 5gL^{-1}	SM	FS	SM	FS	FS	SM
Benzoate 1gL^{-1}	SM	FS	SM	FS	FS	SM
Glucose 5gL^{-1}	SM	SM	FS	SM	FS	FS
Glucose 1gL^{-1}	SM	FS	SM	FS	FS	FS
Pyruvate 5gL^{-1}	SM	FS	FS	FS	FS	SM
Pyruvate 1gL^{-1}	FS	SM	SM	FS	SM	FS

Table 1: Dominant morphologies of bacterial colonies recovered from adhered biofilms, associated with Temperature and Carbon Source at Days 2, 6, and 10. Carbon sources are glycerol, benzoate, glucose, and pyruvate at concentrations of 5gL^{-1} and 1gL^{-1}. All carbon sources were examined at 25°C and 9°C incubation temperatures. Colony morphologies identified as Fuzzy Spreader (FS) or Smooth (SM) are based on descriptions by Rainey & Travisano [27]. All observations were collected from triplicate experiments.

At 25°C, in the case of 1gL^{-1} pyruvate, the FS morphology was dominant at day 2, but had reverted to a SM morphology by day 6; with the FS morphology not emerging again. With both concentrations of sodium benzoate, the FS phenotype temporarily emerged on day 6 before reverting to SM on Day 10. Across all time points and carbon sources at 9°C, the FS morphology was more prevalent than at 25°C at incubation day 2.

Further studies on the relative abundance of the two morphologies observed were undertaken using King's B medium (which contains 19 gL^{-1} glycerol); this medium is widely used for adaptive radiation studies with *P. fluorescens* SBW25.[21,23,27,32–34]. The ancestral SM morphology dominated in early incubation periods; however, the emergence of the FS

phenotype was more rapid at 9°C than 25°C. By day 6, the FS morphology dominated at both temperatures (**Table 2**), but the proportion of SM was higher at 9°C than 25°C, suggesting that the rapid early growth of FS was not sustained at the lower temperature. The rapid emergence of FS at 9°C was also observed with the varied carbon sources and concentrations (Table 1). However by day 10, relatively even mixes of SM and FS morphologies were seen at both 9°C and 25°C.

Morphology	Day 2 – 25°C	Day 2 – 9°C	Day 6 - 25°C	Day 6 - 9°C
FS	4.26	14.14	79.51	64.21
SM	95.74	85.86	20.49	35.79

Table 2: Counts of colony morphology the Fuzzy Spreader (FS) and Smooth (SM) morphologies of adhered biofilm cells, as a percentage of total colonies counted (range 205 - 1535 colonies in total). Measurements were taken after 2 and 6 day incubation periods at either 9°C or 25°C in King's B medium. Measurements were collected from triplicate experiments for each condition.

Previous studies on these phenotypes in King's B Medium have focused on the spatial associated distribution variations, genetic changes, and competition between different *P. fluorescens* SBW25 morphologies. These experiments are generally carried out at room temperature, in a medium that is incorporates glycerol as a carbon source (King's B). These studies have identified that the FS morphology typically occupies the base of test tube microcosms, while the SM morphology colonises the liquid phase.[20] Our results indicate that the FS morphology does dominate the microcosm base as would be expected; however we additionally establish that the proportion of FS and SM morphology observed in this niche will vary as a result of temperature, an effect which has not been observed to date.

Comparison of Biofilm Structures

Although confocal microscopy has been used to study *P. fluorescens* SBW25 morphologies such as the Wrinkly Spreader (WS) and 'small colony variant' (SCV) phenotypes,[35,36] there has been limited studies of the SM and FS morphologies and little investigation to date of any structural variations linked to temperature.

In this study we used confocal microscopy to examine the structures of the biofilms formed with King's B medium at 9°C and 25°C (6 days incubation), and with glycerol or benzoate ($1gL^{-1}$) at 25°C (10 days incubation). With King's B medium, biofilm structure at 9°C was dramatically altered from that observed at 25°C (**Figure 2**). COMSTAT analysis identified that the biofilm formed at 9°C was of reduced biomass and thickness, with increased roughness and surface area to biovolume ratio than the biofilm formed at 25°C (**Table 3**). This is consistent with the reduced growth at 9°C, compared to 25°C, observed with the varying carbon sources (Fig. 1)

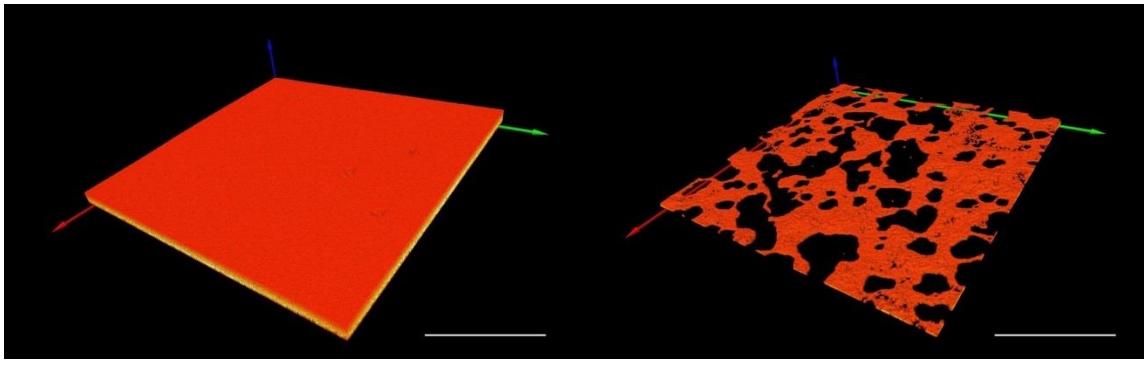

Figure 2 : Confocal microscopy images of P. fluorescens SBW25 biofilms grown at 25°C (Left) and 9°C (Right) after a 6 day incubation period. The biofilm formed at 25°C is clearly thicker and of greater total biomass than the biofilm formed at 9°C. Scale bar is 100µm.

Although the observed variations in biofilm parameters will be significantly affected by differing growth with temperature, the morphological composition is also likely to impact on

the biofilm structure. With King's B medium, FS was the dominant phenotype observed at both temperatures after 6 days incubation, although the percentage FS was lower at 9°C (Table 2). To investigate the effect of morphology on biofilm structure, biofilms were grown on 1gL^{-1} sodium benzoate, and 1gL^{-1} glycerol at 25°C for 10 days. These carbon sources were chosen as the biofilms formed had similar amounts of adhered cells (Fig 1), but had different dominant phenotypes: FS with glycerol; SM with benzoate.

Significant variations in biofilm parameters were observed between the two biofilms (Table 3). The biomass and average thickness of the biofilm were greater with glycerol rather than benzoate, whilst Roughness coefficient and surface area to biovolume ratio were greater with benzoate than glycerol. It is therefore possible that a relative increase in abundance of SM morphology cells within the *P. fluorescens* biofilm may be linked to decreased biofilm density and thickness; and increased roughness and surface area to biovolume ratio.

Medium	**King's B**		**Glycerol 1gL^{-1}**	**Benzoate 1gL^{-1}**
Incubation Temperature	**25°C**	**9°C**	**25°C**	
Biomass (µm^3/µm^2)	152 +/- 60	26 +/- 3	325.7 +/- 110.3	1.61 +/- 1.14
Average Thickness (µm)	192 +/- 83	52 +/- 11	479.9 +/- 126	177 +/- 89.0
Roughness Coefficient (Ra)	0.03 +/- 0.02	0.3 +/- 0.08	0.09 +/- 0.02	1.9 +/- 0.01
Surface Area to Biovolume Ratio	0.21 +/- 0.04	0.46 +/- 0.04	0.42 +/- 0.3	2.04 +/- 0.4

Table 3: Comparison of biofilm parameters measured using confocal microscopy images of biofilms formed at 25^{o}C and 9^{o}C after a 6 day incubation period, or biofilms formed with either a glycerol (observed as FS-dominant) or benzoate (observed as SM-dominant) carbon source after a 10 day incubation period. Measurements were collected from confocal stacks using the software COMSTAT 2. All measurements are mean of at least N=3 +/- SEM.

Previous studies have shown the competition between the FS and SM phenotypes are complex, with a stable maintenance of variation between the two morphologies identified as typical.[27] Adaptation of *P. fluorescens* SBW25 morphologies to different environmental niches has been identified in the past, such as the identified dominance of the WS phenotype at the air-liquid interface, [33] and the niche preference of the FS phenotype to the base of test tube microcosms. Significantly, an inhibitory effect of FS on SM has been noted and attributed to the deprivation of oxygen in the broth phase promoted by the capacity of FS morphology cells utilise 'FS rafts' that allow them to transiently colonise the broth phase of the microcosm.[20] However, there are very few studies investigating the impact of overall environmental conditions on colony morphology.

In the present work we identify that these variations in biofilm structure and morphological abundance suggest adaption to environmental conditions, in particular to temperature. These variations can be associated with changes in bulk biofilm structure that may plausibly impact fitness under different growth conditions. The structure of *Pseudomonas* biofilms is relevant to a number of practical applications; such as wastewater treatment,[37] and biomineralisation.[38] A nascent example is the use of microbial fuel cells, a technology which utilises biofilm formation as a novel method for the generation of electricity while simultaneously removing organic waste material from wastewater streams.[7] Biofilm

formation by *Pseudomonas* species has been exploited in the development of these fuel cells as *Pseudomonas* species are capable of utilising a diverse range of sugars and organic substrates[39], with studies identifying that enhanced *Pseudomonas* biofilm development generates improved power generation and waste organic material clearance.[7]

Methods

Strain and routine growth conditions

Pseudomonas fluorescens strain SBW25 [40] (provided by Dr Nicolas Tucker, Strathclyde Institute of Pharmacy & Biomedical Sciences, University of Strathclyde) was revived from -80^{o}C storage onto King's B agar, incubated for 3 days and an ancestral smooth morphology was recovered for use as an inoculum.

Experimental Conditions for Static Biofilm Test Tube Culture Carbon Source Analysis

Four different carbon sources were examined at temperatures of 25^{o}C and 9^{o}C: Sodium Pyruvate (Sigma-Aldrich), D-glucose (Sigma-Aldrich), Sodium Benzoate (Sigma-Aldrich), or Glycerol (Sigma-Aldrich) were added to a base medium, to final concentrations of either 1gL^{-1} or 5gL^{-1}. The base medium was developed from a formulation used by Allison *et al*. [41] and contained the following components dissolved in deionised water: $MgSO_4$ $7H_2O$ (Sigma-Aldrich) 0.2gL^{-1}, K_2HPO_4 (Sigma-Aldrich) 2.2gL^{-1}, KH_2PO_4 (Sigma-Aldrich) 9.4gL^{-1}, NH_4Cl (VWR) 0.65gL^{-1}, $CaCl_2$.$2H_2O$ (Fisher Scientific) 0.133gL^{-1}.

2ml volumes of each media were dispensed into disposable glass culture tubes (Corning Inc), which were sealed with non-absorbent cotton wool bungs (Cowens Ltd). Tubes were inoculated with 0.05% v/v inocula of *P. fluorescens* culture (OD_{600} of culture inoculum = 0.1) with a calibrated inoculation loop. Glass tubes containing each medium variant for each

time point (2, 6 and 10 days) were incubated at 9^{o}C and 25^{o}C. All samples were prepared and incubated in triplicate.

After 2, 6, and 10 day static incubation periods, biofilm cell density was measured and colony morphology recorded. TSA (Oxoid) and LB (Sigma-Aldrich) media were used as the quantification and propagation medium for the carbon source investigations to avoid any interference from the glycerol present in King's B medium formulations. Quantification was carried out using the drop plate method, allowing results from triplicate microcosms to be analysed on single Petri dishes.[42,43] The use of the drop plate method step enabled the economical screening of a large range of carbon sources and conditions, versus the more resource intensive spread plating method.

Experimental Conditions for Quantification of FS and SM Abundance in King's B Medium

P. fluorescens SBW25 was propagated from the ancestral smooth morphology in triplicate test tube microcosms containing 7ml King's B medium at either 9^{o}C or 25^{o}C for 2 or 6 days.

A quantitation of the abundance of both morphologies was then carried out. This was done via collection of 1ml adhered A-L interface biofilm material from the test tube base, which was diluted in PBS and colony abundances quantified by serial dilution and spread-plating of 100µL aliquots onto King's B agar. Plates were incubated at 20^{o}C for 3 days prior to quantification of SM and FS morphology cells.

> 200 colonies were countable in total for each set of experimental conditions, ranging from 205-1535 colonies dependent upon experimental conditions of time point and temperature. SM and FS colony counts were converted to a percentage of total colonies observed for each set of conditions.

Confocal Microscopy: culture conditions and analysis

Biofilms were grown in a static incubation mode on the inner surface of Nunc^{TM} 35mm glass-bottomed dishes (Thermo Fisher), which allowed the biofilm to be visualised directly on the substrate. Biofilms were grown in King's B medium at 9^{o}C or 25^{o}C, or the base medium described in the earlier section 'Experimental Conditions for Static Biofilm Test Tube Culture Carbon Source Analysis', containing 1gL-1 benzoate or glyercol.

After the selected incubation period (6 or 10 days), the growth medium was removed and the biofilm samples rinsed with 0.9% NaCl to remove any planktonic cells, followed by staining with 3ml 0.1 % w/v acridine orange (Alfa-Aesar) in 1x PBS solution. The biofilms were incubated in the staining solution for 5 minutes, before the staining solution was removed. Biofilms were examined using a confocal microscope (Leica SP5 II).

Confocal microscopy images were prepared using Avizo 8.1.The collected confocal maps were analysed with the COMSTAT2 (version 2.1) software package [44–46] to determine biofilm parameters.

References

[1] F. I. Hai, K. Yamamoto, K. Fukushi, *Desalination* **2006**, *192*, 315.

[2] S. Choi, J. Chae, *Sensors Actuators, A Phys.* **2013**, *195*, 206.

[3] A. Larrosa-Guerrero, K. Scott, I. M. Head, F. Mateo, A. Ginesta, C. Godinez, *Fuel* **2010**, *89*, 3985.

[4] L. H. Li, Y. M. Sun, Z. H. Yuan, X. Y. Kong, Y. Li, *Environ. Technol.* **2013**, *34*, 1929.

[5] S. Oh, B. E. Logan, *Water Res.* **2005**, *39*, 4673.

[6] D. Pant, G. Van Bogaert, L. Diels, K. Vanbroekhoven, *Bioresour. Technol.* **2010**, *101*, 1533.

[7] D. Majumder, J. P. Maity, M.-J. Tseng, V. R. Nimje, H.-R. Chen, C.-C. Chen, Y.-F. Chang, T.-C. Yang, C.-Y. Chen, *Int. J. Mol. Sci.* **2014**, *15*, 16772.

[8] K. R. Suzanne T Read, Paritam Dutta, Phillip L Bond, Jürg Keller, *BMC Microbiol.* **2010**, *10*, 98 (1.

[9] K. Rabaey, W. Verstraete, *Trends Biotechnol.* **2005**, *23*, 291.

[10] A. Khanafari, T. Akbari, M. R. Sohrabi, *Nanomed J* **2014**, *1*, 276.

[11] S. Dupraz, M. Parmentier, B. Ménez, F. Guyot, *Chem. Geol.* **2009**, *265*, 44.

[12] L. E. Macaskie, P. Yong, M. Paterson-Beedle, A. C. Thackray, P. M. Marquis, R. L. Sammons, K. P. Nott, L. D. Hall, *J. Biotechnol.* **2005**, *118*, 187.

[13] R. J. Turner, J. C. Renshaw, A. Hamilton, *ACS Appl. Mater. Interfaces* **2017**, *9*, 31401.

[14] J. L. Ong, D. C. N. Chan, *Crit. Rev. Biomed. Eng.* **2000**, *28*, 667.

[15] S. Mistry, D. Kundu, S. Datta, D. Basu, *Aust. Dent. J.* **2011**, *56*, 68.

[16] E. Sassoni, S. Naidu, G. W. Scherer, *J. Cult. Herit.* **2011**, *12*, 346.

[17] S. Handley-Sidhu, J. A. Hriljac, M. O. Cuthbert, J. C. Renshaw, R. A. D. Pattrick, J. M. Charnock, B. Stolpe, J. R. Lead, S. Baker, L. E. Macaskie, *Environ. Sci. Technol.* **2014**, *48*, 6891.

[18] G. Donnarumma, E. Buommino, A. Fusco, I. Paoletti, L. Auricchio, M. A. Tufano, *Int. J. Immunopathol. Pharmacol.* **2010**, *23*, 227.

[19] M. E. Rhodes, *J. Gen. Microbiol.* **1959**, *21*, 221.

[20] G. C. Ferguson, F. Bertels, P. B. Rainey, *Genetics* **2013**, *195*, 1319.

[21] A. J. Spiers, S. G. Kahn, J. Bohannon, M. Travisano, P. B. Rainey, *Genetics* **2002**, *161*, 33.

[22] P. Goymer, S. G. Kahn, J. G. Malone, S. M. Gehrig, A. J. Spiers, P. B. Rainey, *Genetics* **2006**, *173*, 515.

[23] E. Bantinaki, R. Kassen, C. G. Knight, Z. Robinson, A. J. Spiers, P. B. Rainey, *Genetics* **2007**, *176*, 441.

[24] M. J. McDonald, S. M. Gehrig, P. L. Meintjes, X. X. Zhang, P. B. Rainey, *Genetics* **2009**, *183*, 1041.

[25] R. C. E. Flohr, C. J. Blom, P. B. Rainey, H. J. E. Beaumont, *Proc. Natl. Acad. Sci.* **2013**, *110*, 20663.

[26] R. C. MacLean, *J. Evol. Biol.* **2005**, *18*, 1376.

[27] P. B. Rainey, M. Travisano, *Nature* **1998**, *394*, 69.

[28] P. I. Watnick, C. M. Lauriano, K. E. Klose, L. Croal, R. Kolter, *Mol Microbiol* **2001**, *39*, 223.

[29] W. P. J. Smith, Y. Davit, J. M. Osborne, W. Kim, K. R. Foster, J. M. Pitt-Francis, *Proc. Natl. Acad. Sci.* **2016**, *114*, E280.

[30] M. R. Fishman, K. Giglio, D. Fay, M. J. Filiatrault, *Sci. Rep.* **2018**, *8*, 10156.

[31] A. J. Spiers, *Int. J. Evol. Biol.* **2014**, DOI 10.1155/2014/675432.

[32] A. J. Spiers, *PLoS One* **2007**, DOI 10.1371/journal.pone.0000740.

[33] A. Kuśmierska, A. J. Spiers, *Int. J. Evol. Biol.* **2016**, *2016*, 1.

[34] A. Koza, P. D. Hallett, C. D. Moon, A. J. Spiers, *Microbiology* **2009**, *155*, 1397.

[35] M. L. Workentine, S. Wang, H. Ceri, R. J. Turner, *BMC Microbiol.* **2013**, *13*, DOI 10.1016/0006-291X(63)90549-7.

[36] W. E. Huang, S. Ude, A. J. Spiers, *Microb. Ecol.* **2007**, *53*, 471.

[37] K. Kida, S. Morimura, H. Tadokoro, S. Mashood, A. A. Yusob, Y. B. Ghin, *Environ. Technol.* **1997**, *18*, 517.

[38] S. Handley-Sidhu, J. C. Renshaw, S. Moriyama, B. Stolpe, C. Mennan, S. Bagheriasl, P. Yong, A. Stamboulis, M. Paterson-Beedle, K. Sasaki, R. A. D. Pattrick, J. R. Lead, L. E. MacAskie, *Environ. Sci. Technol.* **2011**, *45*, 6985.

[39] I. A. Ieropoulos, J. Greenman, C. Melhuish, J. Hart, *Enzyme Microb. Technol.* **2005**, *37*, 238.

[40] A. K. Lilley, R. S. Hails, J. S. Cory, M. J. Bailey, *FEMS Microbiol. Ecol.* **1997**, *24*, 151.

[41] D. G. Allison, B. Ruiz, C. SanJose, A. Jaspe, P. Gilbert, *FEMS Microbiol. Lett.* **1998**, *167*, 179.

[42] H. J. Hoben, P. Somasegaran, *Appl. Environ. Microbiol.* **1982**, *44*, 1246.

[43] A. A. Miles, S. S. Misra, J. O. Irwin, *J. Hyg. (Lond).* **1938**, *38*, 732.

[44] A. Heydorn, A. T. Nielsen, M. Hentzer, C. Sternberg, M. Givskov, B. K. Ersboll, S. Molin, *Microbiology* **2000**, *146*, 2395.

[45] M. Vorregaard, Comstat2 - a Modern 3D Image Analysis Environment for Biofilms, Technical University of Denmark, **2008**.

[46] "www.comstat.dk," **n.d.**

Chapter 5: A Characterisation and Comparison of Biogenic and Abiotic Hydroxyapatites

All literature reviews, practical work, data analysis, and manuscript preparation was carried out by Ronald Turner, with guidance provided by Andrea Hamilton and Joanna Renshaw, with the following exceptions:

- Mossbauer spectroscopy was carried out on a collaborative basis by Dr Paul Bingham and Mr Alex Scrimshire, both of Sheffield Hallam University
- Rietveld refinement of XRD patterns to determine lattice parameters, crystallite size, and strain was carried out on a collaborative basis by Dr Pieter Bots (Strathclyde)
- TEM imaging and FIB-SEM lift-outs were carried out on a collaborative basis by Dr Andrew Brown and Mr John Harrington of the University of Leeds, with funding by the Henry Royce Institute
- SAXS data collection and data reduction was carried out as a national service (STFC funded) by Dr Nick Terrill of Diamond Light Source, UK. (Beamline I-22)
- FT-IR data was collected and analysed by Dr Matthew Baker and Dr Cerys Jenkins (Strathclyde), on a collaborative basis.
- CHN/TOC analysis was carried out under contract by Antony Hinchliffe of the University of East Anglia
- Mass-balancing of ICP-OES and CHN/TOC data was carried out on a collaborative basis by Dr Susan Cumberland (Strathclyde)

Chapter 5 – A Characterisation and Comparison of Biogenic and Abiotic Hydroxyapatites

Abstract

The calcium phosphate mineral hydroxyapatite has been a focus of significant research interest. Hydroxyapatites have variable structural morphologies, which may include rod-like and/or plate-like nanostructures. These variations in nanostructure are associated with changes in the properties of the bulk material, such as altered Young's modulus or the promotion of bone formation in the context of medical implant devices. In this work, TEM and SAXS analyses are used to establish that the biogenic hydroxyapatite has a plate-like, anhedral morphology with particle diameters of 20-30nm; in comparison to the abiotic hydroxyapatite which presented a more crystalline, rod-like structure with a larger primary particle size. We also identify that hydroxyapatites synthesised on an OPC substrate appear to uptake a level of carbonate and iron from the cement substrate, with an abiotic hydroxyapatite having an increased level of carbonate relative to the biogenic hydroxyapatite. This effect is likely due to the more immediate pH increase utilised in the abiotic synthesis process. Analysis of the data suggests that this iron and carbonate exists in a separate phase from the hydroxyapatite, although there is some evidence for iron incorporation into the hydroxyapatite lattice. We establish these associations of iron and carbonate with the hydroxyapatites through a combination of ICP-OES, SEM-EDS, FT-IR, and XRD. We utilise ^{57}Fe Mössbauer Spectroscopy to determine that a coating of this biogenic hydroxyapatite on Ordinary Portland Cement associates with iron in the Fe(III) oxidation state, potentially in the Ca(2) sites of the hydroxyapatite structure, in the octahedral coordination. Mossbauer analysis provides also provides some evidence for superparamagnetic nanoparticles associated with the biogenic hydroxyapatite coating. In comparison, the abiotic hydroxyapatite coating appears to contain Fe(III) in the form of FeOOH, again in an octahedral coordination but without any paramagnetic component.

Introduction

Hydroxyapatite is a calcium phosphate mineral, with the general formula [$Ca_5(PO_4)_3(OH)$]. The ability of bacteria to promote formation of hydroxyapatite has been of recent research interest.[1, 2] So-termed 'Biogenic' hydroxyapatite can be formed through the action of *Pseudomonas fluorescens*, in a growth medium containing LB broth, potassium phosphates, and OPC which mediates an increase in pH and production of ammonium; leading to the formation of hydroxyapatite. This process has been examined in previous work, and is suggested to rely upon microbial generation of an alkaline environment.[3]

Hydroxyapatite presents with variable morphologies, and these changes influence the physical properties of the material. Rod-like morphologies [4] as well as spherical or plate-like [5] morphologies have been described in the literature. Spherical or plate-like hydroxyapatites can be found in bone material,[6] and synthetic spherical hydroxyapatites have been associated with enhanced bone formation *in vitro*.[7] Plate-like hydroxyapatites have been identified as the ideal morphology for stiffening isotropic materials, in comparison to spherical and fibrous morphologies.[8]

We characterise these biogenic and abiotic hydroxyapatites using a combination of XRD, SAXS, FT-IR, TEM, and ^{57}Fe Mössbauer spectroscopy. We observe that the biogenic hydroxyapatite formed is associated with both iron and carbonate when formed on Ordinary Portland cement, and that the biogenic hydroxyapatites are associated with lower inorganic carbonate levels than abiotic hydroxyapatites in general. We also observe alterations in lattice parameters when synthesis methods are varied. Biogenic hydroxyapatite was observed to present a plate-like morphology, versus a rod-like morphology for the abiotic hydroxyapatite.

Materials and Methods

Experimental Procedures

Hydroxyapatite synthesis

The *P. fluorescens* SBW25 stock culture used as the inoculum for this study was grown in LB (Lennox) broth (Sigma-Aldrich). Buffered LB broth with added $Ca(OH)_2$ was used as the growth medium for hydroxyapatite synthesis in the absence of OPC. The buffered LB broth consisted of $20gL^{-1}$ LB (Lennox) Broth (Sigma-Aldrich), $9.4gL^{-1}$ KH_2PO_4 (Sigma-Aldrich), $2.2gL^{-1}$ K_2HPO_4 (Fluka), and $1gL^{-1}$ $Ca(OH)_2$. All materials were added in powdered form and dissolved in DI water. 100ml volumes of the buffered LB broth solution were dispensed into Erlenmeyer flasks. The initial addition of $1gL^{-1}$ $Ca(OH)_2$ was observed to immediately raise the pH of the buffered LB medium from 6.0 to 6.4, as measured pre-autoclaving of the medium. All flasks were sealed with non-absorbent cotton wool bungs (Cowdens). The flasks were autoclaved at 121°C for 15 minutes.

Test flasks were inoculated with a 1% v/v inoculum of *P. fluorescens* overnight culture (OD600 = 0.1). Control flasks were not inoculated, acting as abiotic controls. All flasks were incubated for 20 days at ambient temperature with continual shaking inside a fume cabinet. After a 20 day incubation period, pH measurements were taken. In all flasks containing $Ca(OH)_2$, the pH had risen to ~9.6.

To collect the precipitates from the liquid media, 10ml of medium was transferred to a sterile 15ml centrifuge tube, and the precipitate collected via centrifugation at 8000g for 20 minutes, at 20°C. The supernatant was decanted, the collected sediment pellet was re-suspended in distilled water to wash and re-centrifuged. The supernatant was discarded and the precipitate air-dried at 37°C for 24 hours. Precipitates were imaged with a Nikon digital camera. Precipitates were analysed by XRD, SAXS, SEM, FT-IR, and TEM as described further below.

P. fluorescens Biofilm Growth and Hydroxyapatite Synthesis on an OPC Substrate

OPC coupons were rinsed thoroughly in DI water, and one coupon aseptically transferred into each flasks containing 100ml sterile modified buffered LB broth, which did not contain any $Ca(OH)_2$ but was otherwise of the same formulation described earlier. Test flasks were inoculated with 100µL of *P. fluorescens* overnight culture (OD_{600} = 0.1); control flasks were not inoculated. All flasks were incubated at ambient temperature on an orbital shaker.

Unlike the $Ca(OH)_2$ system, in the absence of bacteria there was an insufficient rise in pH to generate hydroxyapatite on an OPC coupon, with brushite forming instead. In order to synthesise an 'abiotic hydroxyapatite coating' on OPC, the protocol was carried out as described for the 'control' samples. However, prior to autoclaving the growth medium the pH was adjusted to 9.0 by preparing 90ml of buffered LB broth made up to a final volume of 100ml with 1M NaOH.

Solid-State Analyses

X-Ray Diffraction (XRD)

XRD spectra were collected using a Bruker D8 Advance instrument. Measurements of lattice parameters based on the collected XRD patterns were carried out using TOPAS (Bruker) using a crystallographic information file for hydroxyapatite with a spacegroup of $P6_3/m$.[9] Instrument peak broadening was estimated by analysing a crystalline silicon standard and fitted in TOPAS simultaneously to each sample of interest.

Small-Angle X-Ray Scattering (SAXS)

Biogenic and abiotically generated hydroxyapatite precipitates were dried and analysed using SAXS at Diamond Light Source (beamline I22). 12.4keV X-rays were used with a camera length of 1.9m, providing a q range of 0.013-0.9$Å^{-1}$. The collected scattering patterns were background subtracted

and radially integrated using the in-house software DAWN, and SasView was used for further data analyses and fitting.[10]

Transmission Electron Microscopy (TEM)

Approximately 10mg of the dried hydroxyapatite powders were separately dispersed in methanol, and a small amount loaded onto a TEM sample grid prior to imaging using an FEI Titan3 Themis 300.

Chemical Speciation Analyses

^{57}Fe Mössbauer Spectroscopy

To prepare the samples for Mössbauer analysis, a clean diamond-coated file (Draper Tools Ltd, UK) was used to scrape the surface of the cement samples to generate a fine powder. Powdered samples were vacuum-packed for storage prior to analysis, to minimise any potential carbonation.

Mössbauer spectroscopy was carried out at 293 K using a constant acceleration spectrometer with a 25 mCi ^{57}Co source in a Rh matrix. Absorbers were prepared from ground samples mixed with graphite powder to ensure a Mössbauer thickness t<1. Spectra were measured in the velocity range ±12 mm s^{-1} relative to α-Fe and were fitted using the Recoil analysis software package. Two broadened Lorentzian paramagnetic doublets were fitted to the resultant spectra. It was assumed for the purposes of fitting that the recoil-free fraction f $(Fe(III)^{))}$f (Fe(II)) = 1.0. Spectral measurements were carried out over 2 weeks per sample. The relatively low signal-to-noise ratio obtained from the measured samples was due to their low Fe contents, and data collection was halted at a point where an unfeasible (> 1 month) additional collection time would be required to produce a statistically significant improvement in spectral signal-to-noise ratio.

Inductively Coupled Plasma Atomic Emission Spectroscopy (ICP-OES)

Biogenic and abiotically generated hydroxyapatite precipitates were collected and dried to produce fine powders. Hydroxyapatites formed on OPC were removed from the surface using clean diamond-

coated files (Draper Tools Ltd, UK), to produce a fine powder. Samples were processed for ICP-OES via microwave digestion using a MARSXpress microwave digestion system (CEM Corporation) in a 10ml solution of concentrated trace-element grade hydrochloric acid (2ml) and nitric acid (8ml). Samples were diluted 1:10 in ultrapure water prior to analysis using an iCAP 7000 Plus series ICP-OES (Thermo-Fisher).

Fourier Transform Infrared Spectroscopy (FT-IR)

Representative portions of biogenic and abiotic hydroxyapatite precipitates were transferred onto the diamond ATR element of the Spectrum Two (PerkinElmer). Pressure was applied to samples at a force gauge of 50. Spectral repeats were taken of three portions of each sample and averaged to produce overall sample representative spectra.

Spectra collected using the Spectrum Two spectrometer were exported as csv files and exported to MATLAB for spectral analysis including processing, peak fitting and plotting using in-house written software.

Total Organic Carbon/Total Inorganic Carbon/Elemental Analysis for CHN

5mg of each sample was weighted out into centrifuge tubes and mixed with 5ml sulphurous acid. Further sulphurous acid was added until effervescence was observed to stop. Samples were then freeze-dried. The dried samples were disaggregated using a spatula, which was then weighed into tin capsules for analysis. Samples were analysed using an Exeter CE440 Elemental Analyser.

Results and Discussion

Structural and morphological characteristics of biogenic and abiotic hydroxyapatite

XRD

Figure 1: XRD Patterns of Biogenic and Abiotic Hydroxyapatite Samples

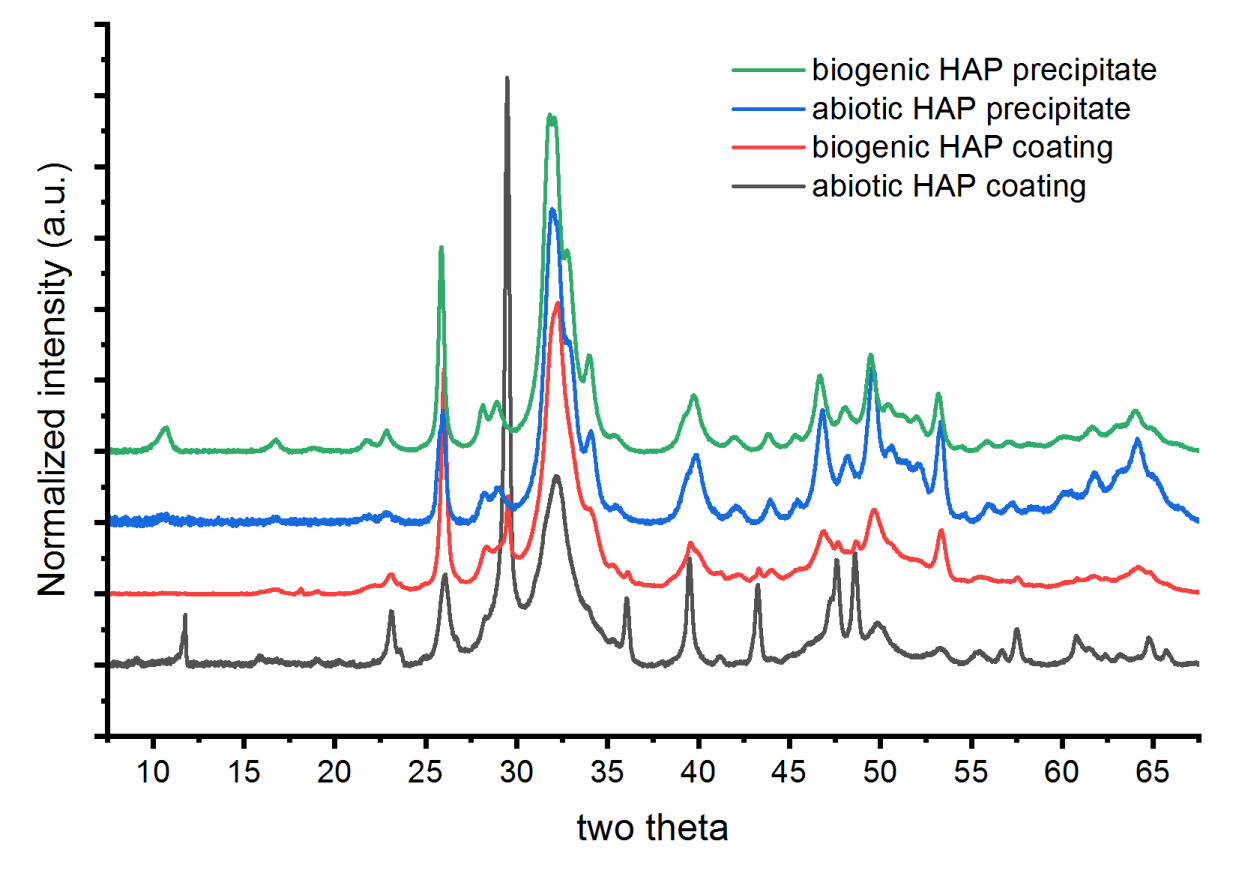

Figure 1 Legend: XRD patterns of biogenic and abiotic hydroxyapatites precipitates, and coatings on an OPC substrate. Library patterns were taken from Sanger & Kuhs (1992) [9] *for hydroxyapatite, and Markgraf & Reeder (1985)* [11] *for calcite.*

The results from the XRD analyses are plotted in Fig. 1, and the results from the Rietveld refinement are summarized in Table 1. Rietveld refinement was possible with a single phase in the precipitate samples (Table 1), identified as hydroxyapatite with a space group *P63/m*.[9] In addition to hydroxyapatite, calcite [11] was identified at 24.15% and 3.60% in the abiotic and biogenic

hydroxyapatite coatings, respectively. The Rietveld refinements also revealed variations in the lattice parameters between the different samples (Table 1); we determined that the biogenic HAP samples have a larger unit cell volume (530.5-531.0 A^3) compared to the abiotic HAP samples (~528.6 A^3). Increases in c/a ratio are associated with B-carbonated hydroxyapatite.[12] We would suggest that it is unlikely that carbonate is selectively substituted into the crystal structure of the hydroxyapatites but rather exists as a separate phase. Silicon incorporation is also associated with expanded lattice parameters and unit cell volumes, which we do not observe.[13] Past work has identified that iron-substitution of hydroxyapatites is associated with a contraction in lattice dimensions;[14, 15]although the literature is conflicting, with other data suggesting that iron incorporation results in expanded lattice parameters.[16] We would therefore not suggest that there is sufficient evidence for any direct incorporation of substituting ions into the hydroxyapatite lattice from investigation of the lattice parameters (Table 1) alone.

Table 1: Lattice and Physical Parameters of Biogenic and Abiotic Hydroxyapatites

Sample	**a (A)**	**c (A)**	**c/a ratio**	**V (A^3)**	**wt% calcite**
Biogenic HAp Precipitate	9.436(1)	6.8854(4)	0.7297	530.95(8)	n.d.
Abiotic HAp Precipitate	9.420(1)	6.879(1)	0.7303	528.57(16)	n.d.
Biogenic HAp Coating	9.434(1)	6.8817(4)	0.7295	530.46(8)	3.60(5)
Abiotic HAp Coating	9.437(3)	6.8541(8)	0.7263	528.61(31)	24.1(5)

Table 1 Legend: Lattice parameter of Biogenic and Abiotically generated hydroxyapatites. All parameters were calculated using TOPAS, (n.d.: not detected)

TEM and Small Angle X-Ray Scattering (SAXS)

Transmission Electron Microscopy identified that the biogenic hydroxyapatite displays a plate-like, anhedral morphology, with particle diameters of approximately 20-30nm (Fig 2A). In contrast, the abiotic hydroxyapatite consisted mainly of relatively crystalline rods, which exceed 50nm in length but are only 1-5nm across (Fig 2C).

Analysis of the SAXS patterns identified that the biogenic hydroxyapatite presents a larger primary particle size than the abiotic hydroxyapatite (Fig 2E), as represented by changes in the 'radius of gyration (Rg) parameter of a Guinier-Porod model fitted to the SAXS patterns. We observed an enlarged Rg for the biogenic hydroxyapatite (4.423 Å +/- 0.0001) in comparison to the abiotic hydroxyapatite (3.772 Å +/- 0.001).

Fig 2: TEM Micrographs, electron diffraction images, and SAXS patterns of biogenic and abiotically synthesised hydroxyapatites

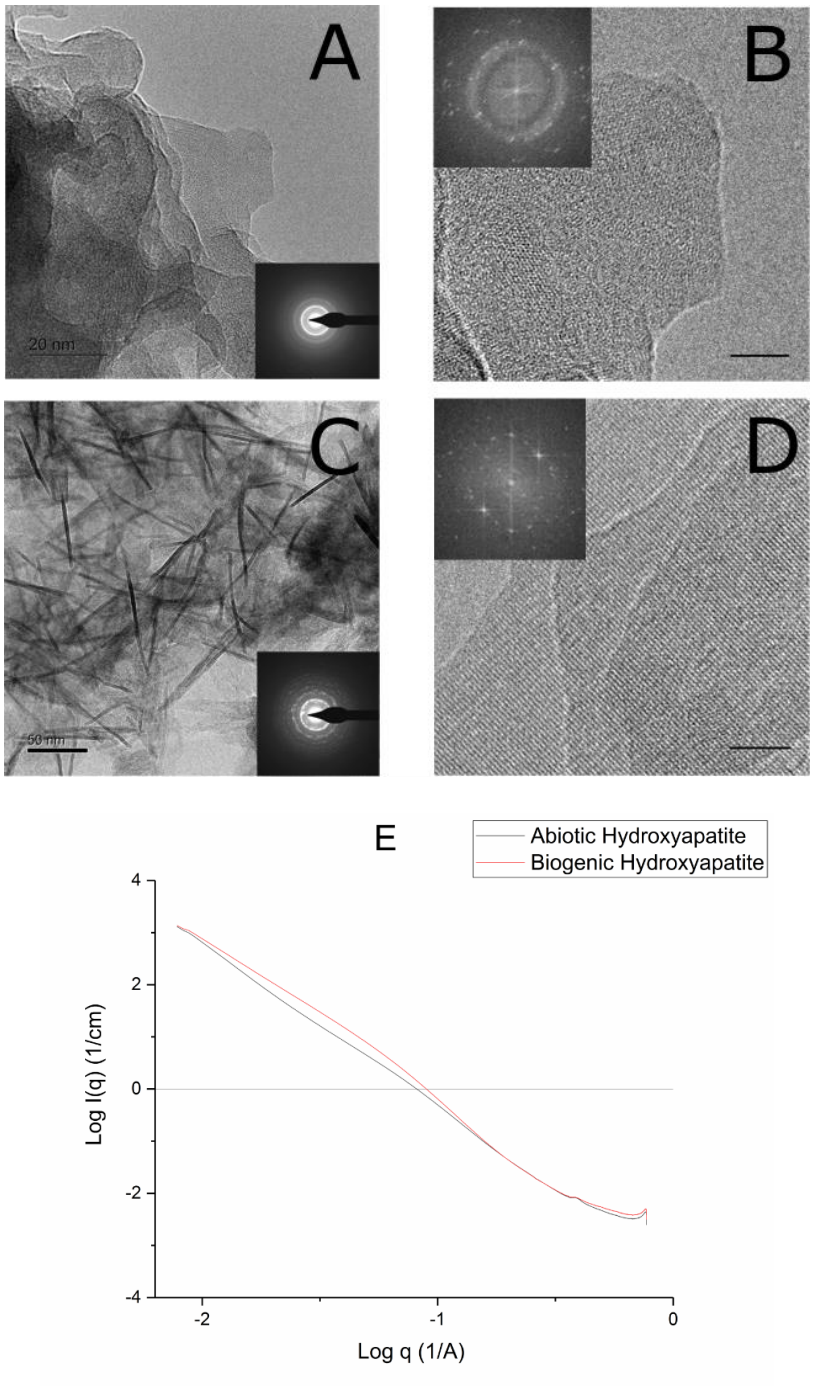

Fig 2 Legend: TEM micrographs of biogenic HAP (A), showing a flat, plate-like nanomorphology with the electron diffraction pattern (inset) demonstrating that this hydroxyapatite has an amorphous, disordered crystal structure. In comparison, the abiotic HAP (C) shows a Needle-like morphology with

a comparatively crystalline, ordered crystal structure (inset). High magnification images show the relative disorder in the atomic lattice structures for the biogenic (B) and abiotic (D) hydroxyapatites, including Fast Fourier Transforms of the images to highlight these changes (inset). The SAXS patterns (E) were fit to a Guinier-Porod model, with a Rg of 3.772 Å +/- 0.001 for the abiotic hydroxyapatite, and a Rg of 4.423 Å +/- 0.0001 for the biogenic hydroxyapatite. SAXS pattern is mean of 3 patterns per sample. Inset images showing lattice fringes and FFT indicate a higher level of disorder in the biogenic precipitate sample in comparison to the abiotic precipitate sample as indicated by increased variations in lattice fringe orientation in the control sample. Scale bar (B & D) is 5nm.

Chemical composition and speciation variations between biogenic and abiotic hydroxyapatite

ICP-OES

Table 2: Elemental Composition of Various Hydroxyapatites as Measured by ICP-OES, TOC, and CHN

	Biogenic HAp Precipitate	**Abiotic HAp Precipitate**	**Biogenic HAp Coating**	**Abiotic HAp Coating**	**Buffered LB Broth**
Ca	18.44 +/- 0.65	47.97 +/- 8.19	37.11 +/- 5.43	40.60 +/- 8.93	0.62 +/- 0.03
Fe	0.02 +/- 0.0008	0.04 +/- 0.02	1.19 +/- 0.19	1.86 +/- 0.24	0.004 +/- 0
P	13.58 +/- 0.68	22.96 +/- 5.64	16.35 +/- 2.3	5.29 +/- 0.95	16.59 +/- 5.03
Si	0.02 +/- 0.002	0.06 +/- 0.01	2.07 +/- 0.17	1.69 +/- 0.62	0.01 +/- 0.001
N	1.38 +/- 0.58	1.48 +/- 1.98	0.06 +/- 0.24	0.05 +/- 0.02	N/A
H	1.59 +/- 0.36	1.05 +/- 0.09	1.22 +/- 0.03	1.14 +/- 0.04	N/A
Total Carbon	6.62 +/- 1.64	1.56 +/- 0.09	3.74 +/- 0.29	5.84 +/- 0.32	N/A

Organic Carbon	5.99 +/- 0.94	0.91 +/- 0.01	0.57 +/- 0.15	0.40 +/- 0.10	N/A
Inorganic Carbon	~0.63	~0.65	~3.17	~5.47	N/A

Table 2 Legend: Elemental Composition of Various Hydroxyapatites as Measured by ICP-OES. All values are mean of N = 3 +/- standard error of the mean. All values are weight %

ICP-OES indicated that iron enrichment was associated with hydroxyapatite formed on OPC, whether the synthesis was carried out in a biogenic or abiotic process. It was identified that high levels of iron were not present in the growth medium in the absence of an OPC substrate (Table 2, 'Buffered LB Broth'). Significant iron enrichment could be observed in both hydroxyapatites formed on OPC, with lower levels observed in both precipitate samples (Table 2).

Inorganic carbon levels were highest in the coating samples, with the abiotic hydroxyapatite having the highest proportion; most likely due to the presence of higher levels of calcite in this sample. Phosphorus levels were lowest in the abiotic HAp coating, being comparable to buffered LB broth alone. This may be linked to the lack of biomass in the abiotic coating deposition process, which could be expected to increase both organic carbon, nitrogen, and phosphorus levels in the biogenic coating versus the abiotic coating; as was generally observed (Table 2).

An increased phosphorus level was observed in the abiotic precipitate, which appears to link with an increased calcium concentration in this same sample. It may be that this increased phosphorus and calcium level is representative of a higher 'purity' hydroxyapatite sample relative to the biogenic system which will contain a higher proportion of biomass. Both total and organic carbon values support this interpretation.

The presence of a cement substrate also has a considerable effect, with ICP-OES revealing similar enrichment in the hydroxyapatite coatings for iron and silicon (Table 2), both of which are present in some quantity in the cement substrate. The influence of the substrate appears to have a greater effect on the association of carbonate and trace metals with the hydroxyapatite, than the changes produced by variation between biogenic and abiotic synthesis methods (Table 2).

FT-IR

Figure 3: FT-IR Analysis of Hydroxyapatite Samples

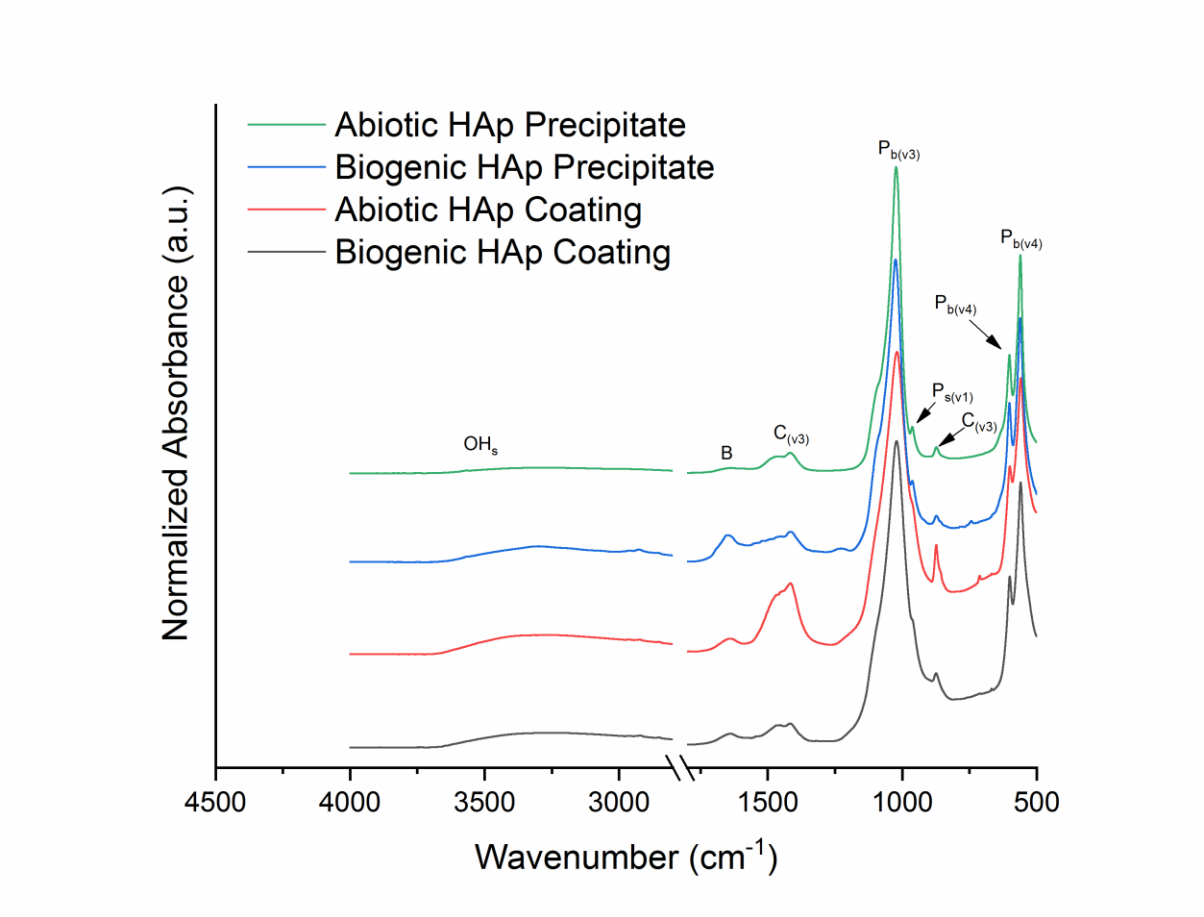

Figure 3: FT-IR analysis of hydroxyapatite samples. '$P_{b(v3)}$' represents the v3 PO_4^{3-} bending vibrational mode , '$P_{b(v4)}$' represents v4 PO_4^{3-} bending vibrational mode.[17] *'$C_{(v3)}$' represents the v3 CO_3^{2-} stretching vibrational mode.*[18, 19] *B represents biological material/amide bonds (likely N-H bending).*[20] *OH_s represents stretching of the O-H group, likely from water.*

Biogenic samples showed broader characteristic phosphate peaks indicating a less ordered lattice structure (Fig 3), which is in agreement with TEM observations (Fig 2). The influence of carbonates from the cement substrate material was clearly observable. A particularly high level of carbonate was noted in the abiotic hydroxyapatite coating.

This observation suggests that the synthesis method may have a significant influence on the ionic content of the hydroxyapatite coating; which is evidenced from the increased carbonate content in the abiotic hydroxyapatite coating sample versus the biogenic coating sample as observed from the XRD patterns, which showed a higher level of calcite in the abiotic hydroxyapatite coating versus the biogenic hydroxyapatite coating (Fig 1, Table 1).

We would suggest this may be attributable to the pH increase in the abiotic coating system was mediated via the use of sodium hydroxide rather than the by-products of bacterial metabolism or gradual dissolution of $Ca(OH)_2$ as in the abiotic precipitate system. The key difference between the methods is a lower rate of pH increase in the biological system versus an immediate increase in the abiotic coating system. Increased pH is associated with increased concentrations of carbonate ions in solution, whereas at low pH bicarbonate and dissolved CO_2 will be of greater abundance.[21] As the treatment times were the same for both methods (20 days), it can be inferred that greater carbonation will be observed in the abiotic coating sample as it was in a carbonate-enriched environment for a larger portion of the incubation period than all other samples examined.

A particularly high 'biological' peak at wavenumber of around 1700cm^{-1} identified a relatively high proportion of biological material in the biogenic precipitate. This would be expected due to the collection of samples using centrifugation leading to more biological material in the analysis versus the coatings, where the biological material can be more easily washed from the solid substrate.

^{57}Fe Mössbauer Spectroscopy

Analysis of the biogenic and abiotic hydroxyapatite coatings on Ordinary Portland Cement (OPC) was undertaken using ^{57}Fe Mössbauer spectroscopy to investigate the oxidation state and coordination environment of iron.[22] A negligible Mössbauer signal was acquired from all other samples, which was expected due to the comparatively low iron content in these materials. The biogenic hydroxyapatite coating on OPC generated a Mössbauer spectrum consistent with the

presence of Fe(III) (Fig 4). Iron in the (III) oxidation state would be the expected form in iron-substituted hydroxyapatite produced under aerobic conditions.[23]

The fitted Mössbauer spectrum (Fig 4) indicates two different Fe(III) sites in the biogenic hydroxyapatite sample. Past investigations have calculated the isomer shift (CS) and quadrupole splitting (Δ) values for iron-substituted hydroxyapatite at 300K.[24] When compared with the results of the present investigation Doublet 1 suggests the presence of Fe(III) in the Ca(2) site of the hydroxyapatite structure, in an octahedral coordination (Table 3).[24]. The results suggest that Doublet 2 identifies iron existing in the 'surface Fe(III)' site; which represents super-paramagnetic nanoparticles similar to haematite with iron in an octahedral coordination.[24]

Figure 4: Fitted Mössbauer Spectrum of Biogenic Hydroxyapatite OPC Coating

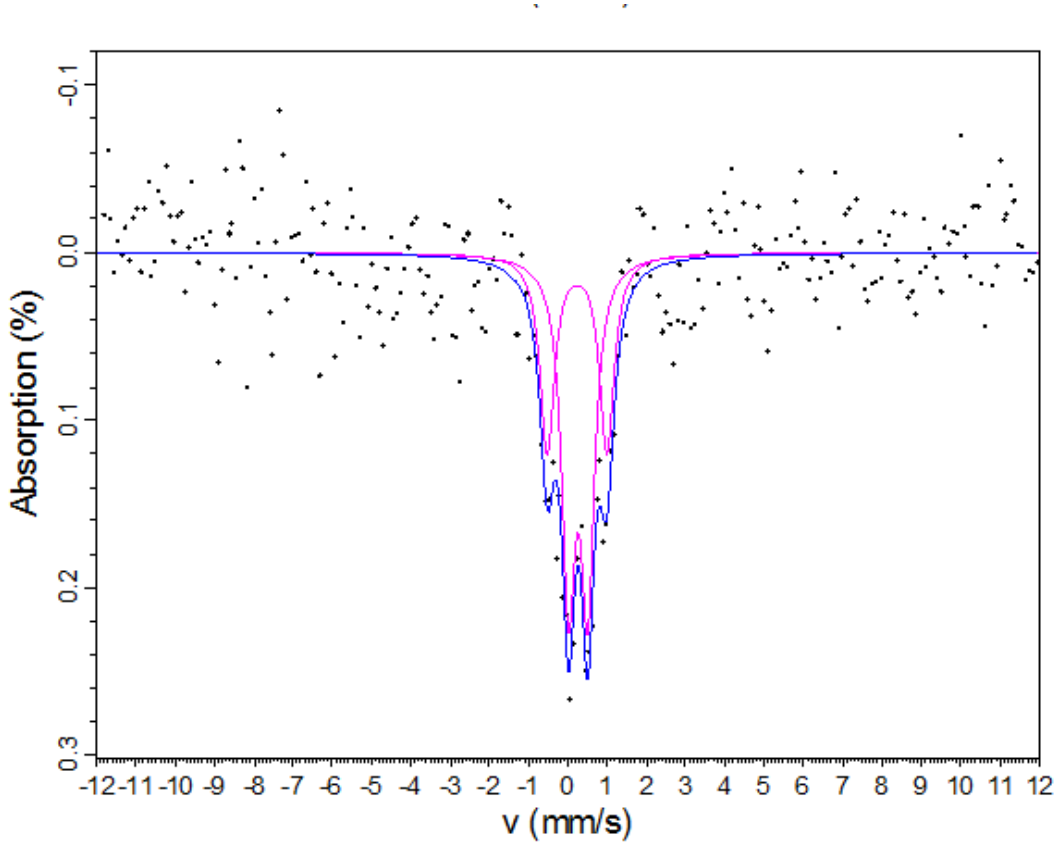

Figure 4: Mössbauer spectrum of biogenic hydroxyapatite OPC coating.

Table 3: Mossbauer Parameters Table

Sample/description		**Centre Shift ($mm\ s^{-1}$)**	**Quadrupole Splitting ($mm\ s^{-1}$)**
Biogenic Hydroxyapatite precipitate	D1	0.23(8)	1.52(20)
	D2	0.26(5)	0.49(10)
Abiotic Hydroxyapatite precipitate	D1	0.48(13)	0.80(41)
	S1	0.1(13)	-
Oct- Fe(III), Ca(2) site (Jiang et al. 2002)		0.23	1.72
Surface Fe(III), superparamagnetic nanoparticles, octahedral coordination (Jiang et al. 2002)		0.22	0.69
Oct- Fe(III) - Ferrihydrite/lepidocrocite (Marco et al. 2000)		0.32	0.61
Oct- Fe(III) - Ferrihydrite (Rout et al. 2014)		0.31	0.68

Table 3: Mossbauer parameters. Doublet (D) and singlet (S) experimental data is included. Data extracted from Marco et al. (2000) [25] *and Rout et al. 2014* [26].

In comparison, the abiotic hydroxyapatite displayed an altered Mössbauer spectrum of which 80% of the spectral area represented Fe(III) in a symmetric six-fold coordination environment [27] with the remaining 20% being metallic or cubic iron (Fig 5). The spectra matches well with reported Mössbauer spectra for Goethite (FeOOH) at 300K (Goethite 125086 “Limonite”, Mineral Spectroscopy Database, Mount Holyoke College)[28], and previously reported magnetite-HAp composites [27] where a six-fold coordination of Fe(III) can be expected.[29]

Figure 5: Fitted Mössbauer Spectrum of Abiotic Hydroxyapatite OPC coating

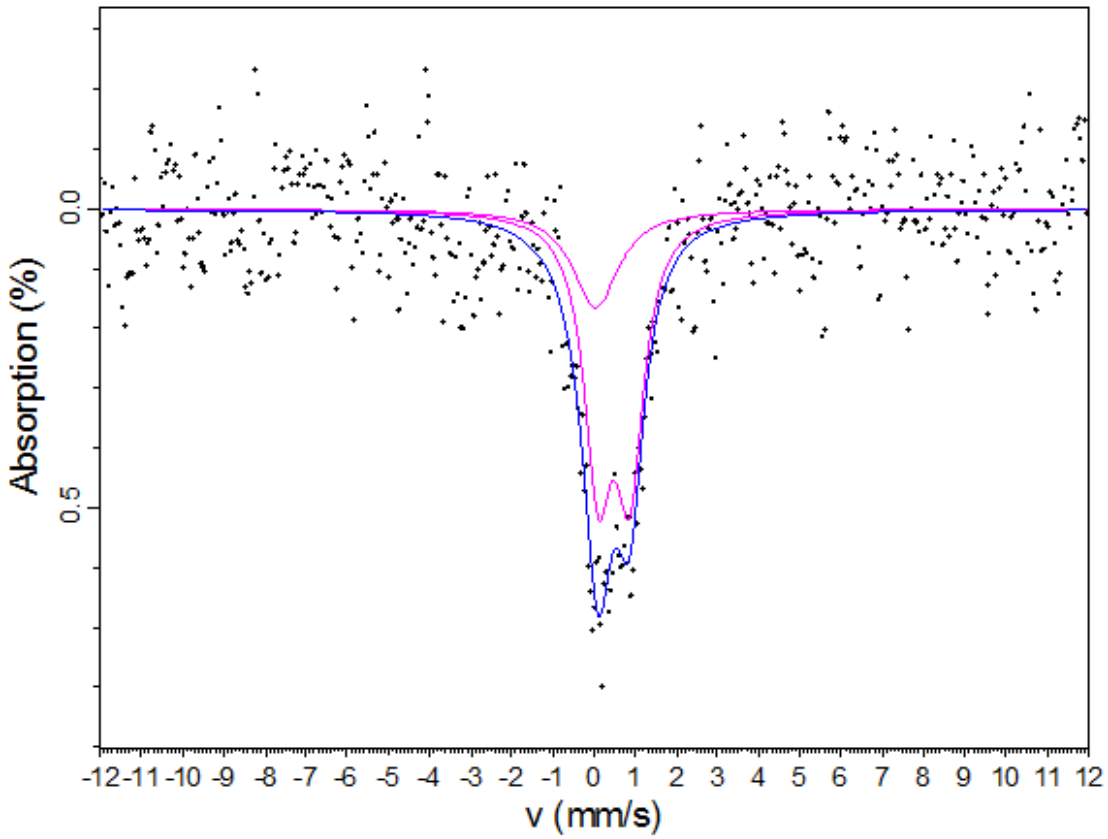

Figure 5: Mössbauer spectrum of abiotic hydroxyapatite OPC coating

Conclusions

We have observed structural and chemical differences between the biogenic and abiotically-synthesised hydroxyapatites via analysis of XRD patterns, SAXS patterns, and TEM. When formed on OPC, we identify that these hydroxyapatites will associate with iron and carbonate, likely drawn from the cement substrate material, as measured using ICP-OES and SEM-EDS.

Crystallite size was observed to be increased in the biogenic hydroxyapatite, with a plate-like and relatively amorphous morphology visible under TEM in comparison to the crystalline rods in the abiotic hydroxyapatite. These observations were consistent across XRD, SAXS, and TEM analysis. The

observed capacity for *Pseudomonas fluorescens* to generate an amorphous hydroxyapatite versus a rod-like abiotic hydroxyapatite has not been reported in the literature to date.

Hydroxyapatite morphology is linked to its physical properties, which will ultimately affect the final applications of the material. The increased surface area of spherical and plate-like morphologies has also been linked to superior drug loading and release in comparison to other hydroxyapatite forms.[30] Spherical or plate-like hydroxyapatites can be found in bone material, and synthetic spherical hydroxyapatites have been associated with enhanced bone formation *in vitro*.[7] Plate-like hydroxyapatites have been identified as the ideal morphology for stiffening isotropic materials, in comparison to spherical and fibrous morphologies. [8] Consequently, *Pseudomonas*-induced hydroxyapatite deposition may offer a novel synthesis method for these plate-like hydroxyapatite morphologies.

FT-IR analysis identified there is a considerable level of carbonate present in the abiotic hydroxyapatites, generally higher than that observed in biogenically synthesised hydroxyapatite; this observed carbonate may be from calcite and XCO2 substitution/surface adsorption into the hydroxyapatite. We suggest that the higher levels of carbonate observed in the abiotic samples may be attributed to a longer time incubation period in a higher-pH and therefore carbonate-rich environment.

Interpretation of the Mössbauer spectra of hydroxyapatite formed directly on Ordinary Portland Cement suggests the presence of 'superparamagnetic' iron-hydroxyapatite nanoparticles. We therefore suggest that the present work identifies *Pseudomonas*-induced biomineralisation as a novel method for the generation of iron- and/or carbonate-associated hydroxyapatites under simple reaction conditions, and that varying synthesis methods has the capacity to alter hydroxyapatite particle morphology.

Acknowledgements

We thank Diamond Light Source for access to beamline I22 (proposal number sm17097-1) that contributed to the results presented here. This work benefited from the use of the SasView application, originally developed under NSF award DMR-0520547. SasView contains code developed with funding from the European Union's Horizon 2020 research and innovation programme under the SINE2020 project, grant agreement No 654000. Thanks to Dr Tatyana Peshkur of the University of Strathclyde for assistance with ICP-OES analyses.

References

1. **Macaskie LE, Yong P, Paterson-Beedle M, Thackray AC, Marquis PM, *et al.*** A novel non line-of-sight method for coating hydroxyapatite onto the surfaces of support materials by biomineralization. *J Biotechnol* 2005;118:187–200.

2. **Gangappa R, Yong P, Singh S, Mikheenko I, Murray AJ, *et al.*** Hydroxyapatite Biosynthesis by a *Serratia* sp. and Application of Nanoscale Bio-HA in the Recovery of Strontium and Europium. *Geomicrobiol J* 2016;33:267–273.

3. **Turner RJ, Renshaw JC, Hamilton A**. Biogenic Hydroxyapatite: A New Material for the Preservation and Restoration of the Built Environment. *ACS Appl Mater Interfaces* 2017;9:31401–31410.

4. **Wang W, Oaki Y, Ohtsuki C, Nakano T, Imai H**. Formation of c-axis-oriented columnar structures through controlled epitaxial growth of hydroxyapatite. *J Asian Ceram Soc* 2013;1:143–148.

5. **Roveri N, Battistella E, Bianchi CL, Foltran I, Foresti E, *et al.*** Surface enamel remineralization: Biomimetic Apatite Nanocrystals and Fluoride Ions Different Effects. *J Nanomater*;2009. Epub ahead of print 2009. DOI: 10.1155/2009/746383.

6. **Zhao W, Xu Z, Yang Y, Sahai N**. Surface energetics of the hydroxyapatite nanocrystal-water interface: A molecular dynamics study. *Langmuir* 2014;30:13283–13292.

7. **Kalia P, Vizcay-Barrena G, Fan JP, Warley A, Di Silvio L, *et al.*** Nanohydroxyapatite shape and its potential role in bone formation: an analytical study. *J R Soc Interface* 2014;11:20140004–20140004.

8. **Gupta HS, Guitia F**. An effective morphology control of hydroxyapatite crystal via hydrothermal synthesis. *Cryst Growth Des* 2009;466–74.

9. **T. Sänger A, Kuhs W**. Structural Disorder in Hydroxyapatite. *Zeitschrift Fur Krist - Z Krist* 1992;199:123–148.

10. http://www.sasview.org/.

11. **Markgraf S, Reeder R**. High-temperature structure refinements of calcite and magnesite. *Am Miner* 1985;70:590–600.

12. **Landi E, Celotti G, Logroscino G, Tampieri A**. Carbonated hydroxyapatite as bone substitute. *J Eur Ceram Soc* 2003;23:2931–2937.

13. **El Yacoubi A, Massit A, Fathi M, Chafik El Idrissi B, Yamni K**. Characterization of silicon-substituted hydroxyapatite powders synthesized by a wet precipitation method. *IOSR J Appl Chem* 2014;7:24–29.

14. **Okazaki M, Takahashi J, Kimura H**. Crystallinity and solubility behavior of iron-containing fluoridated hydroxyapatites. *J Biomed Mater Res* 1986;20:879–886.

15. **Kramer E, Zilm M, Wei M**. A Comparative Study of the Sintering Behavior of Pure and Iron-Substituted Hydroxyapatite. *Bioceram Dev Appl* 2013;3:1–9.

16. **Wang J, Nonami T, Yubata K**. Syntheses, structures and photophysical properties of iron

containing hydroxyapatite prepared by a modified pseudo-body solution. *J Mater Sci Mater Med* 2008;19:2663–2667.

17. **Kabir SF, Ahmed S, Mustafa AI, Ahsan M, Islam S**. Synthesis and Characterization of Fe-doped Hydroxyapatite. *Bangladesh J Sci Ind Res* 2007;47:1–8.

18. **Rehman I, Bonfield W**. Characterization of hydroxyapatite and carbonated apatite by photo acoustic FTIR spectroscopy. *J Mater Sci Mater Med* 1997;8:1–4.

19. **Tavender SM, Johnson SA, Balsom D, Parker AW, Bisby RH**. In solution studied by resonance raman spectroscopy. *Laser Chem* 1999;19:311–316.

20. **Brangule A, Gross KA**. Importance of FTIR spectra deconvolution for the analysis of amorphous calcium phosphates. *IOP Conf Ser Mater Sci Eng*;77. Epub ahead of print 2015. DOI: 10.1088/1757-899X/77/1/012027.

21. **Fresenius W, Quentin KE, Schneider W, others**. *Water analysis; a practical guide to physico-chemical, chemical and microbiological water examination and quality assurance*. Springer-Verlag; 1988.

22. **Gutlieh P, Fitzsimmons BW, Ruffer R, Spiering H**. *Mössbauer Spectroscopy: Proceedings of the Fifth Seeheim Workshop*. Seeheim; 2002.

23. **Li Y, Widodo J, Lim S, Ooi CP**. Synthesis and cytocompatibility of manganese (II) and iron (III) substituted hydroxyapatite nanoparticles. *J Mater Sci* 2012;47:754–763.

24. **Jiang M, Terra J, Rossi AM, Morales MA, Baggio Saitovitch EM, *et al.*** Fe2+/Fe3+ substitution in hydroxyapatite: Theory and experiment. *Phys Rev B* 2002;66:224107.

25. **Marco JF, Gracia M, Gancedo JR, Martín-Luengo MA, Joseph G**. Characterization of the corrosion products formed on carbon steel after exposure to the open atmosphere in the Antarctic and Easter Island. *Corros Sci* 2000;42:753–771.

26. **Rout K, Mohapatra M, Layek S, Dash A, Verma HC, *et al.*** The influence of precursors on phase evolution of nano iron oxides/oxyhydroxides: Optical and magnetic properties. *New J Chem* 2014;38:3492–3506.

27. **Boda SK, Anupama A V., Basu B, Sahoo B**. Structural and magnetic phase transformations of hydroxyapatite-magnetite composites under inert and ambient sintering atmospheres. *J Phys Chem C* 2015;119:6539–6555.

28. **Mount Holyoke College**. Geothite 125086, 'Limonite', Red River, Louisiana, 15 mg, T-Series. *Mineral Spectroscopy Database*. https://www.mtholyoke.edu/courses/mdyar/database/index.shtml?group=hydrox&species=125086 (2015, accessed 1 July 2018).

29. **Bleam W**. Chapter 8 - Surface Chemistry and Adsorption. In: Bleam W (editor). *Soil and Environmental Chemistry (Second Edition)*. Academic Press. pp. 385–443.

30. **Uskoković, Vuk, Batarni Samir Shariff, Schweicher Julien, King Andrew DT a**. The Effect on Calcium Phosphate Particle Shape and Size on their Antibaterial and osteogenic Activity in the Delivery of Antibiotics in vitro. 2014;5:2422–2431.

Chapter 6: Hydroxyapatites as Cement Coating Materials with Varied Surface Properties

All literature reviews, practical work, data analysis, and manuscript preparation was carried out by Ronald Turner, with guidance provided by Andrea Hamilton and Joanna Renshaw, with the following exceptions:

- Focus variation data collection was carried out on a collaborative basis by Dr Alan Richardson of Northumbria University, UK
- Guidance on research direction was provided on a collaborative basis by Dr Alan Richardson of Northumbria University, UK
- Measurements of hardness/elastic modulus were carried out on a collaborative basis by Will Williamson of the University of Manchester, UK
- X-CT data was collected on a collaborative basis by Dr Alice Macente (Strathclyde)

Chapter 6 - Hydroxyapatites as Cement Coating Materials with Varied Surface Properties

Abstract

Cement is the most versatile and widely-used of all building materials. The development of novel cement coatings is a topic of considerable and on-going research interest. One such coating of interest is hydroxyapatite, a naturally forming calcium phosphate mineral found in bone and teeth, which has potential application for medical implants and building materials. In many environments where cement is used, the topographic properties (e.g. roughness) of generated hydroxyapatite coatings are important. Surface roughness is particularly important in the function of building preservation, as it is linked to appearance, texture, and hydrophobicity. Hydroxyapatite also has hydrophobic properties linked to its roughness, which could be usefully applied in building preservation. We identify that the hydrophobicity properties of hydroxyapatite may be variable depending on whether it is produced abiotically or biogenically. We show that in the absence of bacteria, but in the presence of the phosphate, brushite [$Ca(HPO_4) \cdot 2H_2O$] is precipitated onto the cement block. The addition of *Pseudomonas fluorescens* to the medium generates an increased pH, leading to the precipitation of hydroxyapatite [$Ca_{10}(PO_4)_6(OH)_2$]. In this study, we identify that a bacterially-synthesised hydroxyapatite layer presents a higher average roughness compared to untreated cement, and a lower roughness than brushite. We establish that abiotic synthesis of hydroxyapatite produces the smoothest observed surface finish. We demonstrate that the deposited hydroxyapatite layer is more hydrophobic than both untreated cement, and cement coated with brushite; but less hydrophobic than the hydroxyapatite coating produced abiotically. These variations in roughness and hydrophobicity with synthesis method allow for 'tuning' of the hydroxyapatite coating properties depending upon the desired final application. Through X-CT imaging of the sample and observation of positive skewness (Rsk) values of the 3D surface parameters, the hydroxyapatite coatings were observed to form a layer covering over 99.8% of the

substrate with a coating of approximately 130µm thickness. We establish that the hardness of biogenic and abiotic hydroxyapatites is comparable, and both have a lower modulus but higher hardness than values for brushite reported in the literature. We discuss the relevance of these observations to the use of hydroxyapatite coatings in the built environment. We propose that these hydroxyapatites could be applied as a hydrophobic sealant to cementitious materials where water ingress may cause deterioration or be otherwise undesirable. For example, in cases where there is no trapped water that may expand during freezing leading to further damage.

Introduction

Hydroxyapatite, a calcium phosphate mineral with the general formula $Ca_{10}(PO_4)_6(OH)_2$, is found naturally in tooth and bone material. Hydroxyapatite has been investigated as a cement coating material, with relevance to cultural heritage preservation and environmental remediation.[1,2] It has shown promise in recent work for the consolidation and/or repair of building materials such as carbonate stones,[3] limestones,[4] and marbles.[5] Hydroxyapatite coatings are also of interest as a coating material for the uptake of environmental contaminants.[2,6] However, the capacity of bacteria to generate these hydroxyapatite minerals 'in-situ' on cement has received little attention in the literature to date until very recently,[7] and the applied properties of these hydroxyapatites remains unstudied.

The generation of hydrophobic surface coatings for concretes has been of significant recent research interest.[8–11] There is an increasing need for such coatings due to the corrosive effects of water and chloride ingress to cementitious building materials.[11,12] Hydrophobicity is linked to the surface topography parameters, with increased micro- and nano-scale roughness generally associated with increased hydrophobicity.[13,14]

The surface micro- and macro-topography of mineral-coated materials is also associated with altered biocompatibility of medical implant devices.[15,16] Roughened hydroxyapatite coated materials are associated with higher implant bond strength in dental implants.[17] Optimisation of dental implant

topographies therefore has potential to increase the success of implant-related dental restorative work, and recent work has examined the topographic properties of several dental implant materials.[18] Increased roughness is also associated with increased surface area, which may enhance the uptake of environmental contaminants by the hydroxyapatite.

Different levels of roughness and hydrophobicity may be desirable depending upon the ultimate application of the cementitious material. Examples may include architectural restoration or building preservation where a smooth, hydrophobic finish is desirable; or environmental remediation applications where a rougher, less hydrophobic coating is of greater utility. Consequently, the ability to 'tune' these properties will be of considerable value.

In this paper, we examine and compare the surface roughness, topographic parameters, and hydrophobicity of bacterially-generated and abiotically-synthesised hydroxyapatite layers on a cement substrate, compared to cement treated with sterile growth medium which generates a brushite [$Ca(HPO_4) \cdot 2H_2O$] coating, and completely untreated cement. We identify that by utilising different synthesis methods, it is possible to generate variations in the roughness and hydrophobicity of these coatings on a cement substrate.

Experimental Methodology

Cement Substrate Preparation

Ordinary Portland Cement (OPC) coupons (a cuboid block of cured cement; measuring approximately 5 x 2 x 1cm) were manufactured and cured by means of the following: 500 g cement powder ('Multicem 32,5R (CEM-II/A-LL)' , Hanson Heidelberg) was hydrated with 200g water to a water:cement ratio of 0.4 (wt/wt). The grout paste was mixed for 15 minutes at low speed using rotary mixer. The paste was cast into 5x2x1 cm silicone moulds and stored at 100% relative humidity and 20^{o}C for 24 hours. Samples were then demoulded and cured in a saturated solution of $Ca(OH)_2$ at 20^{o}C for at least 28 days.

Phosphate Mineral Formation on Cement

Biotic and abiotic hydroxyapatite [$Ca_5(PO_4)_3(OH)$] and brushite [$CaHPO_4.2H_2O$] layers were generated onto the surfaces of the OPC coupons by means of the following method: For the biogenic apatite, suspensions containing *Pseudomonas fluorescens* biofilms were incubated in flasks each containing one coupon in a buffered lysogeny broth (LB) at 20^{o}C and gently rotated (Yellowline OS2, speed setting = 1) for 20 days, as described previously.[7] The final suspensions were measured at pH 9.1. Control experiments were incubated as above with the OPC coupons but in the absence of a *P. fluorescens* bacterial inoculum.

In the absence of bacteria there was an insufficient rise in pH to generate hydroxyapatite on an OPC coupon, with brushite forming instead. Synthesis of abiotic hydroxyapatite was subsequently generated by adjusting the pH before autoclaving. In order to synthesise an 'abiotic hydroxyapatite coating' on OPC, the protocol was carried out as described for the 'control' samples. However, prior to autoclaving the growth medium the pH was adjusted from an initial pH of 6.3 to 9.0 by preparing 90ml of buffered LB broth made up to a final volume of 100ml with 1M NaOH.

Prior to topographic scanning, the coupons were removed from the flasks; rinsed with deionised water and mild agitation to remove any biofilm material, and vacuum-packed prior to analysis to minimise any degradation. Coupons of fully cured but otherwise untreated cement were also rinsed and topographic scans collected.

Formation of biotic and abiotic hydroxyapatite precipitates

To generate biogenic and abiotic hydroxyapatites in the absence of a cement substrate for nano-indentation studies, the protocol was followed as before but with the addition of 1gL^{-1} $Ca(OH)_2$ to the growth medium, both in the presence and absence of bacteria to respectively synthesise biogenic and abiotic hydroxyapatites. To collect the precipitates from the liquid media, 10ml of medium was transferred to a sterile 15ml centrifuge tube, and the precipitate collected via centrifugation at 8000g for 20 minutes, at 20^{o}C. The supernatant was then decanted and the

collected sediment pellet re-suspended in distilled water to wash and re-centrifuged. The supernatant was discarded and the precipitate air-dried at 37^{o}C for 24 hours.

Topographic Scanning

The surface topography of each sample was mapped using focus-variation microscopy (Alicona 4G infinite focus scanner). Each of the three samples – the biogenic hydroxyapatite, abiotic hydroxyapatite, brushite, and unmodified cement were all analysed following the treatment processes described in the section 'Phosphate Mineral Formation on Cement'.

X-Ray Computed Tomography (X-CT) Analysis

X-CT data was collected using a Nikon XT H 320. X-CT analysis generated a total of 2000 X/Y-Slices, and 600 Z-slices through the sample, with a voxel size of 16.5µm^3. X-CT datasets were segmented into three sections ('coating', 'cement', and 'background') using Trainable Weka Segmentation software.[19] Following segmentation, measurements of coating thickness and substrate coverage were carried out using Fiji.[20]

Hydrophobicity Measurements

Cement coupons were rinsed thoroughly with DI water and dried under a stream of nitrogen gas. Three 20µL droplets of deionised water were spotted onto the surface of each coupon. Images were captured using a Nikon digital camera. Droplet contact angle measurement was performed using Fiji and the LBADSA plugin.[21]

Nano-indentation Measurements

Direct nano-indentation measurements of the coatings on the cement substrate were not feasible due to the low thickness of the coating and high hardness of the substrate, so measurements of modulus and hardness were collected from precipitated biogenic and abiotic hydroxyapatite samples using a Nano Indenter (MTS Nano Indenter XP).

Results and Discussion

Results

Calcium phosphate minerals were precipitated on all coupons incubated in LB media, but the specific mineral formed was dependent upon the presence of bacteria and pH. When bacteria were present hydroxyapatite – a phosphate mineral with the chemical formula $Ca_{10}(PO_4)_6(OH)_2$ - was found to form on the coupons in past XRD and FT-IR studies.[7] The biochemical mechanisms underlying this differential deposition process have been described in previous work.[7] When bacteria were absent, brushite – a phosphate mineral with the formula $CaHPO_4.2H_2O$ - formed on the coupons at pH 6.3 (initial pH of the culture medium). However, if the pH of the abiotic culture medium was raised to pH 9.0, then hydroxyapatite was observed form instead of brushite.

The surface of the biogenic hydroxyapatite-coating, abiotically-generated hydroxyapatite-coating, brushite-coated (no bacteria), and untreated cement samples were examined via focus-variation microscopy, with the results summarised in **Table 1**.

Table 1: Topography of Biogenic Hydroxyapatite, Abiotic Hydroxyapatite, Brushite, and Untreated Cement

Parameter	Biogenic Hydroxyapatite	Abiotic Hydroxyapatite	Brushite	Untreated Cement
Coating Thickness (µm)	130.0 ± 7.1 A	161.6 ± 9.3 A	260.1 ± 26.7 B	N/A
Coating Surface Coverage (%)	99.8 ± 0.1 *	100 ± 0.0 *	100 ± 0.0 *	N/A
Ra (µm)	7.86 ± 2.24 A	1.65 ± 0.13 C	14.59 ± 2.24 B	3.75 ± 0.758 C

Rq (µm)	10.07 ± 2.66 A	2.23 ± 0.16 C	19.76 ± 0.11 B	6.28 ± 1.33 A
Rsk	0.58 ± 0.200 A	-0.07 ± 0.71 A	1.40 ± 0.616 A	-2.76 ± 0.667 B
Rku	3.85 ± 0.592 *	7.93 ± 2.79 *	8.80 ± 6.38 *	14.77 ± 5.28 *

Table 1: images of coated OPC cement coupons. All Results are mean of N =3 ± SEM. Coating thickness and surface coverage were quantified by measurements of segmented 3D X-CT images. Ra (roughness average), Rq (Root-Mean-Squared roughness), Rsk (skewness), and Rku (kurtosis) were measured using focus-variation microscopy. For each parameter, statistical significance ($p<0.05$) was established by a 1-way ANOVA to establish the effect of each treatment, and treatment similarities were identified with an uppercase letter (A-C) via Tukey post-hoc analysis. Differences between values within a single row which share an uppercase letter are not statistically significant ($a = 0.05$). Differences in coating surface coverage and Rku were not found to be statistically significant via 1-way ANOVA ($p>0.05$); these values are indicated by a star (*) symbol.

Both the biogenic hydroxyapatite and brushite coated samples had a higher average roughness (Ra) than an untreated cement coupon, at 7.86 and 14.59µm respectively compared against 3.75µm. However, there was no statistically significant difference in the Root-Mean-Squared roughness (Rq) between the biogenic hydroxyapatite coated and untreated samples, whilst the brushite-coated sample had an Rq three times greater than the untreated sample. This can be expected due to the increased sensitivity of Rq to outlying measurements, representing the rougher, less consistent topography of the brushite coating. Ra for the abiotic hydroxyapatite coating was statistically the same as the untreated sample, and Rq was the lowest of all samples measured, indicating that this abiotic coating presented the smoothest average surface roughness of all samples, by at least a factor of 2. The Ra/Rq ratio for the abiotic hydroxyapatite was 1.35, in comparison to 1.67 for the

untreated sample. This observation suggests that the abiotic coating process reduces the presence of any asperities present on the cement surface, generating a smoother and more ordered surface topography than that present on untreated cement.

Rq, Rsk (skewness), and Rku (kurtosis) analyses offer a statistical description of the distribution of peak width, symmetry, and shape respectively.[18] The negative Rsk value for the untreated sample indicates a surface with more pores than peaks; or a 'perforated' surface.[18] The Rsk values for the biogenic HAP, abiotic HAP and the brushite coatings were all statistically similar and all higher than the untreated sample; this demonstrates reduction in surface porosity. Both biogenic and brushite-coated materials had positive Rsk values, identifying relatively high peaks and shallow valleys; or a pointed surface. Rsk measurements of the abiotic coated sample were approximately zero, which was expected due to the very smooth, flat nature of this coating.

Rku analysis showed that all four samples had a kurtosis greater than 3, representing a 'leptokurtic' surface profile which identifies that the distribution of topographic measurements are concentrated to a high extent around the mean value when compared to a normal distribution. Notably, the Rku of the biogenic hydroxyapatite-coated sample is the lowest and least variable of all the samples, being close to 3. In this analysis, Rku suggests that the peaks and valleys of the biogenic hydroxyapatite-coated substrate are closer together than on the abiotic hydroxyapatite, brushite-coated, and untreated cement samples. However, 1-way ANOVA suggests that the differences in Rku between the four sample materials are not statistically significant. As such, limited inference should be drawn from the Rku analysis.

X-CT analysis of the samples (Table 1) identified that an average of 99.8% of the substrate was coated with hydroxyapatite when the biogenic deposition process was used. The abiotic hydroxyapatite and brushite coatings generated substrate coverage of 100% (Table 1). Image analysis revealed that the average biogenic hydroxyapatite coating thickness was approximately 130µm, which was statistically similar to the abiotic hydroxyapatite coating thickness of

approximately 160µm. The brushite layer exceeded 260µm in thickness, being significantly greater than the other coatings.

In the present study, the abiotic-generated hydroxyapatite coating was the most hydrophobic treatment observed, followed by bacterially-deposited hydroxyapatite (**Figure 1**). Both hydroxyapatite treatments are more hydrophobic than untreated cement; and considerably more hydrophobic than the brushite-coated sample (Fig 1).

Figure 1: Hydrophobicity Measurements of Sample Cements

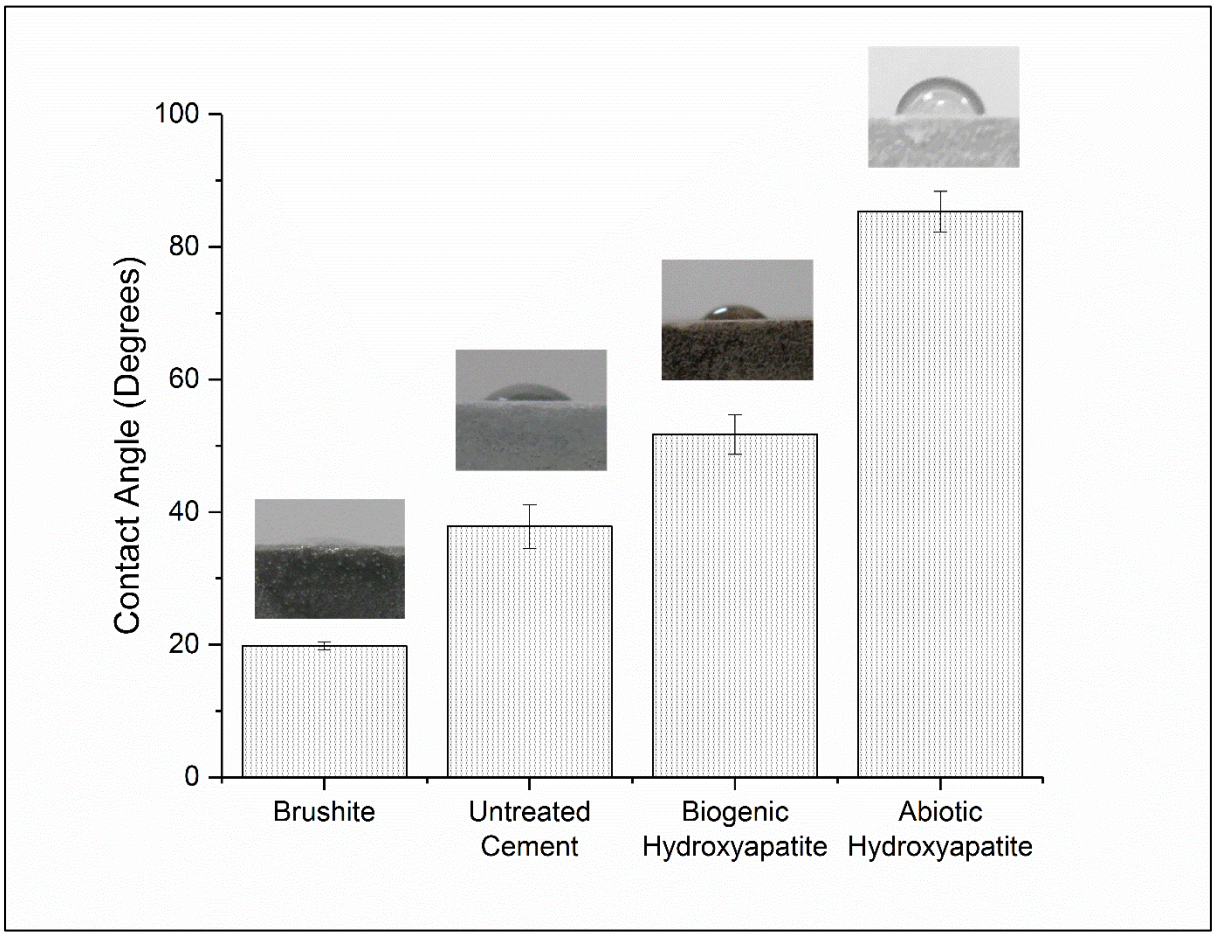

Figure 1: Bar chart of the mean hydrophobicity of the sample's surface measured by water droplet contact angle. The abiotic hydroxyapatite-coated sample is most hydrophobic, and the Brushite-coated sample is the least hydrophobic. Error bars are the SEM (n = 3) and all differences between

samples are statistically significant (ANOVA, $p < 0.001$). Example images of droplets are included above each sample.

Brushite has received attention as a 'calcium phosphate cement' (CPC), which are observed to be generally hydrophilic.[22] It has been observed that high strength hydrogen bonding takes place between water molecules and the brushite coating, which can be expected as brushite contains water layers as part of its crystal structure.[23] Brushite is considerably more soluble than apatites.[24,25] Additionally, brushite has been observed to have an interfacial energy of 4.5mJ.m^{-2}, in comparison to 8mJ.m^{-2} for apatites.[26] Increased interfacial tension can be linked to increased hydrophobicity,[26] although this has not been directly observed in calcium phosphate minerals to date. Together, these factors may account for the low hydrophobicity observed on the brushite-coated cement samples when compared to the hydroxyapatites.

Hardness of the biogenic and abiotic hydroxyapatites formed as precipitates was measured and were statistically similar (**Table 2**). Hardness of the hydroxyapatites is low when compared to literature values for hydroxyapatites sintered at >1150^{o}C,[27] but is comparable to values for lower-temperature sintering at <700^{o}C.[28] The measured hardness for both hydroxyapatites was higher than literature values for brushite, as would be expected based on their respective positions on the Moh's hardness scale; where brushite is typically measured as 2.5, compared to 5 for apatites.[29]

Table 2: Measurements of Modulus and Hardness of different calcium phosphate minerals

Sample	Elastic Modulus (GPa)	Hardness (GPa)
Biogenic hydroxyapatite	4.23 ± 1.32	0.07 ± 0.04
Abiotic hydroxyapatite	4.78 ± 0.46	0.09 ±0.008
Brushite*/**	6.6 ± 0.4*	0.0107 ± 0.002**

*Table 2: Measurements of elastic Modulus (GPa) and Hardness of biogenic hydroxyapatite, abiotic hydroxyapatite, and brushite. Reported measurements for biogenic and abiotic samples are mean of N = 3 ± Standard error of the mean. *Values for brushite are from results reported by Charriere et al (2001).*[30] ***For brushite, measurements were of strength in compression rather than hardness.*[30]

Discussion

Building Preservation – Coverage, Hydrophobicity, and Hardness

The use of hydroxyapatite as a novel consolidant for building materials has been a topic of significant recent research interest.[3,4,31] Hydroxyapatite presents certain advantages over alternative surface coatings such as calcite. Hydroxyapatite has a dissolution rate approximately four orders of magnitude less than calcite.[3] Calcite has been of recent interest as a coating material. However, atmospheric pollutants may react with calcite to produce gypsum, leading to deterioration of the surface of calcite-rich building materials such as marble; a process described as 'sugaring'.[5] In this context, hydroxyapatite coatings may provide similar crack sealing and consolidation effects as calcite precipitation, while generating a cohesive layer which is more resistant to deterioration. Both brushite-coated and hydroxyapatite-coated cement samples presented a 'coated' surface, which minimised pores and cracks and positive Rsk values were observed (Fig 1). This can be expected to reduce the rate of deterioration in real-world applications.[32]

Variations in hydroxyapatite synthesis method generated variable surface roughness values and coating thicknesses (Table 1). This may have significance in a number of contexts, where it is desirable to produce a surface coating to reduce pores and cracks, while minimising the increase in irregularity and roughness and producing a relatively hydrophobic surface.

Hydrophobicity is a desirable property for concretes; with water and chloride ingress associated with the corrosion of concrete reinforcement materials such as steel rebar.[12] The development of hydrophobic concretes has therefore been of recent research interest.[8,9,33] The generation of

hydrophobic cements through the incorporation of biofilm into mortar material has been associated with increased roughness on the micro- and nano-scale.[10] We observed that biogenic hydroxyapatite was considerably less hydrophobic than the abiotic hydroxyapatite (Fig 2), with a contact angle of ~50^{o} versus ~85^{o}. This observation may at first appear surprising, in light of recent work which has identified that biological material enhances the hydrophobicity of ceramics, with contact angles >70 degrees appearing attainable.[10] However, we note that even the biogenic hydroxyapatite is significantly more hydrophobic than the baseline hydrophobicity observed on untreated cement of ~37^{o} (Fig 2). The low measured roughness of the abiotic hydroxyapatite coating would not appear to suggest a high level of hydrophobicity (Fig 1).[34]. However, in the specific case of hydroxyapatite – which has been recognised for its tuneable hydrophobicity under certain conditions [35] – increased roughness has been linked with decreased contact angle and therefore lower hydrophobicity.[36]

The results of the present study do not suggest a truly 'hydrophobic' (Contact Angle >90^{o}) surface coating is generated when hydroxyapatite is deposited. However, the relative increase in hydrophobicity of cements coated with hydroxyapatite is comparable to mortars generated through the incorporation of small amounts of biofilm material,[10] and is significantly higher than reported hydrophobicities for unmodified brushite-coated cements.[10,33] The contact angles achieved using an abiotic coating exceed those measured following silanisation,[37] but cannot attain high contact angles observed using 'super-hydrophobic' treatments such as PTFE.[38]

Hardness is a desirable quality for a building coating material as it will enhance wear resistance. The marginally reduced stiffness of biogenic hydroxyapatite in comparison to abiotic hydroxyapatite – coupled with increased hardness in comparison to alternative calcium phosphates – may confer some resistance to crack formation under environmental pressures. The elastic modulus was lower for both measured hydroxyapatite samples when compared to literature values for brushite (Table 2), however it must be noted that the differences observed were not statistically significant.[30] The

modulus was however lower than the 6.0GPa reported by Martin et al. (1995) as typical of calcium-deficient hydroxyapatites formed at physiological temperatures.[27] The observed reduction in modulus however may identify that the biogenic and abiotic hydroxyapatites investigated in this work have a greater mechanical flexibility when compared to more crystalline calcium phosphates examined by others.[27] The biogenic hydroxyapatite appeared to have a slightly lower and more variable modulus than the abiotic hydroxyapatite, possibly due to residual biofilm material present in the hydroxyapatite. The incorporation of biofilm material with ceramics has been hypothesised to alter its mechanical properties,[10] although there has been no experimental investigation to date. The results of the present study identify that the incorporation of biomass into cement-coating materials such as hydroxyapatite may not have a significant effect on the bulk material hardness and elastic modulus.

Environmental Remediation

Hydroxyapatite is also of interest in producing building material coatings with active environmental remediation capacities. Biogenic hydroxyapatite has shown potential for the remediation of metal contaminated waters and for the sequestration of radionuclide wastes.[2] In these contexts, the structure of hydroxyapatite permits extensive atomic substitution of other ions into the crystal structure, such as fluoride, chloride, carbonate, strontium, and cobalt.[2,39–41] This 'open' structure is significant in allowing the uptake of radionuclides and other metals from the environment.

The finish produced by the bacterial treatment generated Ra and Rq values half that of the brushite-coated samples. This relatively reduced Ra/Rq of the hydroxyapatite coated sample may be significant in terms of generating a surface coating for remediation or preservation. Increased roughness of the surface generates an increased surface area; allowing enhanced trapping of pollutants for remediation purposes. However, this must be balanced against the increased surface area which will be exposed to dissolution via environmental erosion; such as acidic precipitation. In these terms, the reduced roughness of the hydroxyapatite coating may be an advantage. Further

reductions in Ra/Rq were possible by utilising an abiotic hydroxyapatite coating process, with a higher smoothness than untreated cement being attainable (Fig 1).

Conclusions

In this study, we identify that varying between biogenic and abiotic synthesis processes presents the opportunity to influence the surface roughness and hydrophobicity of the hydroxyapatite coating.

We demonstrate that *P. fluorescens* will generate a layer of hydroxyapatite on the surface of OPC that has a greater surface roughness than untreated cement, but a lower surface roughness than the brushite-coated cement. An abiotic synthesis process generated the lowest observed roughness, being even smoother than the untreated cement. The hydroxyapatite layer coats the majority of the surface. We additionally determine that biogenic and abiotic hydroxyapatites have comparable hardness and modulus, which are within the range expected for hydroxyapatite minerals.

We observe that a biogenic hydroxyapatite coating is more hydrophobic than untreated cement, and significantly more hydrophobic than cement coated in brushite. An abiotically synthesised hydroxyapatite coating was observed to have the highest hydrophobicity of all samples examined in this study. The protective capacity of the hydrophobicity produced by these hydroxyapatites may warrant further investigation as an in-situ coating material to enhance water resistance in the built environment.

References

[1] E. Sassoni, *Materials (Basel).* **2018**, *11*, 557.

[2] S. Handley-Sidhu, J. C. Renshaw, S. Moriyama, B. Stolpe, C. Mennan, S. Bagheriasl, P. Yong, A. Stamboulis, M. Paterson-Beedle, K. Sasaki, R. A. D. Pattrick, J. R. Lead, L. E. MacAskie, *Environ. Sci. Technol.* **2011**, *45*, 6985.

[3] E. Sassoni, S. Naidu, G. W. Scherer, *J. Cult. Herit.* **2011**, *12*, 346.

[4] E. Sassoni, G. Graziani, E. Franzoni, *Constr. Build. Mater.* **2016**, *102*, 918.

[5] E. Sassoni, E. Franzoni, *Built Herit. 2013 Monit. Conserv. Manag.* **2013**, 1287.

[6] L. E. Macaskie, P. Yong, M. Paterson-Beedle, A. C. Thackray, P. M. Marquis, R. L. Sammons, K. P. Nott, L. D. Hall, *J. Biotechnol.* **2005**, *118*, 187.

[7] R. J. Turner, J. C. Renshaw, A. Hamilton, *ACS Appl. Mater. Interfaces* **2017**, *9*, 31401.

[8] H. S. Wong, R. Barakat, A. Alhilali, M. Saleh, C. R. Cheeseman, *Cem. Concr. Res.* **2015**, *70*, 9.

[9] S. Muzenski, I. Flores-Vivian, K. Sobolev, *Constr. Build. Mater.* **2015**, *81*, 291.

[10] S. Grumbein, D. Minev, M. Tallawi, K. Boettcher, F. Prade, F. Pfeiffer, C. U. Grosse, O. Lieleg, *Adv. Mater.* **2016**, 8138.

[11] D. Barnat-Hunek, P. Smarzewski, *Constr. Build. Mater.* **2016**, *102*, 367.

[12] S. Ahmad, *Cem. Concr. Compos.* **2003**, *25*, 459.

[13] M. Wu, B. Ma, T. Pan, S. Chen, J. Sun, *Adv. Funct. Mater.* **2016**, *26*, 569.

[14] E. Celia, T. Darmanin, E. Taffin de Givenchy, S. Amigoni, F. Guittard, *J. Colloid Interface Sci.* **2013**, *402*, 1.

[15] M. J. Dalby, L. Di Silvio, E. J. Harper, W. Bonfield, *Biomaterials* **2001**, *22*, 1739.

[16] A. E. Loiselle, L. Wei, M. Faryad, E. M. Paul, G. S. Lewis, J. Gao, A. Lakhtakia, H. J. Donahue, *Tissue Eng. Part A* **2013**, *19*, 1704.

[17] J. L. Ong, D. C. N. Chan, *Crit. Rev. Biomed. Eng.* **2000**, *28*, 667.

[18] A. Mendoza-Arnau, M. F. Vallecillo-Capilla, M. A. Cabrerizo-Vilchez, J. I. Rosales-Leal, *Med. Oral Patol. Oral Cir. Bucal* **2016**, *21*, e631.

[19] I. Arganda-Carreras, V. Kaynig, C. Rueden, K. W. Eliceiri, J. Schindelin, A. Cardona, H. Sebastian Seung, *Bioinformatics* **2017**, *33*, 2424.

[20] J. Schindelin, I. Arganda-Carreras, E. Frise, V. Kaynig, M. Longair, T. Pietzsch, S. Preibisch, C. Rueden, S. Saalfeld, B. Schmid, J.-Y. Tinevez, D. J. White, V. Hartenstein, K. Eliceiri, P. Tomancak, A. Cardona, *Nat. Methods* **2012**, *9*, 676.

[21] A. F. Stalder, T. Melchior, M. Müller, D. Sage, T. Blu, M. Unser, *Colloids Surfaces A Physicochem. Eng. Asp.* **2010**, *364*, 72.

[22] C. Ji, J. G. Ahn, *J. Korean Neurosurg. Soc.* **2010**, *47*, 180.

[23] C. J. Van Oss, R. F. Giese, *Clays Clay Miner.* **1995**, *43*, 474.

[24] G. Vereecke, J. Lemaître, *J. Cryst. Growth* **1990**, *104*, 820.

[25] O. Mekmene, S. Quillard, T. Rouillon, J.-M. Bouler, M. Piot, F. Gaucheron, *Dairy Sci. Technol.* **2009**, *89*, 301.

[26] J. L. Giocondi, B. S. El-Dasher, G. H. Nancollas, C. A. Orme, *Philos. Trans. R. Soc. A Math. Phys. Eng. Sci.* **2010**, *368*, 1937.

[27] R. I. Martin, P. W. Brown, *J. Mater. Sci. Mater. Med.* **1995**, *6*, 138.

[28] I. M. Hung, W. J. Shih, M. H. Hon, M. C. Wang, *Int. J. Mol. Sci.* **2012**, *13*, 13569.

[29] The Editors of Encyclopaedia Britannica, *Encycl. Br.* **2017**.

[30] E. Charrière, S. Terrazzoni, C. Pittet, P. Mordasini, M. Dutoit, J. Lemaître, P. Zysset, *Biomaterials* **2001**, *22*, 2937.

[31] E. Sassoni, G. Graziani, E. Franzoni, *Mater. Des.* **2015**, *88*, 1145.

[32] A. Richardson, K. Coventry, J. Pasley, in *Fourth Int. Conf. Sustain. Constr. Mater. Technol.*, Las Vegas, USA, **2016**.

[33] I. Flores-Vivian, V. Hejazi, M. I. Kozhukhova, M. Nosonovsky, K. Sobolev, *ACS Appl. Mater. Interfaces* **2013**, *5*, 13284.

[34] K. J. Kubiak, M. C. T. Wilson, T. G. Mathia, P. Carval, *Wear* **2011**, *271*, 523.

[35] D. Aronov, R. Rosen, E. Z. Ron, G. Rosenman, *Process Biochem.* **2006**, *41*, 2367.

[36] Y. Abe, Y. Okazaki, K. Hiasa, K. Yasuda, K. Nogami, W. Mizumachi, I. Hirata, *Biomed Res. Int.* **2013**, *2013*, DOI 10.1155/2013/626452.

[37] A. Stewart, B. Schlosser, E. P. Douglas, *ACS Appl. Mater. Interfaces* **2013**, *5*, 1218.

[38] A. Arabzadeh, H. Ceylan, S. Kim, K. Gopalakrishnan, A. Sassani, S. Sundararajan, P. C. Taylor, *Constr. Build. Mater.* **2017**, *141*, 393.

[39] G. Ulian, G. Valdrè, M. Corno, P. Ugliengo, *Am. Mineral.* **2013**, *98*, 410.

[40] Y. Asscher, S. Weiner, E. Boaretto, *Adv. Funct. Mater.* **2011**, *21*, 3308.

[41] K. Sasaki, T. Goto, *Ceram. Int.* **2014**, *40*, 11649.

Chapter 7: Thesis Conclusions

In this thesis, we have demonstrated that a biogenic hydroxyapatite can be biomineralised onto ordinary Portland cement under relatively simple reaction conditions. We have also elucidated the biochemical mechanisms underlying this process. This newly identified deposition method presents a rapid, simple, and cheap method of promoting in-situ biomineralisation of hydroxyapatite onto the OPC substrate.

We have carried out a detailed characterisation of the biogenic hydroxyapatite itself using a combination of synchrotron-SAXS, TEM, SEM-EDS, and Mossbauer spectroscopy. The results suggest that biogenic hydroxyapatite displays a less crystalline; spherical morphology, and reduced primary particle size in comparison to abiotically synthesised hydroxyapatite.

Additionally, we have characterised fundamental properties of the biogenic hydroxyapatite coating on OPC at the bulk scale. Focus-variation microscopy identified that the hydroxyapatite layer is relatively rough, increasing the surface area. X-CT reveals that the biogenic deposition process uniformly coats the entire exposed substrate. We additionally establish that the coating enhances the hydrophobicity of the ceramic substrate material; although an abiotic hydroxyapatite was found to be of even greater hydrophobicity. It was identified that hardness and modulus of the hydroxyapatite did not vary significantly if synthesised biologically or abiotically.

We have also examined the effects of variations in temperature and carbon source composition on *P. fluorescens* biofilm formation and colony morphology. While this initial study has identified that significant variations in biofilm cell concentration and morphology are linked to changes in environmental conditions, we have not examined the full range of environmental conditions which may be present should this coating method be applied in the built environment. Further work may involve the examination of an expanded temperature range, or alterations in pH which are likely in association with high-pH ceramics.

There are a number of potential applications for this newly described hydroxyapatite deposition system, which present opportunities for further applied research. Coating OPC and similar cements with hydroxyapatite using this bacterially-mediated method may be useful in generating a ceramic bone or dental implant material with enhanced biocompatibility.[1] However, the use of an opportunist pathogenic bacterium such as *P. fluorescens* in contact with an implant material will require careful consideration of the potential for infection.

Hydroxyapatite morphology is linked to its physical properties, which will ultimately affect the final applications of the material. The increased surface area of spherical and plate-like morphologies has also been linked to superior drug loading and release in comparison to other hydroxyapatite forms, which we also observe at the bulk scale.[2] Spherical or plate-like hydroxyapatites can be found in bone material, and synthetic spherical hydroxyapatites have been associated with enhanced bone formation *in vitro*.[3] Plate-like hydroxyapatites have been identified as the ideal morphology for stiffening isotropic materials, in comparison to spherical and fibrous morphologies.[4]

OPC is one of the most widely used construction materials in society, and there is an environmental and economic need to preserve and protect concrete structures more widely. The use of organically grown hydroxyapatite offers significant advantages as a protective surface coating. Hydroxyapatite deposition on marble has been investigated, but always via inorganic formation. These methods have been observed to produce a calcium phosphate coating exhibiting pores and/or cracking, offering reduced protection to the marble, and also require the addition of an extra calcium source.[5–11] Significantly, inorganic calcium phosphates often have inferior mechanical properties compared to bacterially generated calcium phosphates, suggesting this method could be appropriate for coating building materials.[12]

Bacterial deposition of bio-hydroxyapatite onto concrete may produce a thinner, more flexible, or stronger film than has been achieved with plasma spraying, electrochemical deposition, or biomimetic deposition.[13, 14] Bacterially generated hydroxyapatite may potentially present

superior strength and crack resistance, as has been observed in other natural hydroxyapatite-bearing systems.[15, 16] A bacterially based deposition method may also help avoid reaction conditions which are unsuitable for architectural conservation, such as extreme alterations of pH, high reaction temperatures, or the use of toxic compounds.[9]

We suggest that biogenic hydroxyapatite may be useful as a coating material for building materials rich in calcium, such as cement and marble.[17] Calcite treatments of building materials are associated with increased strength of the substrate material,[18] but have shown limited capacity to bind stone particles together,[19] and may be more susceptible to environmental degradation than the relatively less soluble hydroxyapatite.[10] The consolidation capacity of hydroxyapatite may exceed that of calcite.

A novel application of bacteria in cement repair is the development of 'self-healing concrete'. This method utilises bacteria packaged as spores within a prepared cement mortar, which activate upon water ingress.[20, 21] This water ingress is typically due to crack formation; as water enters, the bacteria emerge from their spores and precipitate calcite. There is significant potential to examine the ability of bacteria to precipitate hydroxyapatite in this system, due to it's potentially superior crack-sealing properties.

Cements of varied formulations are planned for use in nuclear waste repositories concepts in a number of countries. Some of these concepts use cement blends containing a high quantity limestone, and rely on the leaching of cement minerals to generate a high pH.[22] There is therefore potential for hydroxyapatite layers generated by environmental bacteria which may prevent damage.

Additionally, a recent study has investigated the use of biogenic hydroxyapatite for the uptake of radioisotopes, which established that biogenic hydroxyapatite uptakes radionuclides more efficiently that commercially available hydroxyapatites. In this study, it was found the hydroxyapatite

biologically manufactured by *Serratia* utilising glycerol-2-phosphate and Ca^{2+} precursor chemicals had a smaller crystalline size of ~30nm, and produced the highest level of radionuclide sorption when compared against commercial hydroxyapatite. XRD analysis of this biogenic hydroxyapatite identified a relatively open, semi-crystalline and/or nanoparticle structure.[23]

We would therefore suggest that examinations of this biogenic hydroxyapatite coating in applications such as building material restoration, environmental contaminant remediation, and medical implant devices are potential routes for further research. Additionally, there is significant scope to examine the formation of *P. fluorescens* biofilms under varied environmental conditions, perhaps most significantly under conditions of raised pH or varied calcium concentrations.

References

1. **Li Y, Li Q, Zhu S, Luo E, Li J, *et al.*** The effect of strontium-substituted hydroxyapatite coating on implant fixation in ovariectomized rats. *Biomaterials* 2010;31:9006–9014.

2. **Uskoković, Vuk, Batarni Samir Shariff, Schweicher Julien, King Andrew DT a**. The Effect on Calcium Phosphate Particle Shape and Size on their Antibaterial and osteogenic Activity in the Delivery of Antibiotics in vitro. 2014;5:2422–2431.

3. **Kalia P, Vizcay-Barrena G, Fan JP, Warley A, Di Silvio L, *et al.*** Nanohydroxyapatite shape and its potential role in bone formation: an analytical study. *J R Soc Interface* 2014;11:20140004–20140004.

4. **Gupta HS, Guitia F**. An effective morphology control of hydroxyapatite crystal via hydrothermal synthesis. *Cryst Growth Des* 2009;466–74.

5. **Sassoni E, Naidu S, Scherer GW**. The use of hydroxyapatite as a new inorganic consolidant for damaged carbonate stones. *J Cult Herit* 2011;12:346–355.

6. **Sassoni E, Graziani G, Franzoni E**. An innovative phosphate-based consolidant for limestone.

Part 1: Effectiveness and compatibility in comparison with ethyl silicate. *Constr Build Mater* 2016;102:918–930.

7. **Franzoni E, Sassoni E, Graziani G**. Brushing, poultice or immersion? The role of the application technique on the performance of a novel hydroxyapatite-based consolidating treatment for limestone. *J Cult Herit* 2015;16:173–184.

8. **Sassoni E, Graziani G, Franzoni E**. An innovative phosphate-based consolidant for limestone. Part 2: Durability in comparison with ethyl silicate. *Constr Build Mater* 2016;102:931–942.

9. **Graziani G, Sassoni E, Franzoni E, Scherer GW**. Hydroxyapatite coatings for marble protection: Optimization of calcite covering and acid resistance. *Appl Surf Sci* 2016;368:241–257.

10. **Sassoni E, Franzoni E**. Evaluation of hydroxyapatite effects in marble consolidation and behaviour towards thermal weathering. *Built Herit 2013 Monit Conserv Manag* 2013;1287–1295.

11. **Sassoni E, Graziani G, Franzoni E**. Repair of sugaring marble by ammonium phosphate: Comparison with ethyl silicate and ammonium oxalate and pilot application to historic artifact. *Mater Des* 2015;88:1145–1157.

12. **Dalby MJ, Di Silvio L, Harper EJ, Bonfield W**. Initial interaction of osteoblasts with the surface of a hydroxyapatite-poly(methylmethacrylate) cement. *Biomaterials* 2001;22:1739–1747.

13. **Ong JL, Chan DCN**. Hydroxyapatite and Their Use As Coatings in Dental Implants: A Review. *Crit Rev Biomed Eng* 2000;28:667–707.

14. **Zhang Q, Leng Y, Xin R**. A comparative study of electrochemical deposition and biomimetic deposition of calcium phosphate on porous titanium. *Biomaterials* 2005;26:2857–2865.

15. **Tanner KE**. Small but extremely tough. *Science (80-)* 2012;336:1237–1238.

16. **Weaver JC, Milliron GW, Miserez a., Evans-Lutterodt K, Herrera S, *et al.*** The Stomatopod Dactyl Club: A Formidable Damage-Tolerant Biological Hammer. *Science (80-)* 2012;336:1275–1280.

17. **Sánchez-Román M, Rivadeneyra MA, Vasconcelos C, McKenzie JA**. Biomineralization of carbonate and phosphate by moderately halophilic bacteria. *FEMS Microbiol Ecol* 2007;61:273–284.

18. **Dhami NK, Reddy MS, Mukherjee A**. Improvement in strength properties of ash bricks by bacterial calcite. *Ecol Eng* 2012;39:31–35.

19. **De Muynck W, De Belie N, Verstraete W**. Microbial carbonate precipitation in construction materials: A review. *Ecol Eng* 2010;36:118–136.

20. **Jonkers H, Schlangen E**. Crack repair by concrete-immobilized bacteria. *First Int Conf Self Heal Mater* 2007;1–7.

21. **Jonkers HM, Thijssen A, Muyzer G, Copuroglu O, Schlangen E**. Application of bacteria as self-healing agent for the development of sustainable concrete. *Ecol Eng* 2010;36:230–235.

22. **Hicks TW, D BT, J HP, PJ R, NA C, *et al.*** *Concepts for the Geological Disposal of Intermediate-level Radioactive Waste*. 2008.

23. **Handley-Sidhu S, Hriljac JA, Cuthbert MO, Renshaw JC, Pattrick RAD, *et al.*** Bacterially produced calcium phosphate nanobiominerals: Sorption capacity, site preferences, and stability of captured radionuclides. *Environ Sci Technol* 2014;48:6891–6898.

Appendix 1 - Supplementary Information for Chapter 3

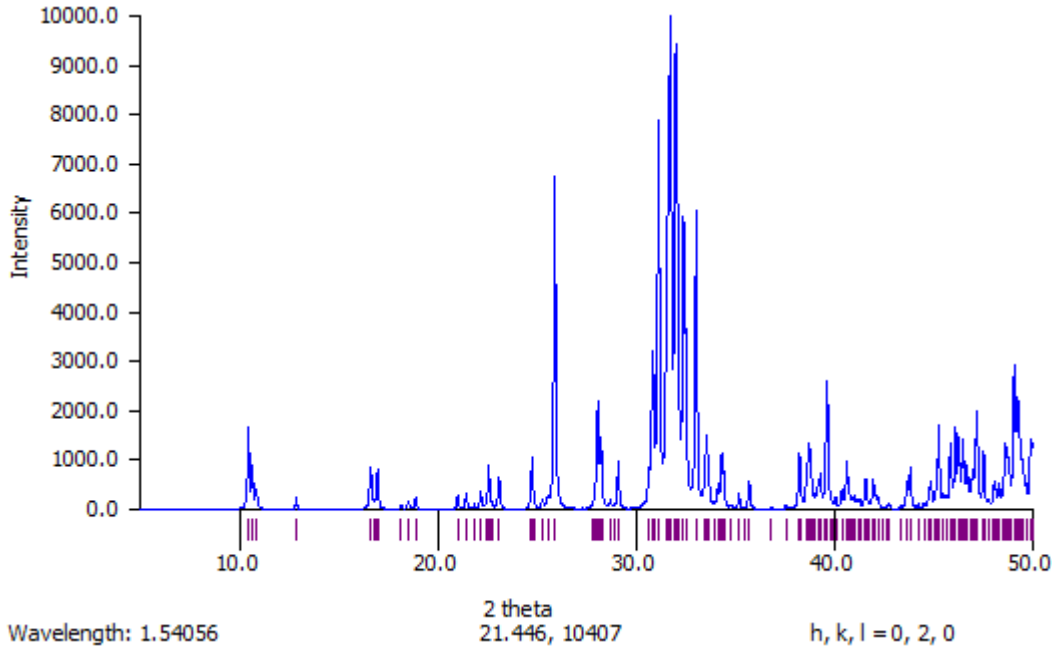

Supplementary Figure 1: Simulated powder diffraction pattern of a carbonate-substituted hydroxyapatite, generated from ICSD-289992

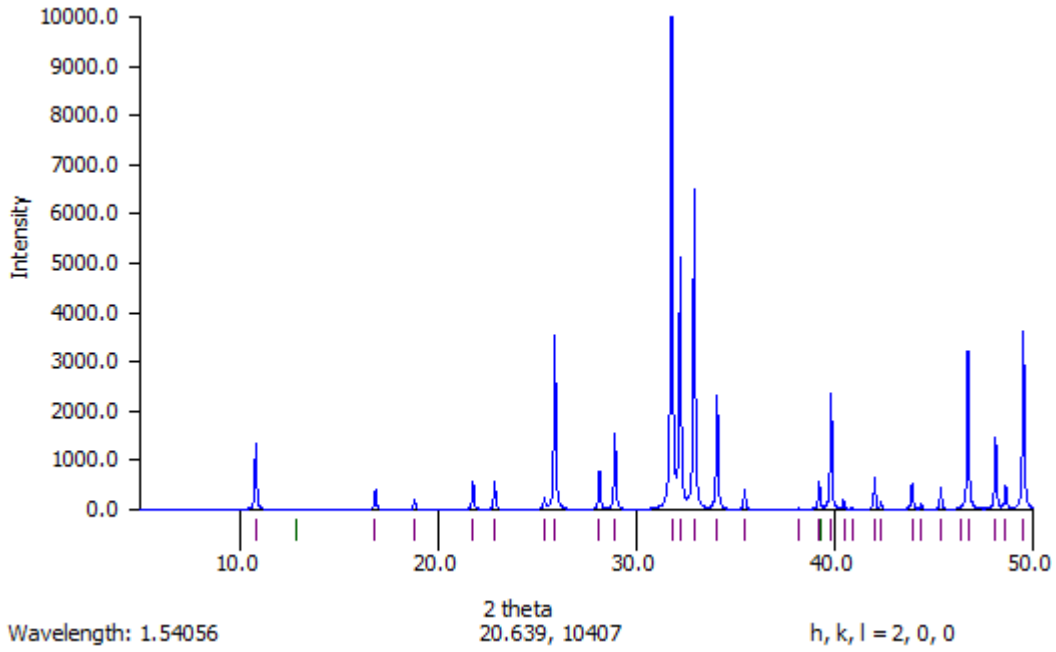

Supplementary Figure 2: Simulated powder diffraction pattern of a synthetic hydroxyapatite, generated from ICSD-203027

S3

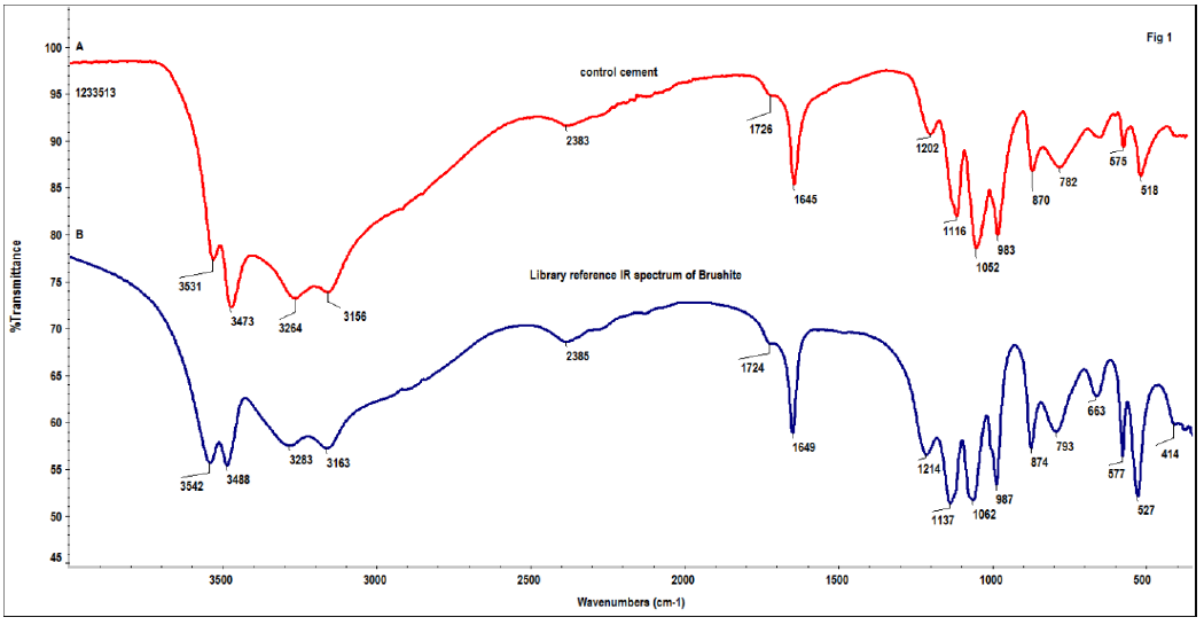

Supplementary Figure 3: The IR spectrum of the surface of the control OPC sample indicated that it consisted predominantly of brushite, a calcium phosphate with the formula CaHPO4.2H2O, with evidence for a possible trace of an organic component. A reference IR spectrum of brushite is shown for comparison.

Appendix 2 - Supplementary Information for Chapter 4

Morphology	Max V	Time at Max V (s)
FS	5.38 +/- 2.9	21937 +/- 8186
SM	8.85 +/- 2.58	24800 +/- 6852

Supplementary Table 1: Maximum growth velocities (Max V), and time at maximum velocity (Time at Max V) for the Fuzzy Spreader (FS) and Smooth (SM) morphologies at 25^{o}C. All measurements are mean of at least N=8 experimental replicates, +/- SEM. The maximum growth rate for the FS morphology was significantly ($p < 0.05$) lower than the SM morphology at 25^{o}C. Differences in Time at Max V were not significant.

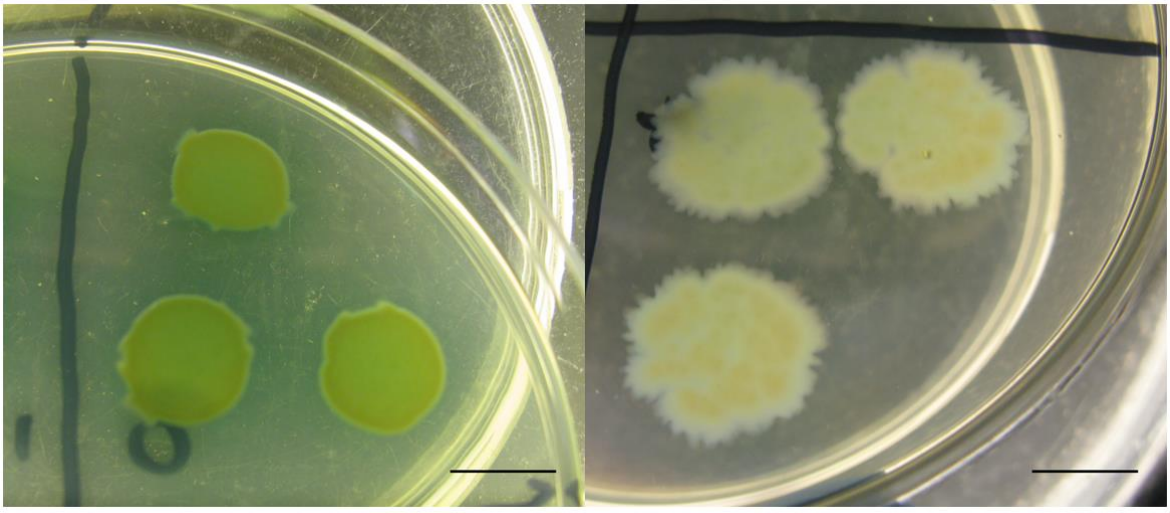

Supplementary Figure 4: Photographic images of colony morphologies of Smooth (Left) and Fuzzy Spreader (Right) P. fluorescens cells, cultured on TSA from adhered biofilm material. Scale bar is 10mm. Identification of colony morphologies was based on that described by Rainey & Travisano (1998).

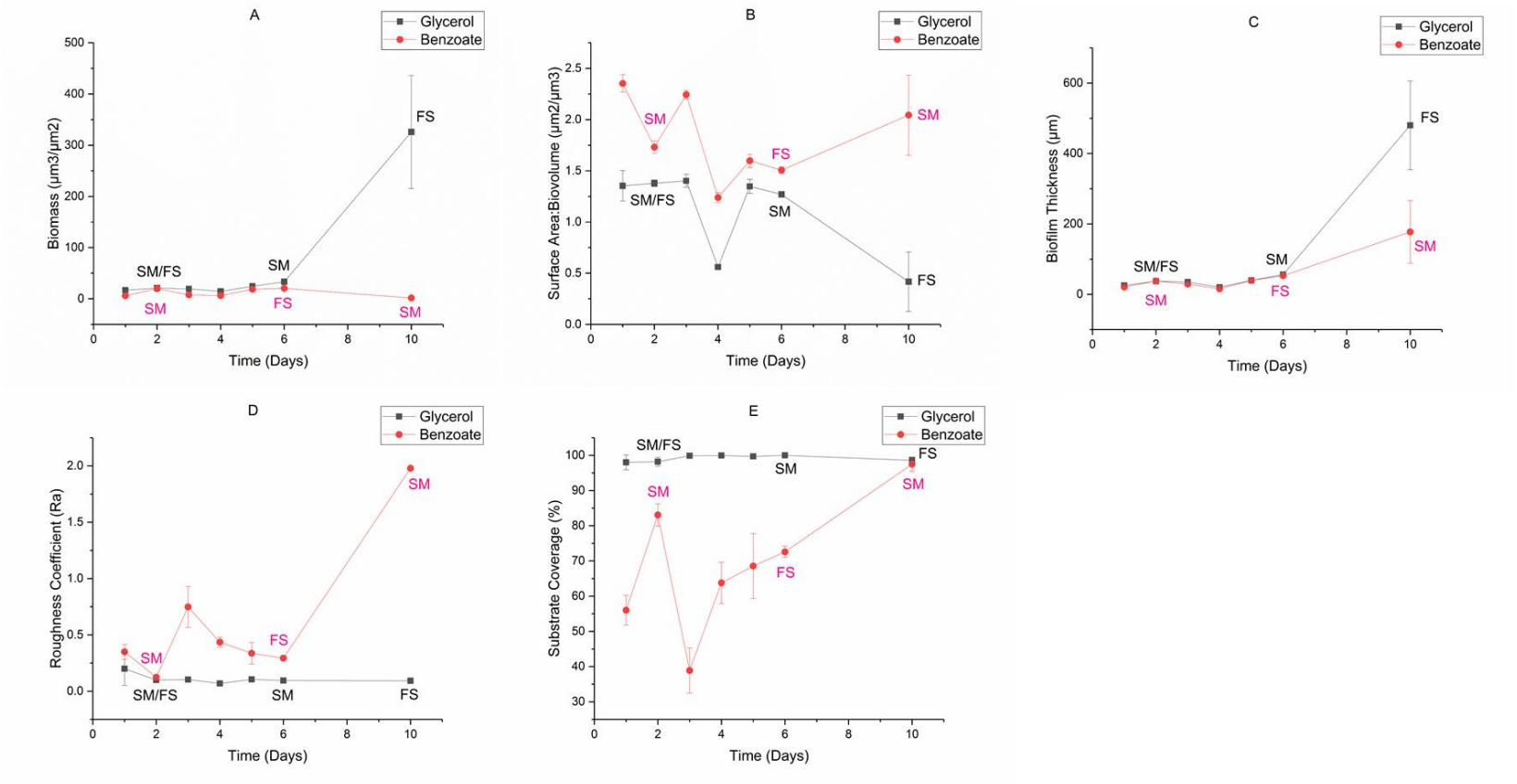

Supplementary Figure 5: Comparisons of biomass, thickness, surface area to biovolume ratio, substrate coverage, and roughness of biofilms formed with either benzoate or glycerol carbon sources at a 25^{o}C incubation temperature. Measurements of A - Biomass (µg,) B - Surface Area

to Biovolume ratio (µm2/µm3), C - Biofilm thickness (µm), D - Roughness coefficient (Ra), E - Substrate Coverage (%), and over a 10 day incubation period. Colony morphology at days 2, 6, and 10 is indicated by 'SM' or 'FS'. Measurements were collected from confocal stacks using the software COMSTAT 2. All measurements are mean of N=3 +/- SEM. Statistical analysis is in supplementary information (SI Table 1).

Appendix 3 - Supplementary Information for Chapter 5

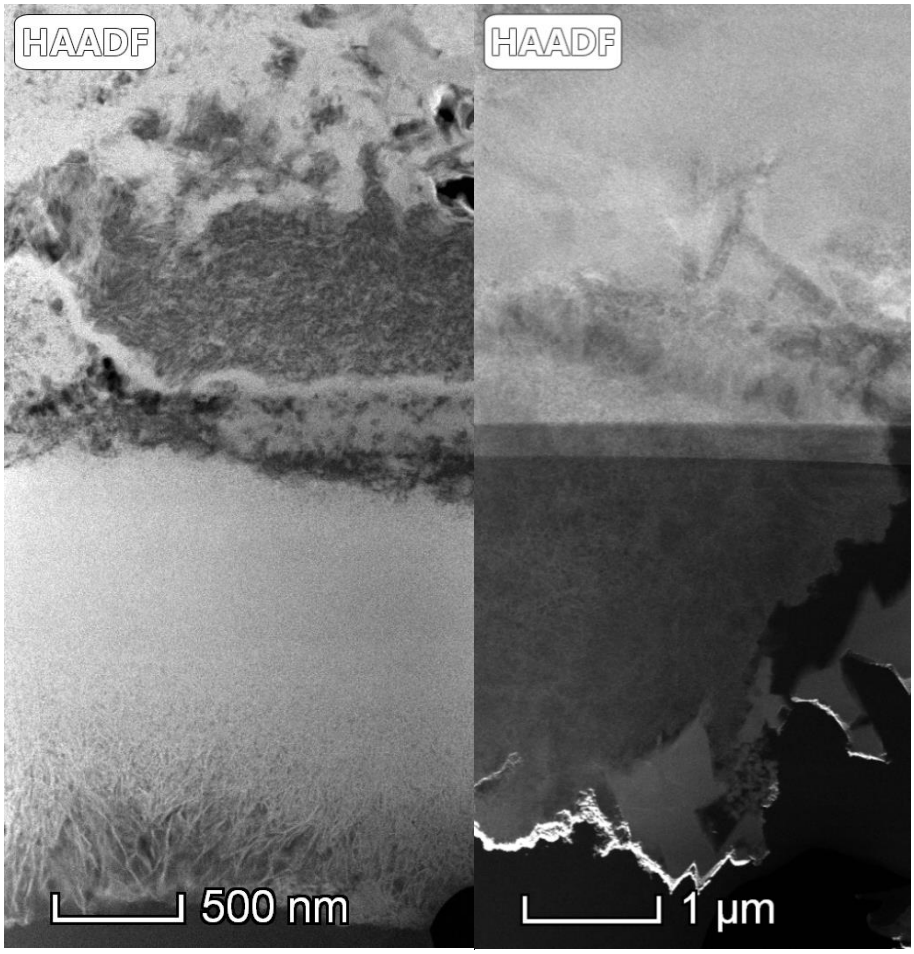

Supplementary Figure 6: TEM images of an abiotic (Left, 500nm scale bar) and biogenic (Right, 1µm scale bar) hydroxyapatite coating on an OPC substrate. The abiotic hydroxyapatite appears to have a needle-like morphology, in comparison to the more plate-like biogenic hydroxyapatite.

	Biogenic HAp Precipitate	Abiotic HAp Precipitate	Biogenic HAp Coating	Abiotic HAp Coating
Ca	19.45	51.35	39.62	43.38
Fe	0.02	0.072	2.20	3.45
P	41.62	70.46	50.13	16.19
Si	0.004	0.10	3.85	3.15
Organic C	5.99	0.91	0.570	0.40
Inorganic C	3.12	3.25	15.87	27.22
Total C	6.62	1.56	3.74	5.84
N	1.59	1.05	1.223	1.14
H	1.59	1.05	1.22	1.14
Calcite content (Rietveld)	nd	nd	3.60	24.10
Ca from Calcite (calculated)	nd	nd	1.44	9.65
Total Weight % Calculated	73.39	128.24	114.67	96.07

Supplementary Table 2: A mass-balanced table of the elemental composition of biogenic and abiotic precipitates and coatings. Mass balance assumed the following phases/compounds were present for the element noted in brackets: PO_4 (P), Ca_5O (Ca), SiO_2 (Si), $Fe(O)_3$ (Fe), CO_3 (inorganic carbon), N (N), H (H). All values are weight %.